Techno-Economic Assessment of Electrolytic Hydrogen Production under Dynamic Operations

by

Doo Hyun Mark Chung

B.S. Engineering, Harvey Mudd College, 2011
M.S. Petroleum Engineering, The University of Texas at Austin, 2013

SUBMITTED TO THE SYSTEM DESIGN AND MANAGEMENT PROGRAM IN PARTIAL FULFILLMENT OF THE REQUIREMENTS OF THE DEGREE OF

MASTER OF SCIENCE IN ENGINEERING AND MANAGEMENT
AT THE
MASSACHUSETTS INSTITUTE OF TECHNOLOGY

September 2022

Signature of Author: _____
System Design and Management Program
August 5, 2022

Certified By: _____
Dharik Mallapragada
Thesis Supervisor
Principal Research Scientist, MIT Energy Initiative

Certified By: _____
Joan Rubin
Thesis Supervisor
Executive Director, System Design and Management Program

Accepted By: _____
Warren Seering
Weber-Shaughness Professor of Mechanical Engineering

(This page intentionally left blank)

Techno-Economic Assessment of Electrolytic Hydrogen Production under Dynamic Operations

by

Doo Hyun Mark Chung

Submitted to the System Design and Management Program

On Aug 5, 2022 in Partial Fulfillment of the Requirement for the
Degree of Master of Science in Engineering and Management

Abstract

Green hydrogen has an important role to play in the future decarbonized world as it has the potential to decarbonize many sectors of the economy. Proton Exchange Membrane (PEM) electrolysis is one of the production pathways for green hydrogen. This study uses a techno-economic optimization model that combines a high-level electrolyzer model and a cost model to evaluate the current (2021) and future (2040) economics of running a PEM electrolyzer under various operating conditions, including dynamic operations and differential-pressure operations. The results show that dynamic operation can reduce the levelized cost of hydrogen (LCOH) by 9% compared to steady operation at a nominal current density. Using direct electrochemical compression without the need for a mechanical compressor is an economically viable solution in the future, while a hybrid approach is preferred in the current scenario. Finally, the LCOH projections show that continued efforts to reduce the capital cost, improve the electrolyzer performance, and integrate more low-cost renewables into the electricity market are necessary for green hydrogen to reach cost-parity with hydrocarbon-based hydrogen.

Thesis Supervisor: Dharik Mallapragada
Title: Principal Research Scientist, MIT Energy Initiative

Thesis Supervisor: Joan Rubin
Title: Executive Director, System Design and Management Program

Keywords —
Hydrogen, Proton Exchange Membrane (PEM) Electrolysis, Techno-economics.

ACKNOWLEDGEMENTS

I would like to first acknowledge my research advisor Dr. Dharik Mallapragada for letting me join him in the journey of learning. He has been a source of inspiration for me as he never ceases to impress me with his vast knowledge, sharp insights, and on-point feedback that kept my research on track. I would also like to thank the other members of the research group, including Landon Schofield, Dr. Ben Paren, Dr. Ed Graham, and Dr. Yang Shao-Horn.

My sincere gratitude also goes to Joan Rubin, who is my other thesis advisor and the Executive Program Director of the System Design and Management Program at MIT. She has been such a supportive advisor and leader throughout my time at MIT.

I am also grateful to Chevron for providing this rare opportunity to become a full-time student again after 8 years in the industry. It is an understatement to say that this past year has been transformational. It forever changed the way I learn, the way I think, and the way I interact with the world. I am eager to give back what I learned in the past year to Chevron. I thank David Meinert and the rest of the PSO Chapter for helping to join the Digital Scholar Program. I thank Chris Lewis, Margery Connor, and Mustafa Kara for steering the program and providing support throughout the year. I also appreciate mentoring and advice from Yaofan Yi and Hari Subramani.

Special thanks to the members of the Chevron Digital Scholar Cohort 3: Amir Ravassipour, Andre Hicks, Anthony Atto, Arman Tanzharikov, Ben Radelet, Jason Lehman, Katherine Papageorge, Mark Tozzi, Matt Barnes, Mo Kittipeerapat, Sarah Coyle, Tara Hong, Will Schwab, and Zhao Zhang. My time at MIT would have never been as complete without you!

Last but not least, I thank and dedicate this thesis to my wife, Jihee Lee. She has been an endless source of support and comfort in the past year. No matter how hard MIT made it look, she emotionally and mentally helped me overcome the challenges one by one. Living 1,846 miles apart only two months after the wedding ceremony was not an easy decision. But, she was magnanimous in her understanding and put herself on a plane 38 times in the past year to cheer me on. Thank you for your dedication and I love you!

Table of Contents

List of Figures

List of Tables

List of Acronyms

BoP	Balance of Plant
BP	Bipolar Plates
CAISO	California Independent System Operator
CAPEX	Capital Expenditures
CEPCI	Chemical Engineering Plant Cost Index
DOE	Department of Energy
eBoP	Electrical Balance of Plant
ERCOT	Electric Reliability Council of Texas
FC	Fuel Cell
FCEV	Fuel Cell Electric Vehicle
GSS	Golden-Section Search
HER	Hydrogen Evolution Reaction
HEV	Hydrogen Electric Vehicles
ICE	Internal Combustion Engine
IF	Installation Factor
KO	Knockout (pots)
LCOH	Levelized Cost of Hydrogen
LMP	Locational Marginal Pricing
mBoP	Mechanical Balance of Plant
MEA	Membrane Electrode Assembly
MINLP	Mixed-Integer Non-Linear Programming
MISO	Midcontinent Independent System Operator

NREL	National Renewable Energy Laboratory
NYSIO	New York Independent System Operator
OCV	Open Circuit Voltage
OER	Oxygen Evolution Reaction
OPEX	Operating Expenses
PEM	Proton Exchange Membrane
PJM	Pennsylvania-New Jersey-Maryland
PTL	Porous Transport Layer
SMR	Steam Methane Reforming
SOEC	Solid Oxide Electrolysis Cell
TCI	Total Capital Investment
TIC	Total Installed Cost
TSA	Temperature Swing Adsorption
WTI	West Texas Intermediate

Chapter 1
Introduction

The past year (2021-2022) marks a tumultuous year that will long be remembered in the history of energy. Energy security has emerged as a top political agenda for many European countries and the rest of the world as a result of an energy shortage triggered by the Russian invasion of Ukraine (European Commission 2022). Sanctions on Russian oil sent the WTI benchmark prices above $130 per barrel in March of 2022 (Kumar 2022), despite the fact that it was trading at historic negative prices less than two years ago (Walker 2020). The Biden Administration also set out to tame rising oil prices, such as by releasing the Strategic Petroleum Reserve, in an effort to fight rising inflation as the world wakes out of dormancy ridden by COVID-19. At the same time, record heat that is battering widespread regions around the world (Newsburger 2022; Fawcett 2022) reminds us that climate change does not wait for us and neither should we. The green energy transition must proceed swiftly; carefully balancing the needs of the present and the advancements for the future.

In 2015, world leaders met in Paris and adopted an international treaty on climate change, referred to as the Paris Agreement or the Paris Accords. As of August 2022, 193 out of 197 parties have agreed to limit global warming to below 2°C compared to pre-industrial levels (United Nations Treaty Collection, n.d.; United Nations, n.d.). This reduction target

requires global annual greenhouse gas emissions to be reduced by 85% by 2050 (Brandon and Kurban 2017). Many states in the United States have adopted plans to decarbonize the electricity sector, which accounted for 25% of the total U.S. greenhouse gas emissions in 2020 (EPA, n.d.). For example, the state of California has a renewable energy mix target of 60% by 2030 and 100% by 2045 (National Conference of State Legislatures 2021). An increasing mix of renewable energy means solution is needed to balance the intermittency that marks the renewable energy sources. The solution may take different forms depending on the storage capacity and discharge time as determined by the mismatch between supply and demand (Ball and Weeda 2015). According to Figure 1.1, hydrogen offers the advantage of storing a large amount of energy (1 GWh to 1 TWh) for both intra-day and inter-seasonal storage (1 hour to 1 month) (Brandon and Kurban 2017). In such a set-up, electrolyzers produce and store hydrogen when excess electricity is available and fuel cells (FC) use the stored hydrogen to generate electricity when the electricity shortage or high electricity price is expected.

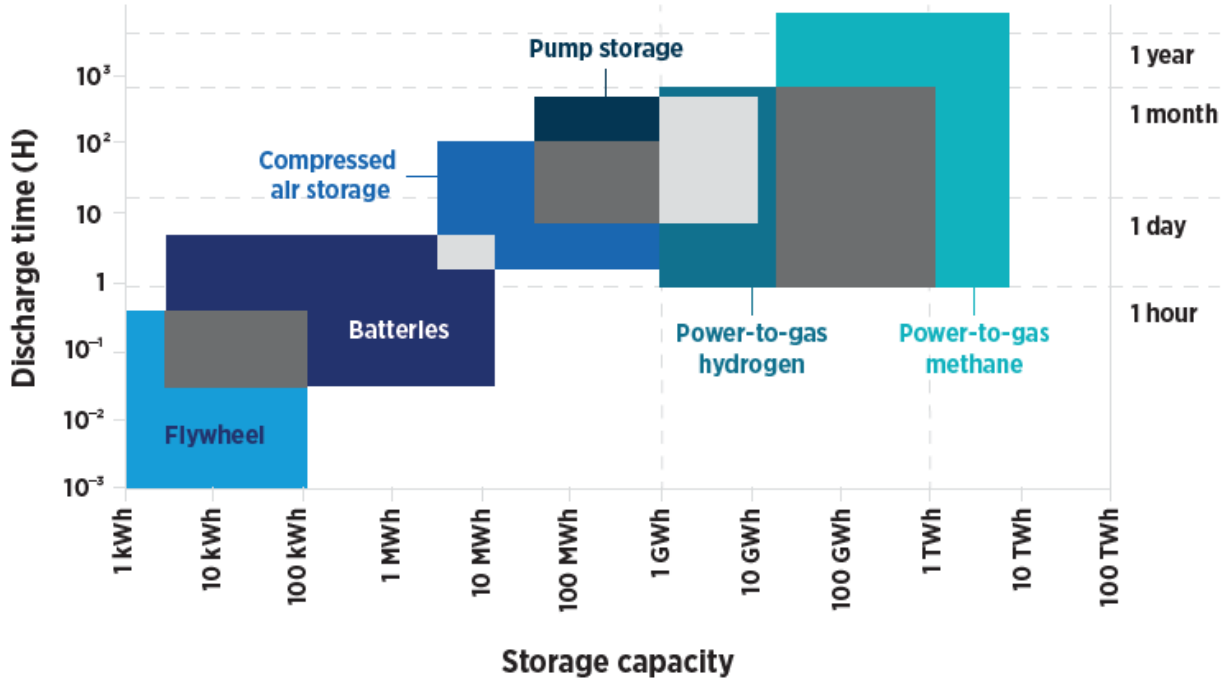

Figure 1.1: Energy storage technologies and power/energy characteristics. Adapted from (Brandon and Kurban 2017).

Hydrogen also has a great potential to be used as a transportation fuel. The transport sector accounts for nearly 25% of the primary energy use and is responsible for 27% of the total greenhouse gas emissions (EPA, n.d.), with 75% of it coming from road transport (Ball and Weeda 2015; Brandon and Kurban 2017). Hydrogen has a few attractive characteristics as a fuel source. Hydrogen offers a gravimetric energy density that is 2.5-3 times greater than hydrocarbon-based fuels (Tashie-Lewis and Nnabuife 2021). The efficiency of a fuel-cell drive train is twice as high as that of an internal combustion engine (ICE). Fuel-cell electric vehicles (FCEV) boast the quiet driving of an electric car and the convenience of fast refueling time and a long driving range (Ball and Weeda 2015). There are several technical and commercial challenges with the mainstream adoption of FCEV. For example, the low volumetric density of hydrogen requires a large space for storage (Tashie-Lewis and Nnabuife 2021). In addition, the cost of an FCEV is relatively high at the moment (Toyota's FCEV Mirai starts at $49,500 in the U.S.) and the refueling infrastructure is not widely available. Despite these challenges, hydrogen makes a compelling case as a transportation fuel, especially for heavy-duty, long-distance vehicles (Brandon and Kurban 2017; IRENA 2020; Godula-Jopek 2015). The shipping and aviation industries are also actively pursuing the use of hydrogen and its derivatives, such as ammonia, for their propulsion systems (IRENA 2020; Tashie-Lewis and Nnabuife 2021).

As of 2022, the industrial sector consumes almost all hydrogen production. 53% of it is used for ammonia production mainly for nitrogen fertilizer and the petrochemical industry uses 40% for hydrocracking, hydrotreating, and desulfurization. The remaining 7% is used for producing polymers and resins (Brandon and Kurban 2017). The steel industry is also looking into hydrogen as a replacement for coke to be used as a reducing agent in iron and steel production (Falcone, Hiete, and Sapio 2021). Figure 1.2 shows various conversion pathways for renewable energy and the role of hydrogen in the decarbonized energy system.

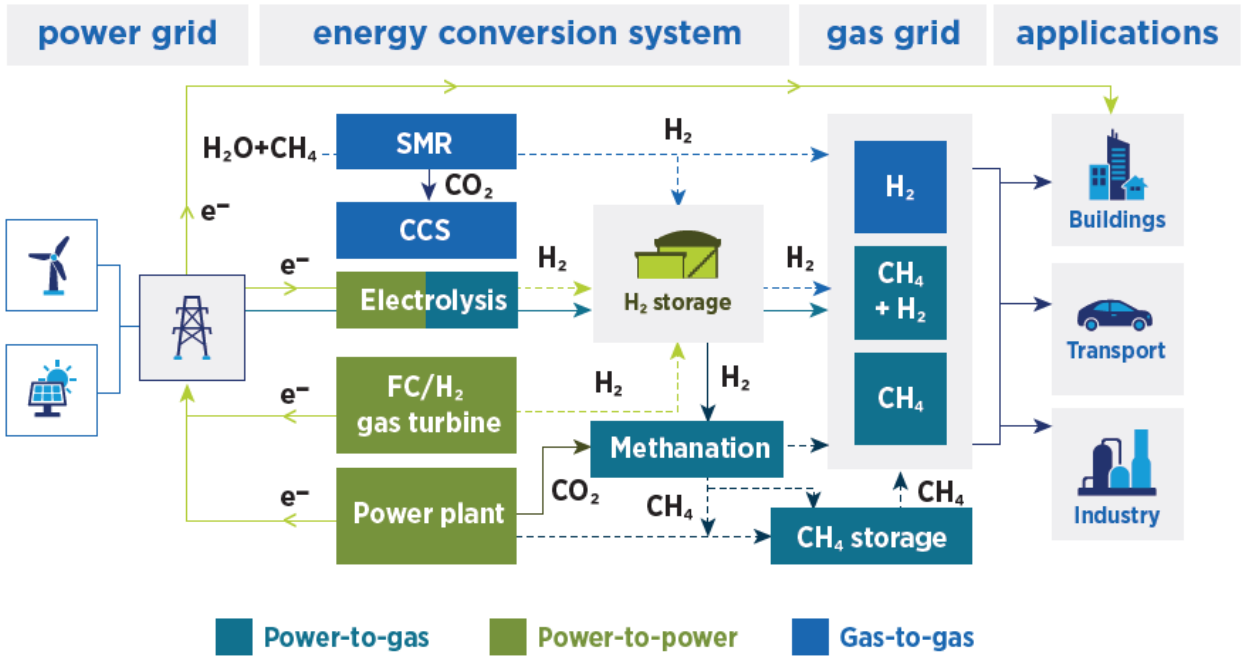

Figure 1.2: Schematic diagram showing the three main energy conversion pathways (power-to-gas, power-to-power and gas-to-gas) in a renewable energy integrated energy system. Adapted from (Brandon and Kurban 2017).

Hydrogen has the potential to decarbonize various economic sectors, including the hard-to-abate sectors (Krishnan et. al. 2022). However, despite being the most common molecule in the universe (Godula-Jopek 2015), hydrogen seldom exists in its molecular structure in nature (Carmo et al. 2013). This means that hydrogen needs to be produced from another primary energy source. As a result, hydrogen is often referred to as an "energy carrier" or "energy vector," rather than as an "energy source," for its ability to move and store energy (Falcone, Hiete, and Sapio 2021). In 2019, the worldwide hydrogen consumption was about 65 million tonnes. Almost 95% of this hydrogen was produced from carbon-intensive processes, with the largest contribution from Steam Methane Reforming (SMR) (El-Emam and Özcan 2019; Godula-Jopek 2015). In SMR, steam is reacted with natural gas in the presence of a metal-based catalyst such as nickel to produce hydrogen. However, hydrogen produced from SMR is low in purity with a high concentration of carbon monoxide (Carmo et al. 2013). Despite this disadvantage, SMR

represents the cheapest method to produce hydrogen, typically at $1.34/kg to $2.27/kg in 2005 dollars (Nikolaidis and Poullikkas 2017).

Only about 1% of hydrogen production comes from electrolysis, which uses electricity to split water to produce hydrogen and oxygen (Bessarabov and Millet 2018). If the electricity comes from renewable sources, the produced hydrogen is dubbed *green hydrogen*. However, the cost of electrolysis is relatively high compared to SMR, ranging from $4.15/kg to $10.49/kg (Nikolaidis and Poullikkas 2017). Therefore, it is imperative to reduce the electrolysis cost to facilitate the widespread adoption of green hydrogen into the energy mix. This thesis focuses on a particular electrolysis technology called the proton exchange membrane (PEM) electrolyzer. A techno-economic model is used to study the levelized cost of hydrogen (LCOH) under various operating conditions. The thesis is organized in the following manner:

Chapter 1 Introduction introduces the potential role of hydrogen in a decarbonized economy and the status quo.

Chapter 2 Literature Review reviews different electrolyzer technologies and analyzes the components of a PEM electrolyzer. Different modes of operating a PEM electrolyzer are introduced. Finally, previous studies on techno-economic modeling of electrolytic hydrogen production are reviewed.

Chapter 3 PEM Electrolyzer Modeling reviews the fundamental electrochemical and physical principles associated with the water-splitting reaction in a PEM electrolyzer and implements them into a model.

Chapter 4 Steady Operations describes the cost model of the PEM electrolysis system and builds the techno-economic model. The techno-economic model is used to study the LCOH under steady operations.

Chapter 5 Dynamic Operations formulates an optimization framework used to model dynamic operations and evaluates the LCOH under dynamic operations.

Chapter 6 Future Cost of Hydrogen uses the techno-economic model to explore different cost drivers and their effect on the LCOH. The cost drivers include the expected reduction in the electrolyzer cost, the expected improvement in the electrolyzer performance, and various future electricity price projections.

Chapter 7 Conclusions summarizes the key findings and makes suggestions for future studies.

References

Ball, Michael, and Marcel Weeda. 2015. "The Hydrogen Economy – Vision or Reality? 1 1This Paper Is Also Published as Chapter 11 'The Hydrogen Economy – Vision or Reality?' In Compendium of Hydrogen Energy Volume 4: Hydrogen Use, Safety and the Hydrogen Economy, Edited by Michael Ball, Angelo Basile and T. Nejat Veziroglu, Published by Elsevier in 2015, ISBN: 978-1-78242-364-5. For Further Details See: Http://Www.Elsevier.Com/Books/Compendium-of-Hydrogen-Energy/Ball/978-1-78242-364-5." *International Journal of Hydrogen Energy* 40 (25): 7903–19. https://doi.org/10.1016/j.ijhydene.2015.04.032.

Bessarabov, Dimitri, and Pierre Millet. 2018. *PEM Water Electrolysis*. United Kingdom: Elsevier.

Brandon, N. P., and Z. Kurban. 2017. "Clean Energy and the Hydrogen Economy." *Philosophical Transactions of the Royal Society A: Mathematical, Physical and Engineering Sciences* 375 (2098): 20160400. https://doi.org/10.1098/rsta.2016.0400.

Carmo, Marcelo, David L. Fritz, Jürgen Mergel, and Detlef Stolten. 2013. "A Comprehensive Review on PEM Water Electrolysis." *International Journal of Hydrogen Energy* 38 (12): 4901–34. https://doi.org/10.1016/j.ijhydene.2013.01.151.

El-Emam, Rami S., and Hasan Özcan. 2019. "Comprehensive Review on the Techno-Economics of Sustainable Large-Scale Clean Hydrogen Production." *Journal of Cleaner Production* 220 (May): 593–609. https://doi.org/10.1016/j.jclepro.2019.01.309.

EPA. n.d. "Sources of Greenhouse Gas Emissions." *United States Environmental Protection Agency*, Accessed Aug 2, 2022. https://www.epa.gov/ghgemissions/sources-greenhouse-gas-emissions.

European Commission. 2022. "Joint Statement by President von der Leyen and President Biden on European Energy Security." Accessed August 2, 2022. https://ec.europa.eu/commission/presscorner/detail/en/STATEMENT_22_4149.

Falcone, Pasquale Marcello, Michael Hiete, and Alessandro Sapio. 2021. "Hydrogen Economy and Sustainable Development Goals: Review and Policy Insights." *Current Opinion in Green and Sustainable Chemistry* 31 (October): 100506. https://doi.org/10.1016/j.cogsc.2021.100506.

Fawcett, Eliza. 2022. "Several Northeast Cities Set New Record Temperatures Amid Heat Wave." *New York Times*, August 4, 2022. https://www.nytimes.com/2022/08/04/us/northeast-heat-wave-record-temperatures.html.

Godula-Jopek, Agata. 2015. "Chapter 1 Introduction." In Hydrogen Production, edited by Agata Godula-Jopek, 1-28. Germany: Wiley-VCH.

IRENA. 2020. "Green Hydrogen Cost Reduction: Scaling up Electrolyzers to Meet the 1.5C Climate Goal." International Renewable Energy Agency, Abu Dhabi.

Krishnan, Mekala, Hamid Samandari, Jonathan Woetzel, Sven Smit, Daniel Pacthod, Dickon Pinner, Tomas Naucler, Humayun Tai, Annbel Farr, Weige Wu, Danielle Imperato. 2022. "The Net-Zero Transition." *McKinsey & Company*, January 2022. https://www.mckinsey.com/business-functions/sustainability/our-insights/the-net-zero-transition-what-it-would-cost-what-it-could-bring.

Kumar, Devika Krishna, and Sheela Tobben. 2022. "Oil Ends at Decade High as Specter of Russia Ban Rattles Market." *Bloomberg*, March 6, 2022. https://www.bloomberg.com/news/articles/2022-03-06/brent-oil-soars-above-135-on-fears-over-tightening-market.

National Conference of State Legislatures. 2021. "State Renewable Portfolio Standards and Goals." *National Conference of State Legislatures*, August 13, 2021. https://www.ncsl.org/research/energy/renewable-portfolio-standards.aspx.

Newsburger, Emma. 2022. "Europe suffers from deadly heat wave as wildfires displace thousands of people." *CNBC*, July 18, 2022. https://www.cnbc.com/2022/07/18/europe-suffers-from-deadly-heat-wave-as-wildfires-displace-thousands.html.

Nikolaidis, Pavlos, and Andreas Poullikkas. 2017. "A Comparative Overview of Hydrogen Production Processes." *Renewable and Sustainable Energy Reviews* 67 (January): 597–611. https://doi.org/10.1016/j.rser.2016.09.044.

Tashie-Lewis, Bernard Chukwudi, and Somtochukwu Godfrey Nnabuife. 2021. "Hydrogen Production, Distribution, Storage and Power Conversion in a Hydrogen Economy - A Technology Review." *Chemical Engineering Journal Advances* 8 (November): 100172. https://doi.org/10.1016/j.ceja.2021.100172.

United Nations Treaty Collection. n.d. "Paris Agreement." Accessed Aug 2, 2022. https://treaties.un.org/Pages/ViewDetails.aspx?src=TREATY&mtdsg_no=XXVII-7-d&chapter=27&clang=_en.

United Nations. n.d. "The Paris Agreement." Accessed Aug 2, 2022. https://www.un.org/en/climatechange/paris-agreement.

Walker, Andrew. 2020. "US oil prices turn negative as demand dries up." *BBC News*, April 21, 2020. https://www.bbc.com/news/business-52350082.

Chapter 2
Literature Review

Hydrogen can be produced from multiple sources, one of which is electrolysis. Eq. 2.1 shows the overall reaction of the water splitting reaction (Carmo et al. 2013):

$$H_2O_{(l)} + 237.2\ kJ\ mol^{-1}(electricity) + 48.6\ kJ\ mol^{-1}(heat) \rightarrow H_2 + \frac{1}{2}O_2$$

Eq. 2.1

In most values of pressure and temperature, electrolysis is a non-spontaneous reaction that requires input of electrical energy and heat to dissociate water into hydrogen and oxygen. There are no other polluting by-products. Electrolysis is capable of producing high-purity hydrogen (>99.9%) that can be directly used in fuel cells (IRENA 2020; Brandon and Kurban 2017). Electrolysis is highly scalable and can be used in both a large-scale central facility and a distributed on-site facility (Ball and Weeda 2015). There are three main types of electrolyzers: Alkaline electrolyzer, Proton-Exchange-Membrane (PEM) electrolyzer, and Solid-Oxide Electrolysis Cell (SOEC) electrolyzer. The following sections provide brief descriptions of each of the electrolyzer types. Then the PEM electrolyzer will be analyzed in more detail. Lastly, previous techno-economic assessments of the PEM electrolyzer are reviewed.

2.1 Alkaline Electrolyzer

Alkaline electrolyzer is the most mature technology for electrolytic hydrogen production up to MW scales. In the alkaline electrolyzer, two electrodes (nickel coated perforated stainless steel) are immersed in the electrolyte solution (5-7 molL^{-1} KOH) (IRENA2020; Carmo et al. 2013). At the cathode, water is split into hydroxide ions and hydrogen. At the anode, the hydroxide ions combine into water and oxygen. The diaphragm separates the anode and the cathode to prevent the mixing of hydrogen and oxygen. At the same time, the diaphragm must be permeable to hydroxide ions and water molecules. A diagram of an alkaline electrolyzer is shown in Figure 2.1.

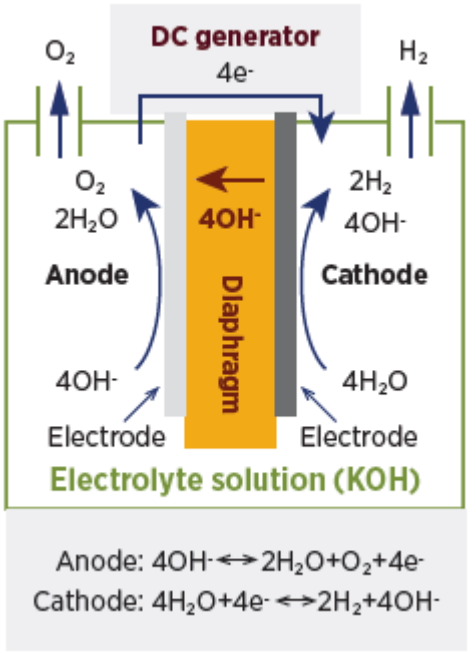

Figure 2.1: Diagram of an Alkaline electrolyzer. Adapted from (IRENA 2020).

Alkaline electrolyzers can be operated at a cell temperature between 60°C and 80°C and at a pressure under 30 bar. The current density can be varied between 0.2 A/cm^2 to 0.8 A/cm^2 (IRENA 2020; Carmo et al. 2013). The low current density limit means that the alkaline electrolyzer can have a large footprint in terms of land use. Thanks to its maturity, alkaline electrolyzers boast a lifetime of 90,000 hours and a capital cost of $500-1,000/kW (IRENA 2020; (El-Emam and Özcan 2019)).

2.2 Solid Oxide Electrolysis Cell (SOEC) Electrolyzer

Solid Oxide Electrolysis Cell (SOEC) electrolyzer is the least mature of the three main electrolyzer types, but has enjoyed great interest from researchers because of its ability to produce a large volume of hydrogen with high efficiency (Carmo et al. 2013) and the potential to operate in reverse as a fuel cell. The SOEC electrolyzer typically operates at a temperature between 700°C and 850°C (IRENA 2020). The electrical energy required to split water at such high temperature decreases significantly compared to other low-temperature systems (El-Emam and Özcan 2019).

The components of the SOEC electrolyzer are ceramic materials (solid oxides), which have the durability to operate at high temperatures. Typical SOEC materials include yttria stabilized zirconia (YSZ) for the electrolyte, nickel-YSZ (Ni-YSZ) for the cathode, and lanthanum-strontium manganoxide (LSM) for the anode (Ni, Leung, and Leung 2006).

The SEOC electrolyzers are still in a R&D stage and have not been widely commercialized due to the limitation imposed by the durability of the materials at high temperatures and long-term operations (IRENA 2020; Carmo et al. 2013).

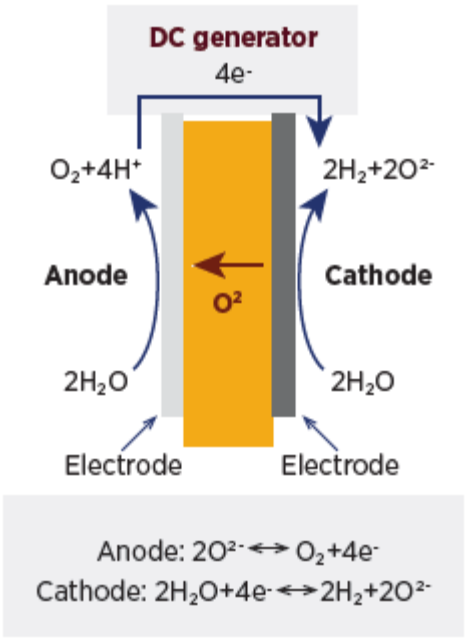

Figure 2.2: Diagram of a Solid Oxide Electrolyzer. Adapted from (IRENA 2020).

2.3 Proton Exchange Membrane (PEM) Electrolyzer

Proton-Exchange-Membrane or Polymer-Electrolyte-Membrane (PEM) electrolyzer is just beginning to experience a widespread commercialization with the growth of interest in green hydrogen. The PEM electrolyzer uses acidic membranes as the solid electrolyte due to the limited self-ionization of pure water (Feng et al. 2017). Typically, a type of perfluorinated ionomer called Nafion is used as the membrane (Carmo et al. 2013). At the anode, water is split into protons and oxygen. The protons migrate from the anode to the cathode through the electrolyte membrane and are combined into hydrogen at the cathode, as shown in Figure 2.3.

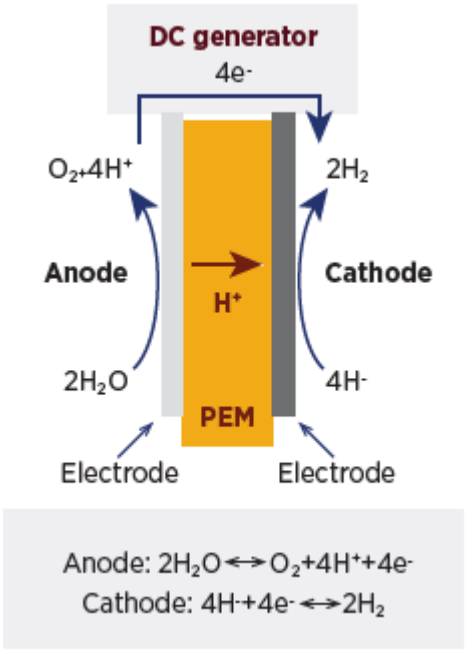

Figure 2.3: Diagram of a PEM Electrolyzer. Adapted from IRENA (2020).

PEM electrolyzers can operate at high current densities from 1 A/cm^2 to 2 A/cm^2 (IRENA 2020). The membrane's low gas crossover rate allows the PEM electrolyzers to operate under a wide range of power input, a trait that well suites the use of renewable energy as a power source (Carmo et al. 2013).

The resistant structural properties of Nafion allows the use of thinner membranes, which

decreases the ohmic losses. It also allows for high-pressure operations. Some manufacturers have demonstrated PEM electrolyzer operations at up to 350 bar (Carmo et al. 2013).

The harsh electrochemical environment characterized by high anodic overpotential, the presence of strong oxidants, and low pH narrows down the list of available materials to precious metal compounds (Feng et al. 2017). As a result, the total capital cost of PEM electrolyzer system sits between $700-1,400/kW (IRENA 2020). In addition, iridium in particular can be a bottleneck in the mass production of the PEM electrolyzers due to its limited supply (Carmo et al. 2013; Minke et al. 2021).

2.3.1 Components of a PEM Electrolyzer

Figure 2.4 shows different components that make up a PEM electrolyzer cell. The bipolar plates (BP) provide mechanical stability and integrity of the device. It ensures charge carrier transport from cell to adjacent cell. It also facilitates mass transport of the feedwater and produced gas as well as heat transfer (Feng et al. 2017). Therefore, BPs must have high electrical conductivity, good mass transport property with integrated flow channels, high mechanical strength, and excellent corrosion resistance in order to withstand the harsh electrochemical environment. As a result, BPs are made up of expensive titanium and can take up to 48% of the total stack cost (IRENA 2020).

The porous transport layer (PTL) acts as a current collector as well as a gas diffusion layer. It is important to supply a continuous stream of feedwater to the catalyst layer (anode electrode) while at the same time removing the produced oxygen that can block the active sites at the electrode (Feng et al. 2017). PTL is typically made of titanium coated with platinum (IRENA 2020).

The anode electrode is the catalyst layer where the conversion of water to oxygen and protons takes place. Therefore, materials that provide lower cathodic potential and robust chemical stability to withstand the hard environment are necessary. As a result, iridium-

based catalysts are used such as Ir, IrO_2, or Ir-transition metal alloys (Feng et al. 2017).

The membrane is typically made up of a solid acidic membrane such as Nafion. It separates the produced oxygen and hydrogen and transport protons from the anode to the cathode. Therefore, it requires excellent chemical stability, mechanical strength, thermal stability, proton conductivity, and gas-crossover resistance (Feng et al. 2017; IRENA 2020).

Finally, the cathode electrode is the catalyst layer where the transported protons combine to form hydrogen. The materials at this layer should provide high anodic potential. Platinum with carbon materials as conductive support materials are typically used (Feng et al. 2017).

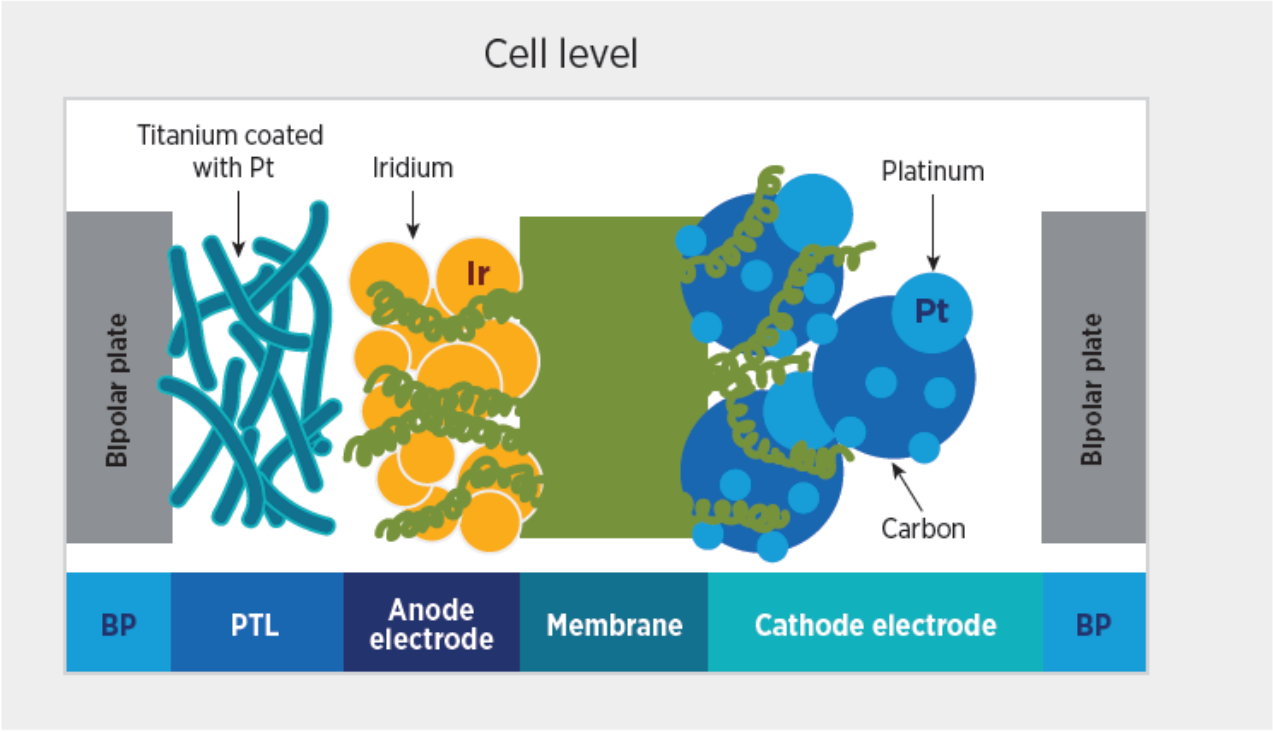

Figure 2.4: Components of a PEM electrolyzer cell. Adapted from (IRENA 2020).

In a typical electrolyzer system, the electrolysis cells are put together in series to form an electrolyzer stack, as shown in Figure 2.5. The number of cells in the stack determine the production volume from the stack. If multiple stacks are present, they can be arranged in different configurations to cater to the needs of the system. For example, if the electrolyzer system is designed for flexibility, a modular design that is made up of small stacks with its own rectifiers would be more suitable than a single-stack, single-rectifier electrolyzer (IRENA 2020). However, such system-level arrangement of multiple stacks is out of scope of this thesis.

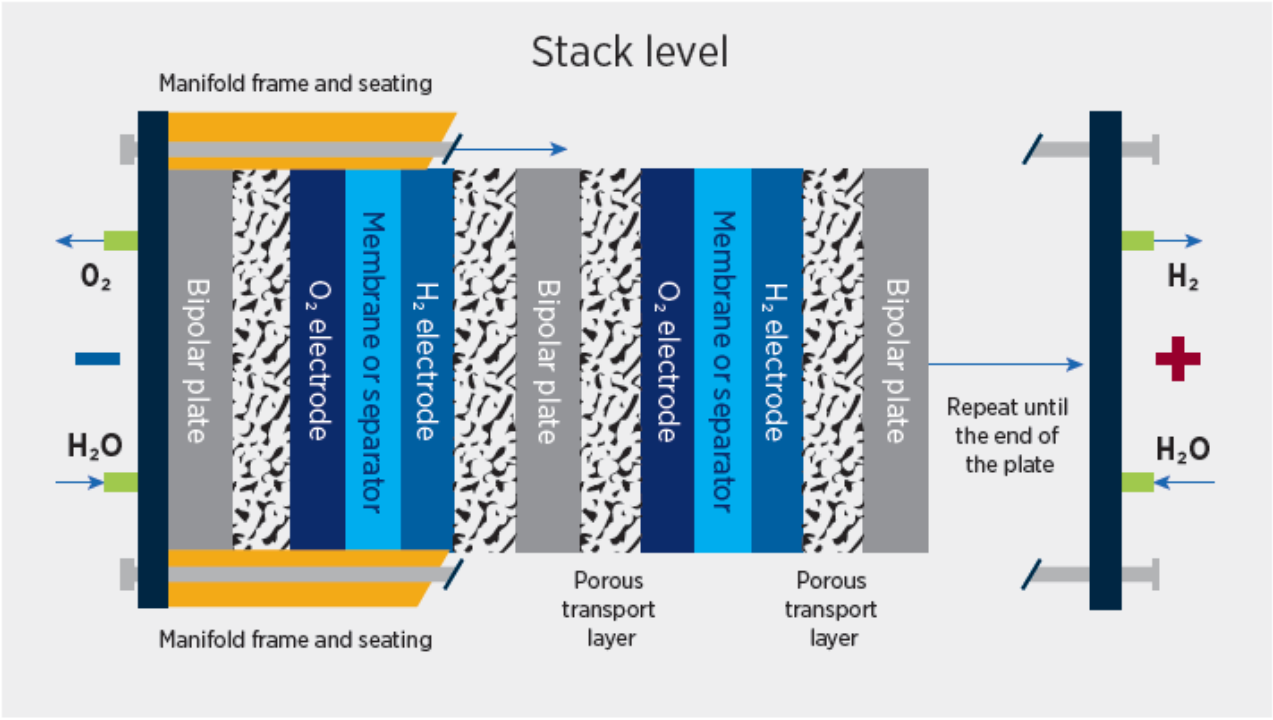

Figure 2.5: Composition of a PEM Electrolyzer Stack. Adapted from (IRENA 2020).

2.3.2 Different Modes of Operations

The PEM electrolyzer can work in different operating modes. In this section, three particular modes of operation are described: Steady operations, dynamic operations, and differential-pressure operations.

In *steady operations*, the electrolyzer operates with a constant, continuous power. The electrolyzer operates at a nominal current density that leads to optimal cell performance. The production capacity can be controlled by changing the number of cells that are in operation.

In *dynamic operations*, the electrolyzer operates at a varying load. Because the proton transport can quickly respond to the power input, the PEM electrolyzers are able to work under a wide range of power input (Carmo et al. 2013). This feature offers the flexibility to complement the intermittent renewable energy sources. Also, dynamic operation has the potential to reduce the cost of production as an excess amount of hydrogen can be produced and stored when the energy price is inexpensive (IRENA 2020).

In *differential-pressure operations*, the structural robustness of the Nafion membrane allows the electrolyzer to operate under different pressures at the anode and the cathode. Typically, the anode stays near the ambient pressure while the cathode is pressurized to the target pressure. This mode presents a potential economic case if direct electrochemical compression removes the necessity for a separate mechanical compression system (Hancke, Holm, and Ulleberg 2022).

2.4 Techno-Economic Modeling

A techno-economic analysis combines a physics-based model and a cost model to assess the economic performance of a system (Burk C 2018). (Orella et al. 2020) presents a generalized techno-economic model that can be used for various electrolytic processes. The model is used to evaluate the economics of PEM electrolysis and found the LCOH to be ~$5.00/kg. (Badgett et al. 2021) provides a techno-economic assessment of the future production of hydrogen based on the reduced capital cost as determined from a learning rate, manufacturing economies of scale, reduced material consumption, and improved electrolyzer performance. (Mallapragada et al. 2020) uses a techno-economic optimization model to evaluate the economics of a PV-PEM Electrolyzer system and find the system configurations that result in LCOH that is competitive with hydrocarbon-based production methods. (Yates et al. 2020) evaluates the potential of PV-PEM Electrolyzer system using a Monte-Carlo approach to identify key drivers for reducing the LCOH. (Hancke, Holm, and Ulleberg 2022) uses a techno-economic model to evaluate the economics of differential-pressure operation of a PEM electrolyzer system by comparing the cost of direct electrochemical compression with the cost of mechanical compression. This study uses a techno-economic optimization model to study the economics of dynamic operations and differential-pressure operations of a large-scale PEM electrolyzer plant (with a daily output of 50 tonne/day) connected to the grid. The model will be also used to understand how the future LCOH would respond to reduction in capital costs and improvement in electrolyzer performance under various future electricity price predictions.

A high-level electrolyzer model based on standard electrochemical principles is used as the physics-based model. The cost modeling approach is adopted from the Department of Energy (DOE)'s H2A model (James et al. 2013), which frequently serves as the benchmark in other studies.

2.5 References

Badgett, Alex, Mark Ruth, Brian James, and Bryan Pivovar. 2021. "Methods Identifying Cost Reduction Potential for Water Electrolysis Systems." *Current Opinion in Chemical Engineering* 33 (September): 100714. https://doi.org/10.1016/j.coche.2021.100714.

Ball, Michael, and Marcel Weeda. 2015. "The Hydrogen Economy – Vision or Reality? 1 1This Paper Is Also Published as Chapter 11 'The Hydrogen Economy – Vision or Reality?' In Compendium of Hydrogen Energy Volume 4: Hydrogen Use, Safety and the Hydrogen Economy, Edited by Michael Ball, Angelo Basile and T. Nejat Veziroglu, Published by Elsevier in 2015, ISBN: 978-1-78242-364-5. For Further Details See: Http://Www.Elsevier.Com/Books/Compendium-of-Hydrogen-Energy/Ball/978-1-78242-364-5." *International Journal of Hydrogen Energy* 40 (25): 7903–19. https://doi.org/10.1016/j.ijhydene.2015.04.032.

Brandon, N. P., and Z. Kurban. 2017. "Clean Energy and the Hydrogen Economy." *Philosophical Transactions of the Royal Society A: Mathematical, Physical and Engineering Sciences* 375 (2098): 20160400. https://doi.org/10.1098/rsta.2016.0400.

Burk C. 2018. "Techno-Economic Modeling for New Technology Development." *Chemical Engineering Progress* 114 (1): 43–52.

Carmo, Marcelo, David L. Fritz, Jürgen Mergel, and Detlef Stolten. 2013. "A Comprehensive Review on PEM Water Electrolysis." *International Journal of Hydrogen Energy* 38 (12): 4901–34. https://doi.org/10.1016/j.ijhydene.2013.01.151.

El-Emam, Rami S., and Hasan Özcan. 2019. "Comprehensive Review on the Techno-Economics of Sustainable Large-Scale Clean Hydrogen Production." *Journal of Cleaner Production* 220 (May): 593–609. https://doi.org/10.1016/j.jclepro.2019.01.309.

Feng, Qi, Xiao−Zi Yuan, Gaoyang Liu, Bing Wei, Zhen Zhang, Hui Li, and Haijiang Wang. 2017. "A Review of Proton Exchange Membrane Water Electrolysis on Degradation Mechanisms and Mitigation Strategies." *Journal of Power Sources* 366 (October): 33–55. https://doi.org/10.1016/j.jpowsour.2017.09.006.

Hancke, Ragnhild, Thomas Holm, and Øystein Ulleberg. 2022. "The Case for High-Pressure PEM Water Electrolysis." *Energy Conversion and Management* 261 (June): 115642. https://doi.org/10.1016/j.enconman.2022.115642.

IRENA. 2020. "Green Hydrogen Cost Reduction: Scaling up Electrolyzers to Meet the 1.5C Climate Goal." International Renewable Energy Agency, Abu Dhabi.

James, Brian, Whitney Colella, Jennie Moton, G. Saur, and T. Ramsden. 2013. "PEM Electrolysis H2A Production Case Study Documentation." NREL/TP--5400-61387, 1214980. https://doi.org/10.2172/1214980.

Mallapragada, Dharik Sanchan, Emre Gençer, Patrick Insinger, David William Keith, and Francis Martin O'Sullivan. 2020. "Can Industrial-Scale Solar Hydrogen Supplied from Commodity Technologies Be Cost Competitive by 2030?" *Cell Reports Physical Science* 1 (9): 100174. https://doi.org/10.1016/j.xcrp.2020.100174.

Minke, Christine, Michel Suermann, Boris Bensmann, and Richard Hanke-Rauschenbach. 2021. "Is Iridium Demand a Potential Bottleneck in the Realization of Large-Scale PEM Water Electrolysis?" *International Journal of Hydrogen Energy* 46 (46): 23581–90. https://doi.org/10.1016/j.ijhydene.2021.04.174.

Ni, M., M. K. H. Leung, and D. Y. C. Leung. 2006. "An Electrochemical Model of a Solid Oxide Steam Electrolyzer for Hydrogen Production." *Chemical Engineering & Technology* 29 (5): 636–42. https://doi.org/10.1002/ceat.200500378.

Orella, Michael J., Steven M. Brown, McLain E. Leonard, Yuriy Román-Leshkov, and Fikile R. Brushett. 2020. "A General Technoeconomic Model for Evaluating Emerging Electrolytic Processes." *Energy Technology* 8 (11): 1900994. https://doi.org/10.1002/ente.201900994.

Yates, Jonathon, Rahman Daiyan, Robert Patterson, Renate Egan, Rose Amal, Anita Ho-Baille, and Nathan L. Chang. 2020. "Techno-Economic Analysis of Hydrogen Electrolysis from Off-Grid Stand-Alone Photovoltaics Incorporating Uncertainty Analysis." *Cell Reports Physical Science* 1 (10): 100209. https://doi.org/10.1016/j.xcrp.2020.100209.

Chapter 3
PEM Electrolyzer Modeling

The core component of the PEM electrolyzer is the membrane electrode assembly (MEA), which consists of the cathode layer, anode layer, and solid polymer electrode membrane that divides the two layers, as shown in Figure 2.4. This chapter lays out the theoretical model that is used to derive the operating cell voltage as a function of operating current density:

$$V = E + \eta_{ohmic} + \eta_a + \eta_{conc} \qquad \text{Eq. 3.1}$$

where V is the operating voltage, E is the thermodynamic equilibrium voltage, η_{ohmic} is the ohmic overpotential, η_a is the activation overpotential, and η_{conc} is the concentration overpotential. The operating voltage, V, is the electrical energy necessary to initiate the water dissociation electrochemical reaction to produce hydrogen. The derivation of each of these components is presented in the following sections. Much of this material is drawn from standard textbooks on electrochemical engineering (Millet 2015, Chapter 2; Bessarabov and Millet 2018). The electrolyzer model assumes that liquid water feed (temperature < 100°C) is at the same temperature as the operating cell. The additional energy required to maintain a constant temperature has not been accounted for in the derivation.

3.1 Thermodynamic Equilibrium Voltage

3.1.1 Nernst Equation for Electrolysis

The electrical potential that is required to create the chemical potential that drives the hydrogen generation process is called the thermodynamic equilibrium voltage or the open-circuit voltage and is given by the Nernst Equation:

$$E = E^0 - \frac{RT}{zF} lnQ \qquad \text{Eq. 3.2}$$

where E^0 is the standard electrode potential at 1 bar and 298 K (25 ℃), R is the gas constant, T is the temperature, z is the number of electrons transferred, F is the Faraday constant, and Q is the reaction quotient. In a PEM electrolyzer, the oxygen evolution reaction (OER) occurs at the anode and the hydrogen evolution reaction (HER) occurs at the cathode:

$$Anode: H_2O(l) \rightarrow \frac{1}{2} O_2(g) + 2H^+ + 2e^- \qquad \text{Eq. 3.3}$$

$$\text{Cathode: } 2H^+ + 2e^- \rightarrow H_2(g) \qquad \text{Eq. 3.4}$$

$$\text{Overall: } H_2O(l) \rightarrow \frac{1}{2} O_2(g) + H_2(g) \qquad \text{Eq. 3.5}$$

The anode reaction needs to be expressed in the form of a reduction reaction, which is the standard form to compute potentials for the Nernst Equation:

$$\frac{1}{2} O_2(g) + 2H^+ + 2e^- \rightarrow H_2O(l) \qquad \text{Eq. 3.6}$$

$$E_{an} = E^{\circ}_{H_2O/O_2} - \frac{RT}{2F} ln \frac{\alpha_{H_2O}}{\sqrt{\alpha_{O_2}}\alpha_{H^+}^2} \qquad \text{Eq. 3.7}$$

where $E^{\circ}_{H_2O/O_2}$ is 1.229 V and α is the activity coefficient of each species.

The Nernst Equation for the cathode reaction is:

$$E_{cat} = E^{\circ}_{H_2/H^+} - \frac{RT}{2F} ln \frac{\alpha_{H_2}}{\alpha^2_{H^+}}$$

Eq. 3.8

where $E^{\circ}_{H_2/H^+}$ is 0 V. Therefore, the cell voltage required to split water is the difference in potential between the anodic and cathodic reactions:

$$E_{an} - E_{cat} = E^{\circ}_{H_2O/O_2} - \frac{RT}{2F} ln \frac{\alpha_{H_2O}}{\sqrt{\alpha_{O_2}}\alpha^2_{H^+}} - E^{\circ}_{H_2/H^+} + \frac{RT}{2F} ln \frac{\alpha_{H_2}}{\alpha^2_{H^+}}$$

$$= E^{\circ}_{H_2O/O_2} - E^{\circ}_{H_2/H^+} - \frac{RT}{2F} ln \frac{\alpha_{H_2O}}{\sqrt{\alpha_{O_2}}\alpha^2_{H^+}} \frac{\alpha^2_{H^+}}{\alpha_{H_2}}$$

$$= E^{\circ}_{H_2O/O_2} - E^{\circ}_{H_2/H^+} - \frac{RT}{2F} ln \frac{\alpha_{H_2O}}{\sqrt{\alpha_{O_2}}\alpha_{H_2}}$$

$$= E^{\circ}_{rev} - \frac{RT}{2F} ln \frac{\alpha_{H_2O}}{\sqrt{\alpha_{O_2}}\alpha_{H_2}}$$

Eq. 3.9

Assuming that water is always in liquid state (operating temperature is always less than 100°C), the membrane can be assumed to be fully hydrated with $\alpha_{H_2O} = 1$ (Awasthi, Scott, and Basu 2011). Then, the activity coefficients of the gaseous species can be approximated with the partial pressures and the voltage requirement for PEM electrolysis can be written as:

$$E = E^{\circ}_{rev} + \frac{RT}{2F} ln \sqrt{p_{O_2}} p_{H_2}$$ Eq. 3.10

where E°_{rev} is the reversible potential, p_{O_2} is the partial pressure of oxygen, and p_{H_2} is the partial pressure of hydrogen. Eq. 3.10 corrects the thermodynamic voltage for different operating pressures. We can further account for the temperature dependence of Eq. 3.10 by expressing E°_{rev} as a function of T:

$$E = \mathrm{E}(\mathrm{T}, 1\ \mathrm{bar}) + \frac{RT}{2F} ln\sqrt{p_{O_2}} p_{H_2} \qquad \text{Eq. 3.11}$$

Researchers have used empirical correlations to calculate E(T, 1 bar) (Awasthi, Scott, and Basu 2011; Marangio, Santarelli, and Cali 2009). However, Eq. 3.10 and Eq. 3.11 are only valid for operating pressures less than 10 bars. For higher-pressure conditions, a more accurate calculation method using state equations is required (Millet 2015, Chapter 2), as presented in the next section.

3.1.2 Thermodynamic Equilibrium Voltage based on Gibbs Free Energy

In order to express the dependence of E on pressure and temperature, we formulate the dependence of ΔG on pressure and temperature and convert to E using the expression:

$$\Delta G = -\mathrm{nFE} \qquad \text{Eq. 3.12}$$

Based on the stoichiometry of the overall reaction (Eq. 3.5), we can also express ΔG as follows (Marangio, Santarelli, and Cali 2009):

$$\Delta G = G_{H_2}(T_{cat}, P_{cat}) + \frac{1}{2} G_{O_2}(T_{an}, P_{an}) - G_{H_2O}(T_{an}, P_{an}) \qquad \text{Eq. 3.13}$$

We also know that

$$G(\mathrm{T}, \mathrm{P}) = H(\mathrm{T}, \mathrm{P}) - TS(T, P) \qquad \text{Eq. 3.14}$$

Therefore, we compute $H(\mathrm{T}, \mathrm{P})$, $S(T, P)$, and $G(\mathrm{T}, \mathrm{P})$ for each species and use Eq. 3.13 to calculate the overall ΔG. For water, the enthalpy and entropy of formation can be obtained from the steam tables, which are available in Appendix A: Steam Table Used for Thermodynamic Voltage Calculations. For the gas molecules, the temperature and pressure dependence of enthalpy and entropy is analytically computed.

The temperature dependence of enthalpy can be expressed as the following empirical model (Millet 2015, Chapter 2):

$$\mathrm{H(T,1\ bar)} - \mathrm{H(298\ K,1\ bar)} = \mathrm{a(T} - T_0) + \frac{b}{2}10^{-3}(T^2 - T_0^2) - c10^5\left(\frac{1}{T} - \frac{1}{T_0}\right) - \frac{e}{2}10^8\left(\frac{1}{T^2} - \frac{1}{T_0^2}\right)$$

Eq. 3.15

Similarly, the temperature dependence of entropy can be expressed as the following (Millet 2015, Chapter 2):

$$\mathrm{S(T,1\ bar)} - \mathrm{S(298\ K,1\ bar)} = \mathrm{a(LnT} - \mathrm{Ln}T_0) + b10^{-3}(T - T_0) - \frac{c}{2}10^5\left(\frac{1}{T^2} - \frac{1}{T_0^2}\right) - \frac{e}{3}10^8\left(\frac{1}{T^3} - \frac{1}{T_0^3}\right)$$

Eq. 3.16

The coefficients for the gas molecules are provided in Table 3.1 (Millet 2015, Chapter 2):

Table 3.1: Coefficients for Hydrogen and Oxygen for Temperature Correction

Molecules	a	b	c	e
H_2 (g)	26.57	3.77	1.17	–
O_2 (g)	34.35	1.92	-18.45	4.06

Since the values of $H(298\ \mathrm{K}, 1\ \mathrm{bar})$ and $\mathrm{S(298\ K,1\ bar)}$ are known, $H(\mathrm{T}, 1\ \mathrm{bar})$ and $\mathrm{S(T,1\ bar)}$ can be calculated for each species. Finally, we use Eq 3.14 to compute $G(\mathrm{T}, 1\ \mathrm{bar})$ for each species.

With the analytical expression for the Gibbs Free Energy at any temperature at 1 bar, another analytical expression using the virial expansion is used to describe the pressure dependence of the Gibbs Free Energy (Millet 2015, Chapter 2):

$$G(\mathrm{T,P}) - G(\mathrm{T},1\ \mathrm{bar}) = \mathrm{RTLnP} + \mathrm{BP} + \frac{C-B^2}{2RT}P^2 \qquad \text{Eq. 3.17}$$

where

$$\mathrm{B} = b_1 + \frac{b_2}{T}\ (cm^3 mol^{-1}) \qquad \text{Eq. 3.18}$$

$$\mathrm{C} = c_1 + \frac{c_2}{T^{\frac{1}{2}}}\ (cm^3 mol^{-1}) \qquad \text{Eq. 3.19}$$

The virial coefficients for the gas molecules for pressure up to 1000 atm are given in Table 3.2 (Millet 2015, Chapter 2).

Table 3.2: Virial Coefficients for Hydrogen and Oxygen for Pressure Correction

Molecules	b1	b2	c1	c2
H_2 (g)	20.5	-1,857	-351	12,760
O_2 (g)	42.6	-17,400	-2,604	61,457

3.1.3 Trends of Thermodynamic Equilibrium Voltage

Using the two-step procedure of 1) correcting for temperature (Eq. 3.15 – Eq. 3.16) and then 2) correcting for pressure (Eq. 3.17 – Eq. 3.19), we can calculate G of each species at any temperature and pressure. Then, we use Eq. 3.13 to calculate ΔG and Eq. 3.12 to calculate E.

Figure 3.1 shows the thermodynamic voltage as a function of operating pressure for different temperatures. In this calculation, the pressures in both cathode and anode were set to be the same value (balanced pressure). The plots show that temperature and pressure have the opposite effect on the thermodynamic voltage. The thermodynamic voltage decreases as temperature increases while the thermodynamic voltage increases as pressure increases. As can be deduced from Eq. 3.11, the thermodynamic voltage increases logarithmically with increasing pressure.

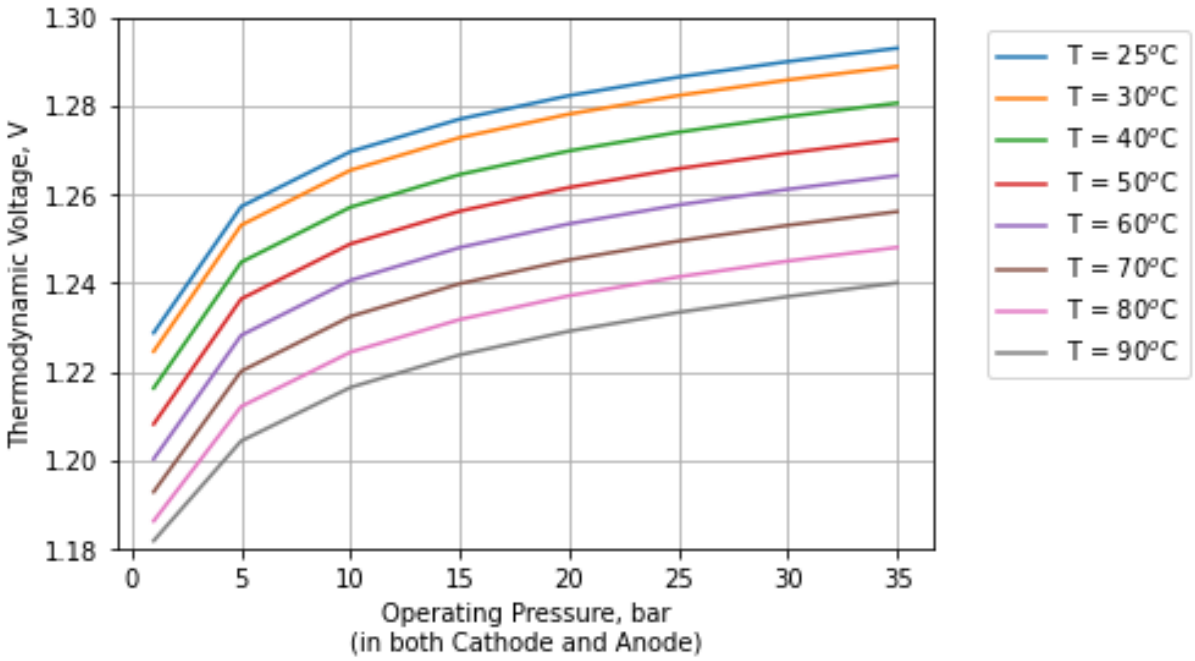

Figure 3.1 Thermodynamic voltage as a function of operating pressure for different temperatures. Both cathode and anode are pressurized.

Figure 3.2 shows the thermodynamic voltage as a function of differential cathode pressure (vs. anode pressure at 1 bar) for different temperatures. While cathode pressure increases, the anode pressure stays the same at 1 bar. Figure 3.2 exhibits similar general trends seen in Figure 3.1. However, the voltage in the differential-pressure system does not increase as much as in the balanced system. This difference highlights one of the advantages of operating in a differential pressure mode: The lower thermodynamic voltage results in lower operational costs for the same hydrogen delivery pressure. In addition, it avoids the safety risk associated with handling high-pressure oxygen, which can self-ignite in the presence of high-purity titanium on a rough surface (Suermann et al. 2017; Hancke, Holm, and Ulleberg 2022).

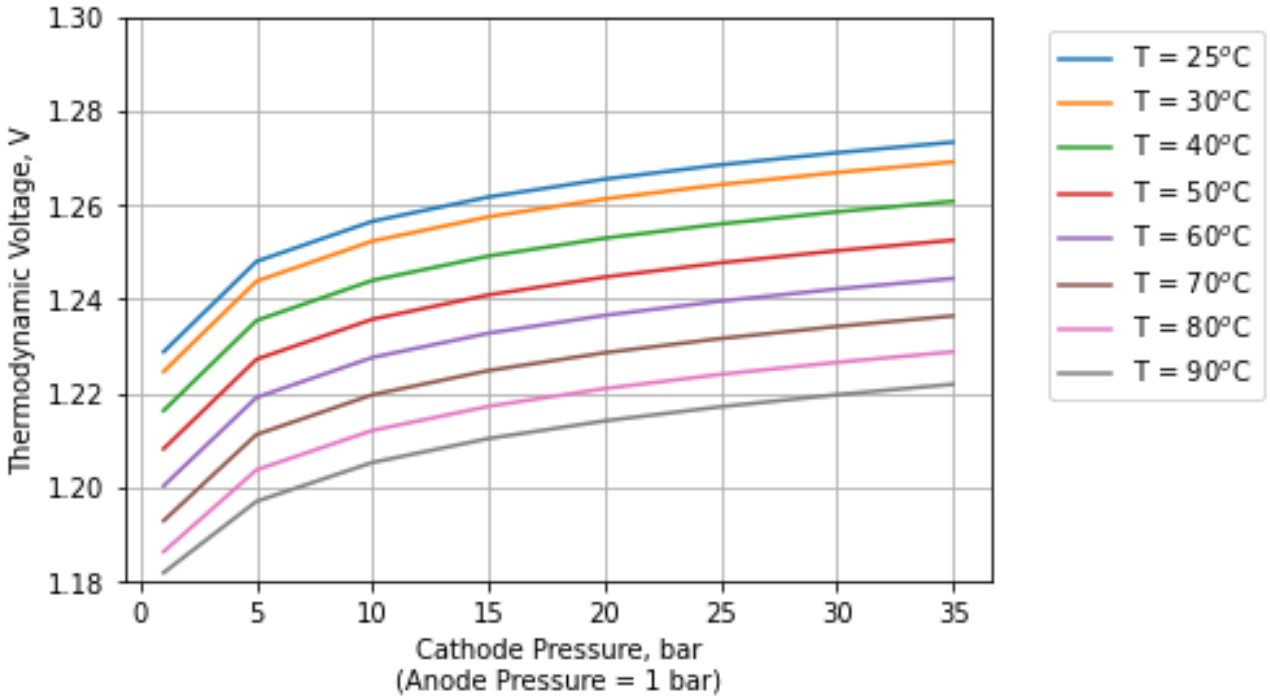

Figure 3.2: Thermodynamic voltage as a function of cathode pressure for different temperatures. The electrolyzer works in a differential pressure mode with the anode pressure at 1 bar.

3.2 Ohmic Overpotential

3.2.1 Ohmic Overpotential due to Membrane

The ohmic overpotential arises from the resistances from the electron flow, proton flow, electrical contact in the membrane. The biggest contributor to the ohmic resistance in the PEM electrolyzer is the membrane (Biaku et al. 2008; Marangio, Santarelli, and Cali 2009). The area-dependent resistance of a membrane is given by the formula:

$$R_{membrane} = \frac{t}{\sigma_{mem}} \qquad \text{Eq. 3.20}$$

where t is the thickness of the membrane and σ_{mem} is the conductivity of the membrane. Average thicknesses of different membranes are shown in Table 3.3 (Bessarabov and Millet 2018).

Table 3.3: Nafion Trade Names and Thicknesses (Bessarabov and Millet 2018)

Trade Name	Thickness (μm)
Nafion N1110 (Nafion 110)	254
Nafion 117	178
Nafion 115	127
Nafion NR212	50.8
Nafion NR211	25.4

The membrane conductivity is given by empirical correlations as shown below (Gorgun 2006; Abdol Rahim et al. 2016):

$$\lambda_m = 0.043 + 17.81a_{H_2O} - 39.85a_{H_2O}^2 + 36a_{H_2O}^3 \qquad \text{Eq. 3.21}$$

$$\sigma_{mem} = (0.00514\lambda_m - 0.00326)e^{\left(1268\left(\frac{1}{303}-\frac{1}{T}\right)\right)} \qquad \text{Eq. 3.22}$$

where λ_m is the water hydration factor. Since the membrane is fully immersed in water during electrolytic operations (Springer, Zawodzinski, and Gottesfeld 1991; García-Valverde, Espinosa, and Urbina 2012), a_{H_2O} is assumed to be 1. Eq. 3.22 suggests that membrane conductivity increases with increasing temperature, but it entails no dependence on pressure.

3.3 Activation Overpotential

In reaction kinetics, an activation energy is required for reactants to initiate the reaction process. Butler and Volmer applied this theory to electrochemical processes and derived the additional voltage needed to supply this activation energy and initiate the exchange of electrons (Bessarabov and Millet 2018; Abdol Rahim et al. 2016). This additional voltage is called the activation overpotential, also known as the kinetic overpotential. The Butler-Volmer equation, which is a commonly-used model for water electrolysis, describes the relationship between current density and activation overpotential (Bessarabov and Millet 2018):

$$j = j_0 \left[exp\left(\frac{-\alpha_1 F z \eta_a}{RT}\right) - exp\left(\frac{\alpha_2 F z \eta_a}{RT}\right)\right]$$

Eq. 3.23

where j_0 is the exchange current density, α is the charge transfer coefficient, and η_a is the activation overpotential. Assuming that $\alpha = \alpha_1 = \alpha_2$, Eq. 3.23 can be simplified to the following equation using the hyperbolic sine function:

$$\eta_a = \frac{RT}{\alpha z F} \operatorname{arcsinh}\left(\frac{j}{2j_0}\right)$$

Eq. 3.24

Previous studies have reported experimental values for the anode charge transfer coefficient and cathode charge transfer coefficient as 2 and 0.5, respectively (Ni, Leung, and Leung 2008; García-Valverde, Espinosa, and Urbina 2012; Lebbal and Lecœuche 2009; Marangio, Santarelli, and Cali 2009; Dale, Mann, and Salehfar 2008; Gorgun 2006; Abdin, Webb, and Gray 2015). However, theoretical value for a charge transfer coefficient is between 0 and 1.

The exchange current density, j_0, is an intensive physical property that measures the ease with which the charge transfer occurs (Millet 2015, Chapter 2). It is a function of the physical characteristics of the electrolyte such as material and morphology, catalyst, age,

and operating conditions (Liso et al. 2018; García-Valverde, Espinosa, and Urbina 2012). For the Pt catalyst in the cathode, j_0 of 10^{-4}-10^{-3} A/cm^2 has been suggested (Escobar-Yonoff et al. 2021; Choi 2004). For the Ir and Pt-Ir catalyst in the anode, j_0 of 10^{-13}-10^{-6} A/cm^2 has been used (Escobar-Yonoff et al. 2021; Marangio, Santarelli, and Cali 2009).

In this study, an approach from (Carmo et al. 2013; García-Valverde, Espinosa, and Urbina 2012; Coutanceau, Baranton, and Audichon 2018) is adopted to express the temperature dependence of j_0:

$$j_0 = j_0^{ref} exp\left[\frac{E_{act}}{R}\left(\frac{1}{T^{ref}} - \frac{1}{T}\right)\right]$$

Eq. 3.25

where j_0^{ref} is the reference exchange current density at the reference temperature, T^{ref}, and E_{act} is the activation energy corresponding to the OER (in the anode) or HER (in the cathode). The values of j_0^{ref} and E_{act} are summarized in Table 3.4 .

Table 3.4: Values of Reference Current Density and Activation Energy for OER and HER

Variable	Value	Units	Reference
$j_{0,cathode}^{ref}$	0.75×10^{-3}	A/cm^2	(Carmo et al. 2013; García-Valverde, Espinosa, and Urbina 2012; Coutanceau, Baranton, and Audichon 2018)
$E_{act,cathode}$	30,000	J/mol	(He et al. 2017)
$j_{0,anode}^{ref}$	1.0×10^{-7}	A/cm^2	(Carmo et al. 2013; García-Valverde, Espinosa, and Urbina 2012; Coutanceau, Baranton, and Audichon 2018)
$E_{act,anode}$	90,000	J/mol	(Suermann, Schmidt, and Büchi 2018; García-Valverde, Espinosa, and Urbina 2012)
T^{ref}	318	K	(García-Valverde, Espinosa, and Urbina 2012)

Therefore, the total activation overpotential of an electrolytic cell is:

$$\eta_a = -\frac{RT}{F}\text{arcsinh}\left(\frac{j}{2j_{0,anode}}\right) + -\frac{RT}{F}\text{arcsinh}\left(\frac{j}{2j_{0,cathode}}\right)$$

Eq. 3.26

3.4 Concentration Overpotential

The concentration overpotential arises due to overpopulation of reacting gases near the electrodes interface. As long as the flow field is well designed for gas removal and the water circulation rate is high enough, the concentration overpotential can be neglected for PEM electrolysis (Yigit and Selamet 2016; Biaku et al. 2008; Gorgun 2006; Abdol Rahim et al. 2016; Choi 2004; Awasthi, Scott, and Basu 2011).

3.5 Polarization (VI) Curve Benchmarking

The polarization curve as calculated from Eq. 3.1 shows the relationship between the operating voltage as a function of the operating current density. In order to validate the electrolyzer model that is developed in this chapter, the model is benchmarked with data from the literature.

3.5.1 Validation with Cell Experiment

The first benchmarking case used data from a single-cell experiment referenced in (Liso et al. 2018). In the experiment, Nafion 117 membrane with a thickness of 178 μm was used. This experiment was conducted at temperatures of 60°C and 80°C under ambient pressure. Table 3.5 summarizes the parameters that were used in the model.

Table 3.5: Electrolyzer Model Parameters for Single-Cell Experiment at 60°C and 80°C

Parameters	Values	Units
Membrane Thickness, t	178	μm
Electrodes and Plates Resistance, R_{elec}	0	ohms
Temperature, T	60 and 80	°C
Cathode Pressure, P_{cat}	1	bar
Anode Pressure, P_{an}	1	bar

Figure 3.3 compares the electrolyzer model with the input from Table 3.5 with experimental data. The model predictions and experimental data match well for both the 60°C and 80°C experiments.

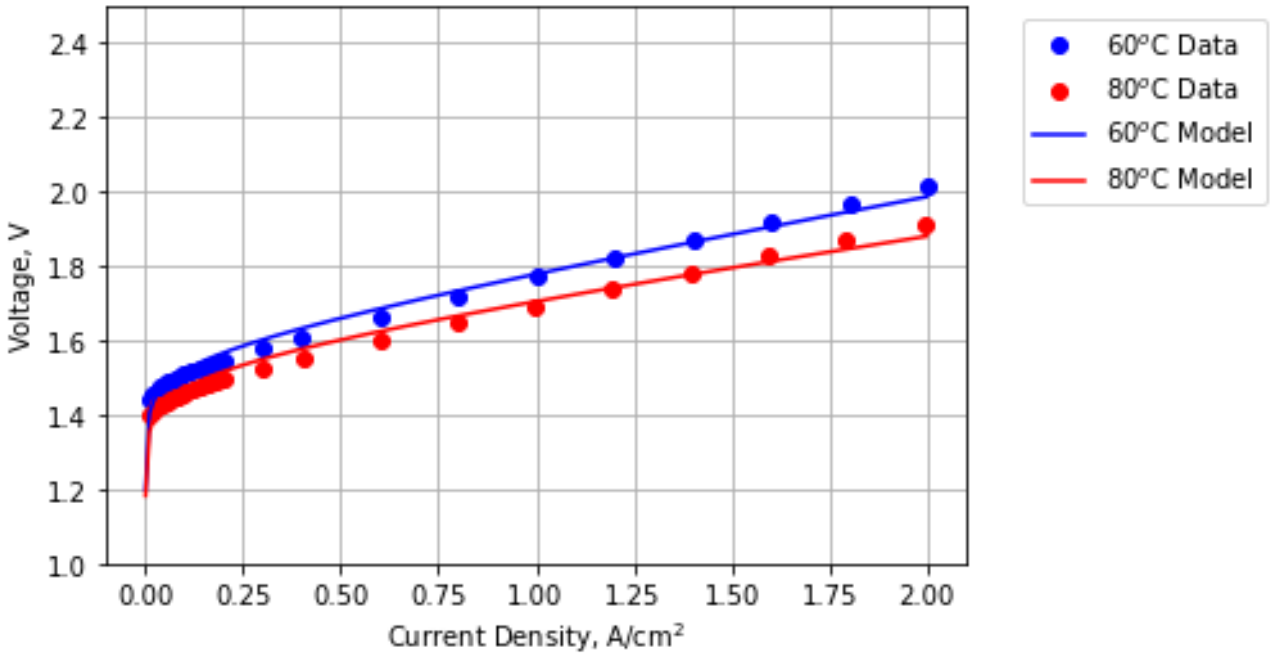

Figure 3.3: Comparison of the electrolyzer model (line) with experimental data (circles) at 80°C (red) and 60°C (blue) in ambient pressure. Data from (Liso et al. 2018).

3.5.2 Validation with Stack Experiment

The model was further benchmarked with data from stack experiments that were conducted in a differential pressure mode, which has been suggested as the preferred mode for commercial electrolyzer operations (Hancke, Holm, and Ulleberg 2022). (Marangio, Santarelli, and Cali 2009) conducted high-pressure experiments with a commercial electrolyzer system from Giner Electrochemical Systems LLC. The stack is made up of twelve cells with an active area of 160 cm^2 each. The experiments were conducted at a temperature between 40 – 55°C and cathode pressures between 1 and 70 bar. The model predictions were overlaid against the data generated from two experiments that were conducted at two different temperatures and pressures, as shown in Figure 3.4.

Nafion 110 with a thickness of 254 μm was used in the experiment. In order to match the experimental results, an additional resistance term was added to the model since the

resistance from the electrodes, plates, and other wires may no longer be negligible in a stack of 10-15 cells (Awasthi, Scott, and Basu 2011). The values of the model parameters are summarized in Table 3.6 and Table 3.7 for the 10-bar-55°C experiment and the 70-bar-40°C experiment, respectively.

Table 3.6: Electrolyzer Model Parameters for Stack Experiment at 55°C and 10 bar

Parameters	Values	Units
Membrane Thickness, t	254	μm
Electrodes and Plates Resistance, R_{elec}	2.5×10^{-5}	ohms
Cathode Exchange Current Density, $j_{0,cathode}$	1.1×10^{-3} (Calculated)	A/cm^2
Anode Exchange Current Density, $j_{0,anode}$	2.87×10^{-7} (Calculated)	A/cm^2
Temperature, T	55	°C
Cathode Pressure, P_{cat}	10	bar
Anode Pressure, P_{an}	1	bar

Table 3.7: Electrolyzer Model Parameters for Stack Experiment at 40°C and 70 bar

Parameters	Values	Units
Membrane Thickness, t	254	μm
Electrodes and Plates Resistance, R_{elec}	2.5×10^{-5}	ohms
Cathode Exchange Current Density, $j_{0,cathode}$	0.6×10^{-3} (Calculated)	A/cm^2
Anode Exchange Current Density, $j_{0,anode}$	5.9×10^{-8} (Calculated)	A/cm^2
Temperature, T	40	°C
Cathode Pressure, P_{cat}	70	bar
Anode Pressure, P_{an}	1	bar

Figure 3.4 shows that the electrolyzer model can reasonably predict the experimental results for different pressures and temperatures just by changing the operating pressure and temperature while maintaining the rest of parameters the same.

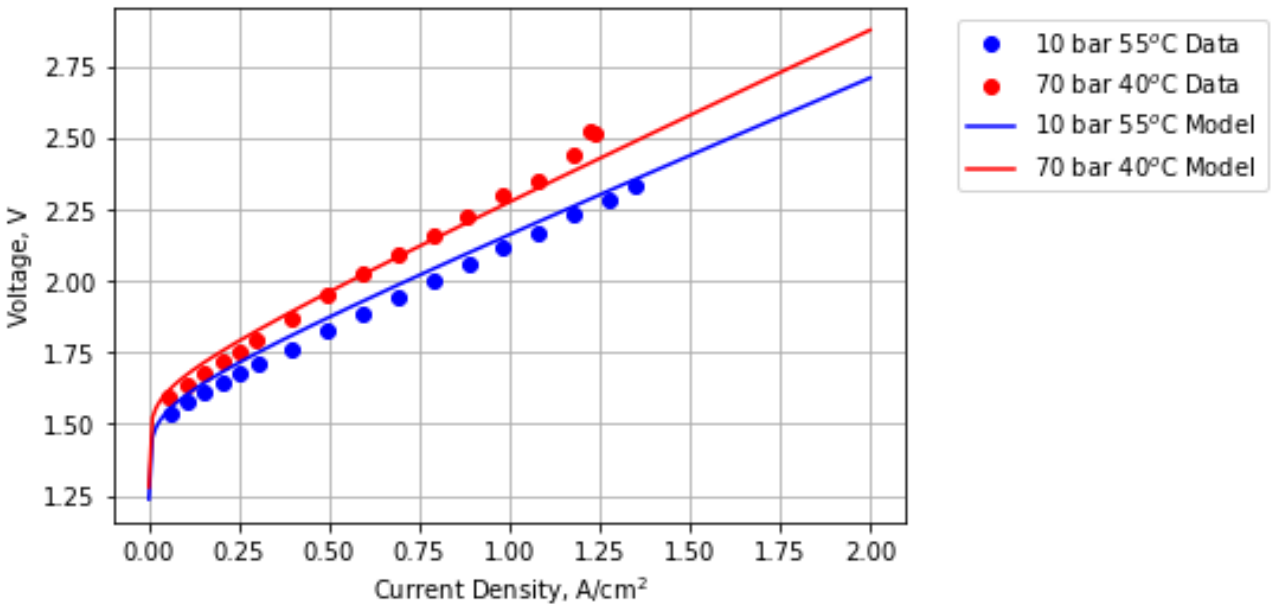

Figure 3.4: Comparison of the electrolyzer model (line) with experimental data (circles) at (a) 55°C and 10 bar (blue); (b) 40°C and 70 bar (red). Data from (Marangio, Santarelli, and Cali 2009).

3.5.3 Comparison with the State-of-the-Art Electrolyzers

A baseline electrolyzer model that represents the state-of-the-art technology as of 2021 was built with the parameters shown in Table 3.8 and compared with data from other PEM electrolyzers in Figure 3.5. The baseline model performance is in line with the published data from some of the leading PEM electrolyzer manufacturers and research labs.

Table 3.8: Baseline Electrolyzer Model Parameters at 80°C and 1 bar

Parameters	Values	Units
Membrane Thickness, t	178	μm
Cathode Exchange Current Density, $j_{0,cathode}$	2.3×10^{-3} (Calculated)	A/cm²
Anode Exchange Current Density, $j_{0,anode}$	3.0×10^{-6} (Calculated)	A/cm²
Temperature, T	80	°C
Cathode Pressure, P_{cat}	1	bar
Anode Pressure, P_{an}	1	bar

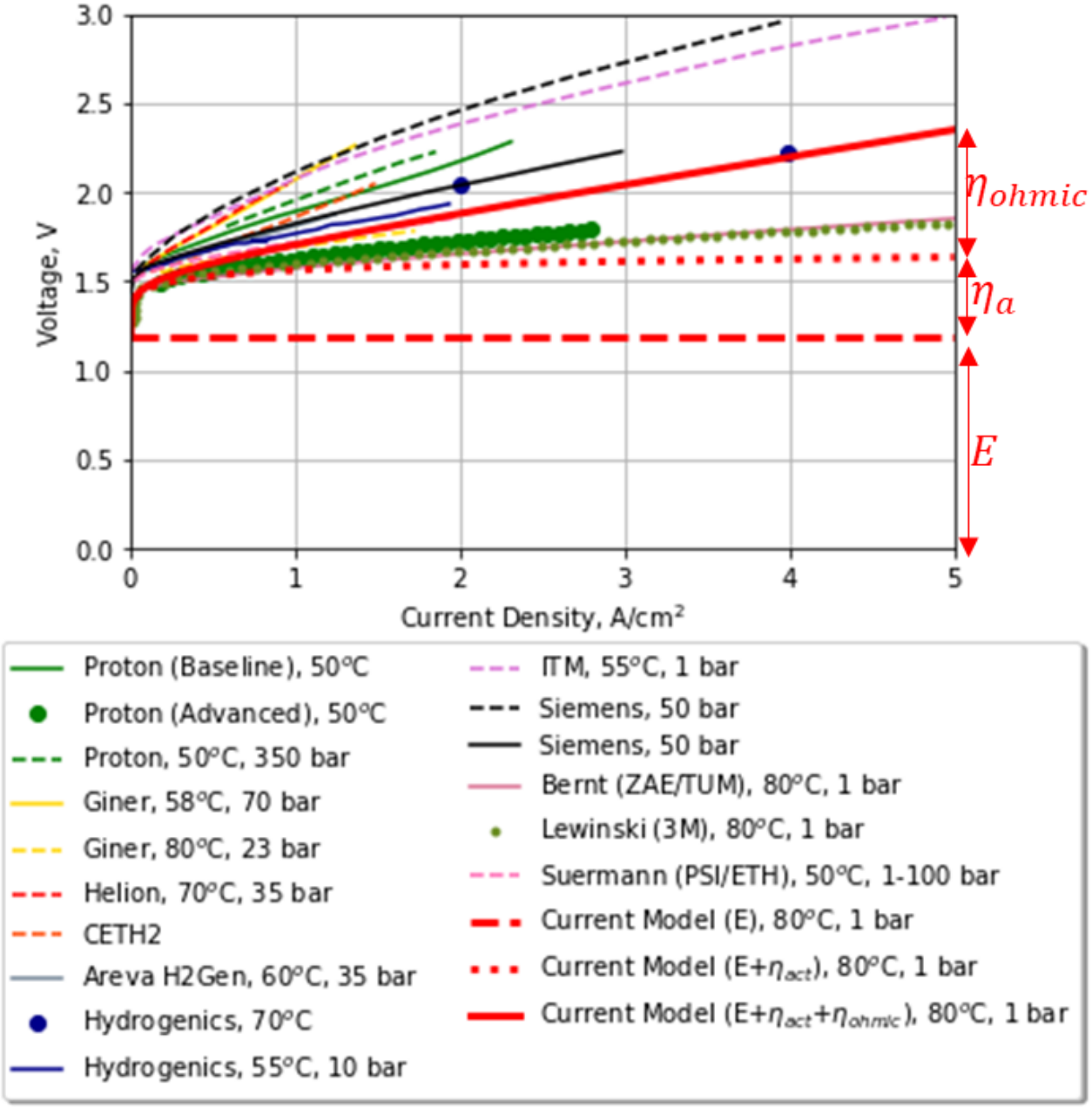

Figure 3.5: Comparison of the electrolyzer model (80°C and 1 bar) with other PEM electrolyzer IV curves from the literature. Figure adopted from (Buttler and Spliethoff 2018).

Figure 3.5 further breaks down the polarization curve into different components. It can be seen that the contribution from the ohmic overpotential, η_{ohmic}, grows with current density while the contribution of the activation overpotential, η_{ohmic}, remains relatively constant. To further illustrate this point, pie charts in Figure 3.6 show the relative

contributions of the different voltage components at three different current densities. At a low current density of 0.25 A/cm^2, the majority of the voltage comes from the thermodynamic equilibrium voltage. Activation overpotential contributes 20.5% and the contribution of the ohmic overpotential is relatively small at 2.3%. At a current density of 1 A/cm^2, the relative contribution of the ohmic overpotential grows to 8.4% while the contribution of the activation overpotential grows to 22.2%. At a high current density of 2 A/cm^2, the contributions of the ohmic overpotential and activation overpotential are 15.2% and 21.8%, respectively. This result is similar to (Liso et al. 2018)'s model which shows an ohmic overpotential contribution of 20.4% at 2 A/cm^2 under similar operating conditions. Furthermore, the model's voltage breakdown is similar to that calculated for (Bernt and Gasteiger 2016)'s data when the model is fitted to represent the experimental conditions (50-µm membrane). Model shows contributions of 24.5% and 7.7% for activation overpotential and ohmic overpotential, respectively, at 3 A/cm^2 and (Bernt and Gasteiger 2016) data show contributions of 20.9% and 9.3% for activation overpotential and ohmic overpotential, respectively. Because the relative contribution of the ohmic overpotential grows drastically with higher operating current density, development of a thin membrane that can support safe and reliable operations will be an important milestone as the operating current density limit is pushed higher in the future.

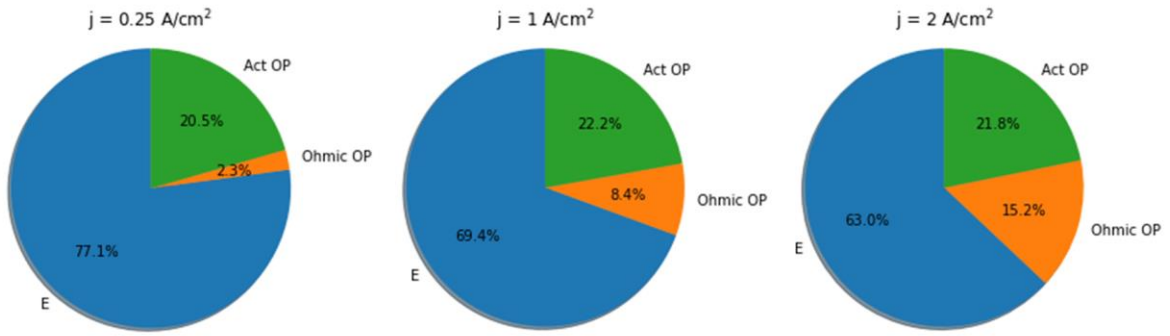

Figure 3.6: Relative contributions of Thermodynamic Equilibrium Voltage (E), Ohmic Overpotential (η_{ohmic}), and Activation Overpotential (η_a) to the overall voltage at j = 0.25 A/cm^2 (left), j = 1 A/cm^2 (middle), and j = 2 A/cm^2 (right)

3.6 Polarization (VI) Curve Sensitivity

With the electrolyzer model validated with various experimental data, the model is used to understand the effects of different electrolyzer designs and operating parameters on electrolyzer performance. The base design and operating parameters are a membrane thickness of 178-μm, temperature of 60, and cathode pressure of 1 bar.

3.6.1 Membrane Thickness Sensitivity

Figure 3.7 shows the impact of membrane thickness on the polarization curve. Membrane thickness changes the polarization curve by changing the slope; the thicker the membrane, the steeper the slope. As a result, the industry is heading towards using thinner and thinner membranes even down to 20 μm (IRENA 2020; Bessarabov and Millet 2018). However, there are technical and safety issues with this approach. First, thinner membranes may be more prone to damages under differential pressures due to lower mechanical strength (Hancke, Holm, and Ulleberg 2022; IRENA 2020). Second, thinner membranes can be more conducive to hydrogen crossover from the cathode to the anode, thereby increasing the risk of catastrophic failure (Schalenbach et al. 2013).

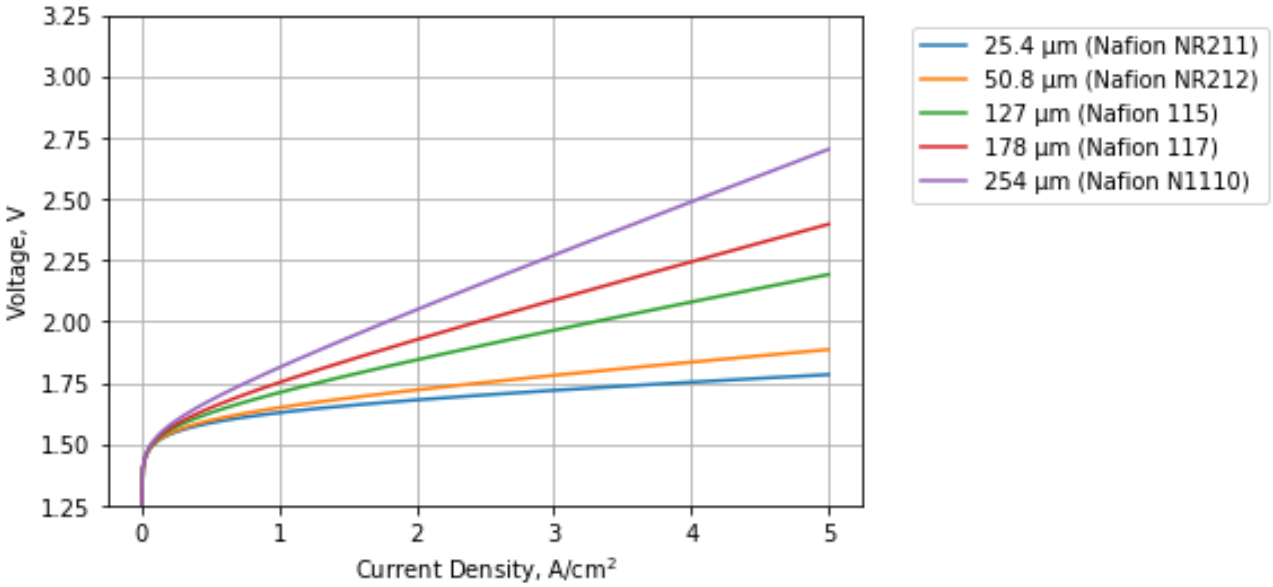

Figure 3.7: Electrolyzer voltage as a function of current density for different membrane thicknesses.

3.6.2 Operating Temperature Sensitivity

Figure 3.8 shows the effect of temperature on the polarization curve. With increasing pressure, the thermodynamic voltage, ohmic overpotential, and activation overpotential all decrease, leading to a decrease in the overall cell voltage (Marangio, Santarelli, and Cali 2009). Despite the advantage of operating at higher temperatures, there is an upper limit set by the thermal robustness of the Nafion membranes.

Nafion is a type of perfluorinated ionomer, which provides high ionic conductivity and chemical stability in aqueous acidic electrolytes (Bessarabov and Millet 2018). However, above 90°C, the membrane can lose its mechanical properties due to excessive water-swelling (Millet 2015, Chapter 3). Experiments testing the thermal stability of Nafion membranes suggest that the release of fluoride release rate (FRR), which is indicative of membrane disintegration, increases by approximately two orders of magnitude when the temperature increases from 55°C to 150°C (Feng et al. 2017). Therefore, with today's commercial PEM electrolyzers, the operating temperature is set below 90°C.

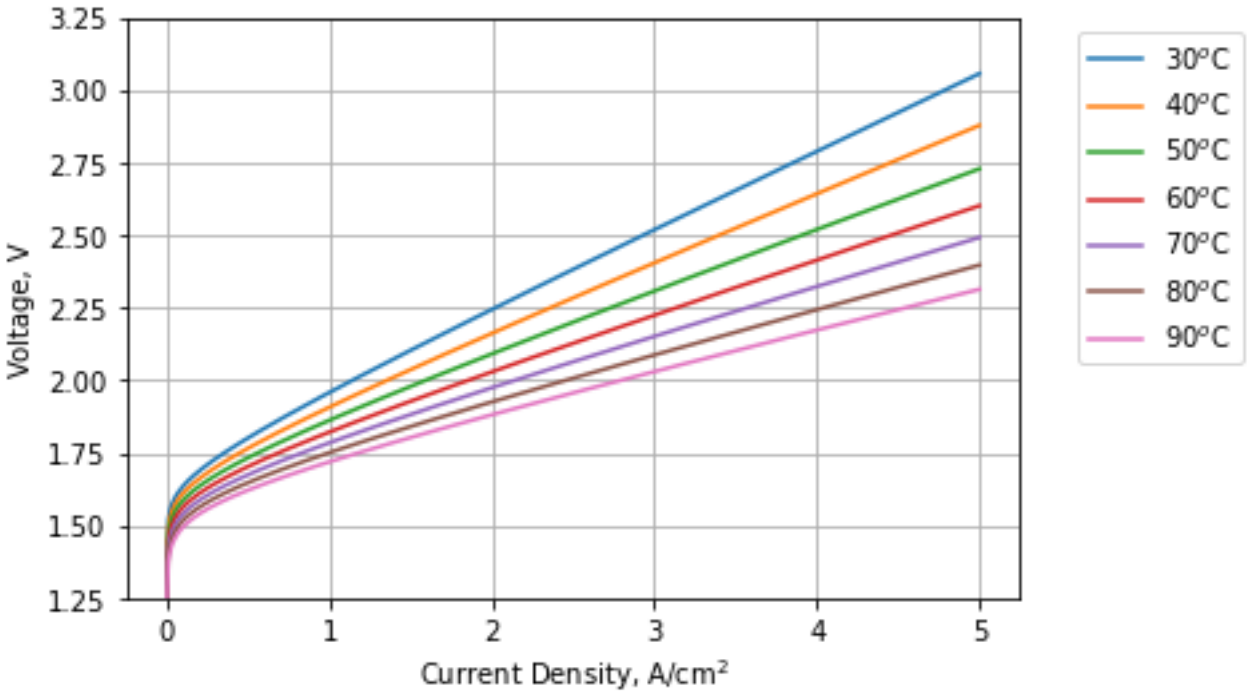

Figure 3.8: Electrolyzer voltage as a function of current density for different temperatures.

3.6.3 Operating Pressure Sensitivity

Figure 3.9 shows the effect of cathode pressure on the polarization curve. Increasing cathode pressure increases the overall voltage by mainly increasing the thermodynamic equilibrium voltage (Buttler and Spliethoff 2018). The model does not include any potential effects of pressure on the membrane resistance, exchange current density, electrode and plate resistance, and limiting current density.

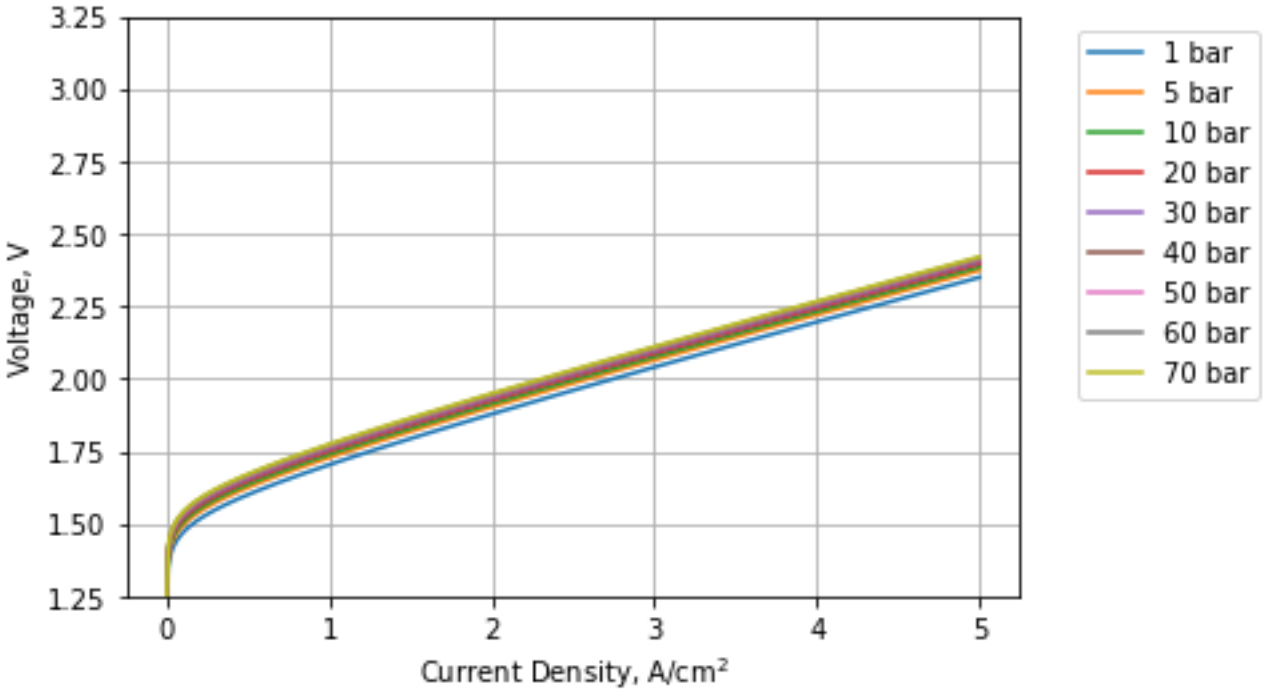

Figure 3.9: Electrolyzer voltage as a function of current density for different differential cathode pressures.

3.6.4 Anode Exchange Current Density Sensitivity

Exchange current density is determined by various factors such as material, morphology, catalyst, age, and operating conditions. There are ongoing efforts to optimize catalyst loadings and morphology (Bernt and Gasteiger 2016; Bernt, Siebel, and Gasteiger 2018; Weiß et al. 2019), an area that is particularly important for iridium due to its limited supply (Minke et al. 2021). The anode exchange current density sensitivity shown in Figure 3.10 is created by changing the reference exchange current density. It can be seen that the anode exchange current density shifts the polarization curve up and down in the y-direction. Furthermore, its effect can be seen across the entire range of current densities.

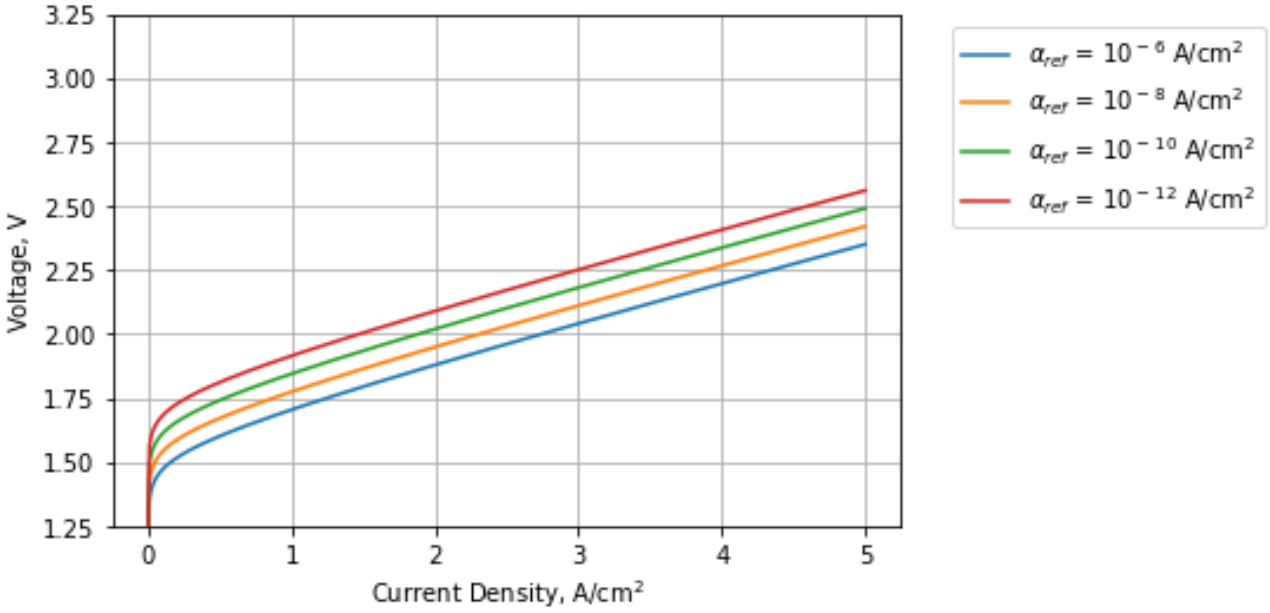

Figure 3.10: Electrolyzer voltage as a function of current density for different reference anode exchange current densities.

3.7 References

Abdin, Z., C.J. Webb, and E.MacA. Gray. 2015. "Modelling and Simulation of a Proton Exchange Membrane (PEM) Electrolyser Cell." *International Journal of Hydrogen Energy* 40 (39): 13243–57. https://doi.org/10.1016/j.ijhydene.2015.07.129.

Abdol Rahim, A.H., Alhassan Salami Tijani, S.K. Kamarudin, and S. Hanapi. 2016. "An Overview of Polymer Electrolyte Membrane Electrolyzer for Hydrogen Production: Modeling and Mass Transport." *Journal of Power Sources* 309 (March): 56–65. https://doi.org/10.1016/j.jpowsour.2016.01.012.

Awasthi, A., Keith Scott, and S. Basu. 2011. "Dynamic Modeling and Simulation of a Proton Exchange Membrane Electrolyzer for Hydrogen Production." *International Journal of Hydrogen Energy* 36 (22): 14779–86. https://doi.org/10.1016/j.ijhydene.2011.03.045.

Bernardi DM, Verbrugge MW. 1991. "Mathematical Model of a Gas Diffusion Electrode Bonded to a Polymer Electrolyte." *AIChE Journal* 37(8): 1151–63.

Bernt, Maximilian, and Hubert A. Gasteiger. 2016. "Influence of Ionomer Content in IrO_2 /TiO_2 Electrodes on PEM Water Electrolyzer Performance." *Journal of The Electrochemical Society* 163 (11): F3179–89. https://doi.org/10.1149/2.0231611jes.

Bernt, Maximilian, Armin Siebel, and Hubert A. Gasteiger. 2018. "Analysis of Voltage Losses in PEM Water Electrolyzers with Low Platinum Group Metal Loadings." *Journal of The Electrochemical Society* 165 (5): F305–14. https://doi.org/10.1149/2.0641805jes.

Bessarabov, Dimitri, and Pierre Millet. 2018. *PEM Water Electrolysis*. United Kingdom: Elsevier.

Biaku, C, N Dale, M Mann, H Salehfar, A Peters, and T Han. 2008. "A Semiempirical Study of the Temperature Dependence of the Anode Charge Transfer Coefficient of a 6kW PEM Electrolyzer." *International Journal of Hydrogen Energy* 33 (16): 4247–54. https://doi.org/10.1016/j.ijhydene.2008.06.006.

Buttler, Alexander, and Hartmut Spliethoff. 2018. "Current Status of Water Electrolysis for Energy Storage, Grid Balancing and Sector Coupling via Power-to-Gas and Power-to-Liquids: A Review." *Renewable and Sustainable Energy Reviews* 82 (February): 2440–54. https://doi.org/10.1016/j.rser.2017.09.003.

Carmo, Marcelo, David L. Fritz, Jürgen Mergel, and Detlef Stolten. 2013. "A Comprehensive Review on PEM Water Electrolysis." *International Journal of Hydrogen Energy* 38 (12): 4901–34. https://doi.org/10.1016/j.ijhydene.2013.01.151.

Choi, P. 2004. "A Simple Model for Solid Polymer Electrolyte (SPE) Water Electrolysis." *Solid State Ionics* 175 (1–4): 535–39. https://doi.org/10.1016/j.ssi.2004.01.076.

Coutanceau, Christophe, Stève Baranton, and Thomas Audichon. 2018. "Hydrogen Production From Water Electrolysis." In *Hydrogen Electrochemical Production*, 17–62. Elsevier. https://doi.org/10.1016/B978-0-12-811250-2.00003-0.

Dale, N.V., M.D. Mann, and H. Salehfar. 2008. "Semiempirical Model Based on Thermodynamic Principles for Determining 6kW Proton Exchange Membrane Electrolyzer Stack Characteristics." *Journal of Power Sources* 185 (2): 1348–53. https://doi.org/10.1016/j.jpowsour.2008.08.054.

Escobar-Yonoff, Rony, Daniel Maestre-Cambronel, Sebastián Charry, Adriana Rincón-Montenegro, and Ivan Portnoy. 2021. "Performance Assessment and Economic Perspectives of Integrated PEM Fuel Cell and PEM Electrolyzer for Electric Power Generation." *Heliyon* 7 (3): e06506. https://doi.org/10.1016/j.heliyon.2021.e06506.

Feng, Qi, Xiao−Zi Yuan, Gaoyang Liu, Bing Wei, Zhen Zhang, Hui Li, and Haijiang Wang. 2017. "A Review of Proton Exchange Membrane Water Electrolysis on Degradation Mechanisms and Mitigation Strategies." *Journal of Power Sources* 366 (October): 33–55. https://doi.org/10.1016/j.jpowsour.2017.09.006.

García-Valverde, R., N. Espinosa, and A. Urbina. 2012. "Simple PEM Water Electrolyser Model and Experimental Validation." *International Journal of Hydrogen Energy* 37 (2): 1927–38. https://doi.org/10.1016/j.ijhydene.2011.09.027.

Gorgun, H. 2006. "Dynamic Modelling of a Proton Exchange Membrane (PEM) Electrolyzer." *International Journal of Hydrogen Energy* 31 (1): 29–38. https://doi.org/10.1016/j.ijhydene.2005.04.001.

Hancke, Ragnhild, Thomas Holm, and Øystein Ulleberg. 2022. "The Case for High-Pressure PEM Water Electrolysis." *Energy Conversion and Management* 261 (June): 115642. https://doi.org/10.1016/j.enconman.2022.115642.

He, Zheng-Da, Jie Wei, Yan-Xia Chen, Elizabeth Santos, and Wolfgang Schmickler. 2017. "Hydrogen Evolution at Pt(111) – Activation Energy, Frequency Factor and Hydrogen Repulsion." *Electrochimica Acta* 255 (November): 391–95. https://doi.org/10.1016/j.electacta.2017.09.127.

IRENA. 2020. "Green Hydrogen Cost Reduction: Scaling up Electrolyzers to Meet the 1.5C Climate Goal." International Renewable Energy Agency, Abu Dhabi.

Lebbal, M.E., and S. Lecœuche. 2009. "Identification and Monitoring of a PEM Electrolyser Based on Dynamical Modelling." *International Journal of Hydrogen Energy* 34 (14): 5992–99. https://doi.org/10.1016/j.ijhydene.2009.02.003.

Liso, Vincenzo, Giorgio Savoia, Samuel Simon Araya, Giovanni Cinti, and Søren Knudsen Kær. 2018. "Modelling and Experimental Analysis of a Polymer Electrolyte Membrane Water Electrolysis Cell at Different Operating Temperatures." *Energies* 11 (12): 3273. https://doi.org/10.3390/en11123273.

Marangio, F, M Santarelli, and M Cali. 2009. "Theoretical Model and Experimental Analysis of a High Pressure PEM Water Electrolyser for Hydrogen Production." *International Journal of Hydrogen Energy* 34 (3): 1143–58. https://doi.org/10.1016/j.ijhydene.2008.11.083.

Millet, Pierre. 2015. "Chapter 2 Fundamentals of Water Electrolysis." In Hydrogen Production, edited by Agata Godula-Jopek, 33-61. Germany: Wiley-VCH.

Millet, Pierre. 2015. "Chapter 3 PEM Water Electrolysis." In Hydrogen Production, edited by Agata Godula-Jopek, 63-114. Germany: Wiley-VCH.

Minke, Christine, Michel Suermann, Boris Bensmann, and Richard Hanke-Rauschenbach. 2021. "Is Iridium Demand a Potential Bottleneck in the Realization of Large-Scale PEM Water Electrolysis?" *International Journal of Hydrogen Energy* 46 (46): 23581–90. https://doi.org/10.1016/j.ijhydene.2021.04.174.

Ni, Meng, Michael K.H. Leung, and Dennis Y.C. Leung. 2008. "Energy and Exergy Analysis of Hydrogen Production by a Proton Exchange Membrane (PEM) Electrolyzer Plant." *Energy Conversion and Management* 49 (10): 2748–56. https://doi.org/10.1016/j.enconman.2008.03.018.

Schalenbach, Maximilian, Marcelo Carmo, David L. Fritz, Jürgen Mergel, and Detlef Stolten. 2013. "Pressurized PEM Water Electrolysis: Efficiency and Gas Crossover." *International Journal of Hydrogen Energy* 38 (35): 14921–33. https://doi.org/10.1016/j.ijhydene.2013.09.013.

Springer, T. E., T. A. Zawodzinski, and S. Gottesfeld. 1991. "Polymer Electrolyte Fuel Cell Model." *Journal of The Electrochemical Society* 138 (8): 2334–42. https://doi.org/10.1149/1.2085971.

Suermann, Michel, Thomas J. Schmidt, and Felix N. Büchi. 2018. "Comparing the Kinetic Activation Energy of the Oxygen Evolution and Reduction Reactions." *Electrochimica Acta* 281 (August): 466–71. https://doi.org/10.1016/j.electacta.2018.05.150.

Weiß, A., A. Siebel, M. Bernt, T.-H. Shen, V. Tileli, and H. A. Gasteiger. 2019. "Impact of Intermittent Operation on Lifetime and Performance of a PEM Water Electrolyzer." *Journal of The Electrochemical Society* 166 (8): F487–97. https://doi.org/10.1149/2.0421908jes.

Yigit, Tevfik, and Omer Faruk Selamet. 2016. "Mathematical Modeling and Dynamic Simulink Simulation of High-Pressure PEM Electrolyzer System." *International Journal of Hydrogen Energy* 41 (32): 13901–14. https://doi.org/10.1016/j.ijhydene.2016.06.022.

Chapter 4
Steady Operations

Commercial electrolyzer systems consist of three primary components: 1) Electrolyzer Stack, 2) Mechanical Balance of Plant (mBoP), and 3) Electrical Balance of Plant (eBoP), as shown in Figure 4.1 (Peterson, Vickers, and DeSantis 2019; Briguglio et al. 2010). An electrolyzer stack consists of several cells put together in series as illustrated in Figure 2.5.

The mechanical BoP (mBoP) consists of subsystems that perform secondary functions to support the electrolyzer stack (Mayyas et al. 2019). First, there is the water management subsystem. Because membrane degradation mechanisms such as membrane thinning, ion exchange site blocking, and permeability loss, are caused by metallic ion content in the feedwater (Feng et al. 2017), a charcoal bed filter and deionizer are used to purify the feed water. The water pump delivers and circulates water throughout the system. The knockout (KO) pots with condensers separate gas phases (oxygen and hydrogen) from the water. Finally, the temperature swing adsorption (TSA) process removes any remaining water content from the hydrogen stream (Sadighi et al. 2016). Second, the temperature regulation subsystem controls the temperature of the electrolyzer. During electrolyzer operations, about 20% of the input power is converted to heat and the electrolyzer needs to be cooled in order to maintain a constant operating temperature (Tiktak, 2019). Cooling is typically achieved by flowing excess water through the stack and/or running a separate cooling fluid around the system (Rashidi et al. 2022).

The electrical BoP (eBoP) is the power supply system and consists of an AC transformer to change the voltage of the AC power supply from the grid and a rectifier to convert the AC current to a DC current.

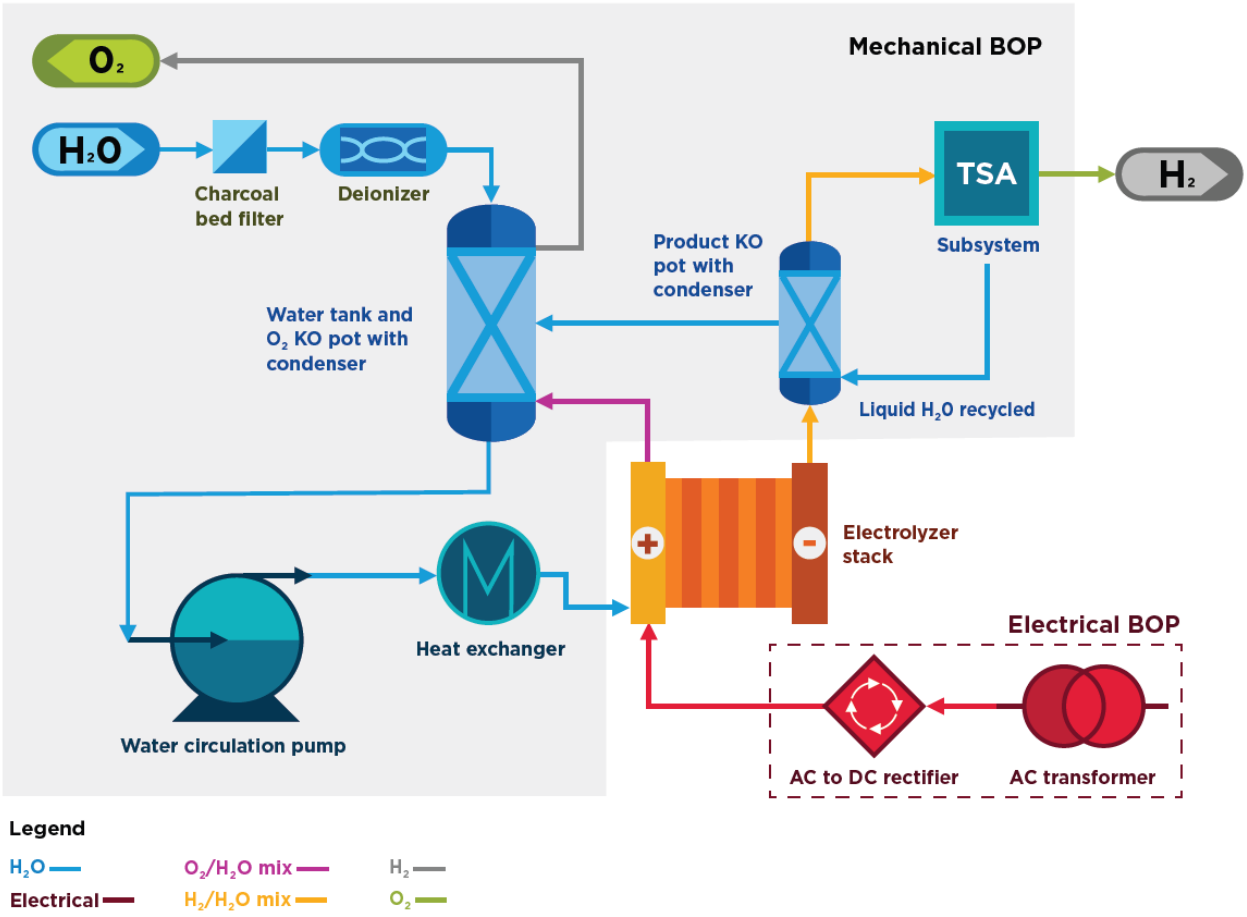

Figure 4.1: Schematic of the PEM electrolysis system showing the electrolyzer stack, mechanical balance of plant, and electrical balance of plant. Adapted from (Peterson, Vickers, and DeSantis 2020).

When constant, continuous power is supplied to an electrolyzer, it produces a steady flow of hydrogen. This operational mode is referred to as *steady operations*. In this case, the electrolyzer operates at a nominal current density that leads to optimal cell performance.

This chapter builds the techno-economic model that combines the electrolyzer model from Chapter 3 and a discounted cost model to explore the economic prospective of operating an electrolyzer system in a steady operations mode.

4.1 Techno-Economic Model of the Electrolyzer System

Using the system described in Figure 4.1 as the archetypical configuration of a PEM hydrogen production system, a cost model was developed to complement the physics-based model developed in Chapter 3. Together, they form a techno-economic model which is used to evaluate the changes in the costs and performance of a PEM electrolyzer system. In this model, the DOE's H2A framework was extensively used to calculate the system's capital costs, replacement costs, fixed operating costs, and variable operating costs (James et al. 2013).

All the cost factors used for direct capital calculations in this model are obtained from the current central H2A model (James et al. 2013), adjusted with the Chemical Engineering Plant Cost Index (CEPCI). In addition, all the dollar values are adjusted with the Consumer Price Deflator (U.S. Bureau of Economic Analysis) to price the costs in 2021 dollars. Finally, all the hourly labor rates were updated with the Labor Index from the U.S. Bureau of Labor Statistics.

4.1.1 Capital Cost

The total capital expenditure (CAPEX) is the sum of the depreciable capital cost and the non-depreciable capital cost:

$$C_{CAPEX} = CAPEX_{total} = CAPEX_{depreciable} + CAPEX_{non-depreciable}$$

Eq. 4.1

The depreciable capital cost covers the direct capital cost, site preparation cost, engineering cost, contingency cost, and permitting cost:

$$CAPEX_{depreciable} = \text{Direct Capital} + \text{Site Preparation Cost} + \text{Engineering Cost} + \text{Contingency Cost} + \text{Permitting Cost}$$

Eq. 4.2

Direct capital cost covers the equipment purchases for the electrolyzer stack, mechanical BoP, and electrical BoP:

$$\text{Direct Capital} = \text{Stack Cost} + \text{mBoP Cost} + \text{eBoP Cost}$$

Eq. 4.3

The stack cost is proportionally scaled based on the total active area of the electrolyzer, which is the number of cells multiplied by the area of a unit cell:

$$\text{Active Area} = \text{Unit Cell Area} \times \text{Number of Cells}$$

Eq. 4.4

$$\text{Stack Cost} = \text{Stack System Cost Factor} \times \text{Active Area} \times \text{Installation Cost Factor}$$

Eq. 4.5

The stack system cost factor is an aggregated cost of an electrolyzer stack system per unit area. Based on the current central H2A model, the stack system cost factor is \$2.00/cm^2 (James et al. 2013). The installation cost factor is a multiplier used to cover the costs associated with installation and is assumed to be 1.2 (James et al. 2013).

In order to estimate the costs of mBoP and eBoP, we first need to estimate the plant's daily hydrogen production rate. Since the active area of the electrolyzer is known, the total current consumed by the system can be calculated as:

$$\text{Total Current } (i) = \text{Current Density (j)} \times \text{Active Area (A)}$$

Eq. 4.6

The production of hydrogen is proportional to the amount of current that is flowing through the electrolyzer to power the electrolysis reaction:

$$\dot{M}_{H_2} = \frac{i}{2F} \qquad \text{Eq. 4.7}$$

This molar production rate, $\dot{M}_{H_2}$, is converted to the mass production rate by:

$$\dot{m}_{H_2} = \dot{M}_{H_2} \times \frac{3600\ s}{hr} \times \frac{24\ hr}{day} \times \frac{1\ kg}{1000\ g} \times \frac{2.02\ g}{mole} \qquad \text{Eq. 4.8}$$

The daily production rate is used to size the mBoP and eBoP and therefore determine the costs of mBoP and eBoP. The cost of mBoP can be calculated by:

$$\text{mBoP Cost} = \text{mBoP Cost Factor} \times \text{Daily } H_2\ Production \qquad \text{Eq. 4.9}$$

Similar to the stack system cost factor, the mBoP cost factor is an aggregated cost per unit production. In the current central H2A model, the mBoP cost factor is \$117/kg H_2 per day (James et al. 2013).

While the mBoP depends on the hydrogen production rate alone, the cost of the eBoP is also dependent on the peak power of the electrolyzer. The peak power is defined as:

$$\text{Peak Power (in kW)} = \frac{V \times j \times ActiveArea}{1000}$$

Eq. 4.10

where j is the operating (nominal) current density and V is the corresponding voltage at j. This peak power rating is plugged into Eq. 4.11 to calculate the eBoP cost:

$$\text{eBoP cost} = \text{eBoP Cost Factor} \times \text{Peak Power} \times \text{Installation Cost Factor}$$

Eq. 4.11

The eBoP Cost Factor in the current central H2A model is \$126/kW and the installation cost factor is 1.2 (James et al. 2013). With this cost information, the direct capital cost can be calculated using Eq. 4.3.

The rest of the items under the depreciable cost category—site preparation cost, engineering cost, contingency cost, and permitting cost—are all some proportions of the direct capital cost:

$$\text{Site Preparation Cost} = \text{Site Preparation Cost Rate} \times \text{Direct Capital} \quad \text{Eq. 4.12}$$

$$\text{Engineering Cost} = \text{Engineering Cost Rate} \times \text{Direct Capital} \quad \text{Eq. 4.13}$$

$$\text{Contingency Cost} = \text{Contingency Cost Rate} \times \text{Direct Capital} \quad \text{Eq. 4.14}$$

$$\text{Permitting Cost} = \text{Permitting Cost Rate} \times \text{Direct Capital} \quad \text{Eq. 4.15}$$

For the current central H2A model, the site preparation cost rate is 2%, the engineering cost rate is 10%, the contingency cost rate is 15%, and the permitting cost rate is 15% (James et al. 2013).

The non-depreciable capital costs just comprise of the land cost:

$$\text{Land Cost} = \text{Cost of Land} \times \text{Area of Required Land} \quad \text{Eq. 4.16}$$

For the current central H2A model, the cost of land is $50,000/acre and the required area is 5 acres (James et al. 2013).

4.1.2 Pressure Correction Factor for Electrolyzer

The electrolyzer stack cost in the H2A model is based on a 300 psi (20.68 bar) operating pressure. In order to calculate the stack cost for any operating cathode pressure design, a modification factor needs to be incorporated. (Hancke, Holm, and Ulleberg 2022) calculated the cost of direct electrochemical compression and compared it with a hybrid compression system that combined direct electrochemical compression and mechanical compression, but they did not adjust the capital cost of the electrolyzer system while admitting that the cost would increase due to the higher-pressure ratings.

(Saba et al. 2018) reported an industry survey that showed that the specific investment costs of a pressurized alkaline electrolyzer system are ~34% higher than the specific investment costs of an ambient system. (Saba et al. 2018) also reported specific cost data for PEM electrolyzers—one ambient system and one pressurized system—from NEL, as shown in Figure 4.2.

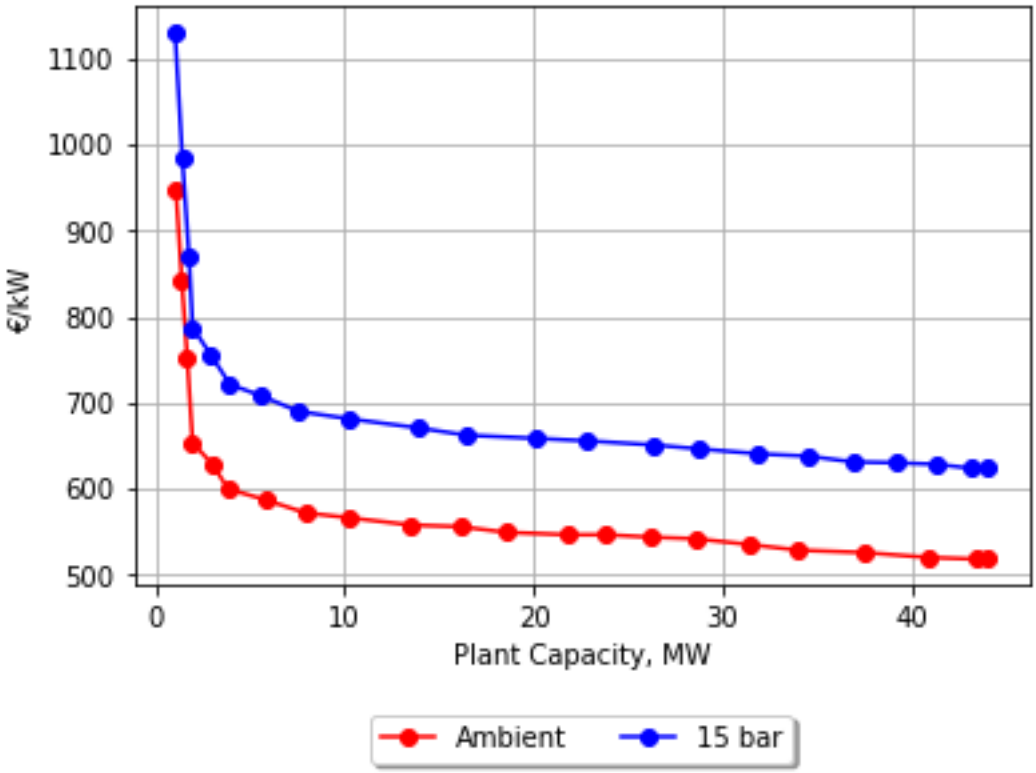

Figure 4.2: Specific costs of a 15-bar electrolyzer system (blue) and an ambient electrolyzer system (red) as a function of plant capacity. Adapted from (Saba et al. 2018).

Figure 4.2 shows that the 15-bar system is approximately 20% more expensive than the ambient system. Assuming that the correction factor increases linearly with operating pressure, a linear correction factor that passes through 1 at 1 bar and 1.2 at 15 bar is constructed, as shown with a red line in Figure 4.3.

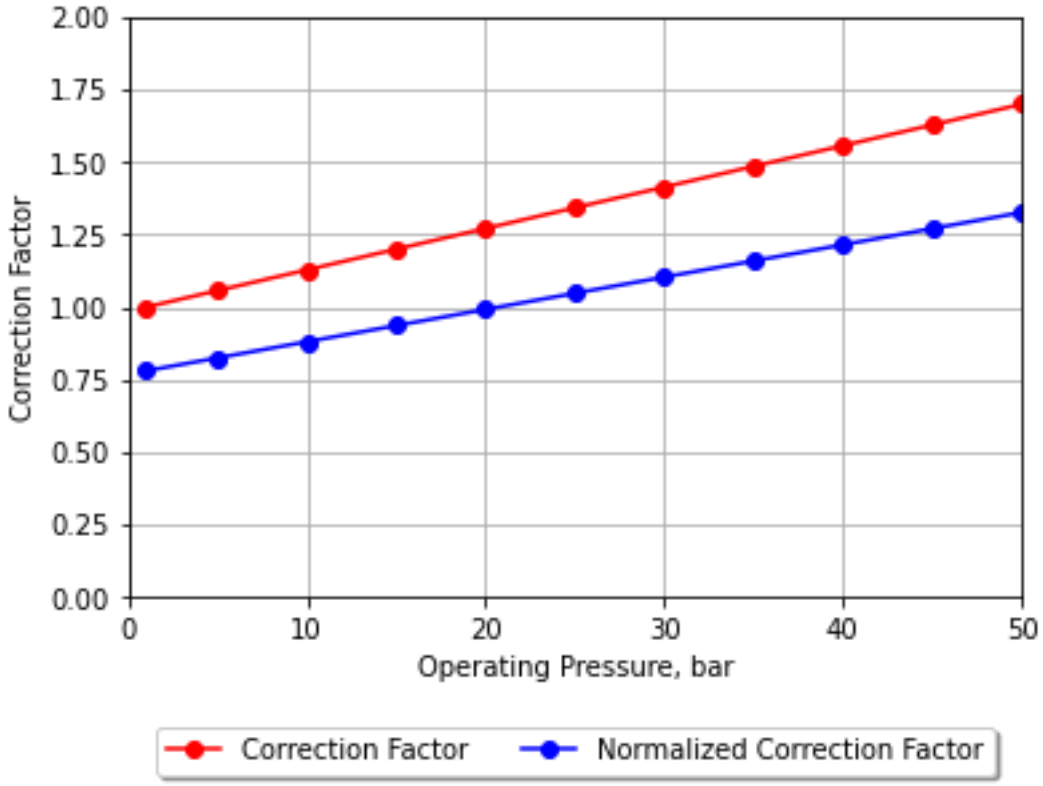

Figure 4.3: Original and normalized pressure correction factor as a function of operating pressure from 0 bar to 50 bar.

Since the electrolyzer cost model in this chapter is based on an operating pressure of 300 psi (20.68 bar), the pressure correction factor was normalized by diving each correction factor by the correction factor at 20.68 bar. The resulting normalized correction factor is shown with a blue line in Figure 4.3.

While some manufacturers have demonstrated that the electrolyzers can operate at a pressure up to several hundred bars (Grigoriev et al. 2011; Millet et al. 2009), most commercial electrolyzers as of 2022 have maximum delivery pressure limits of 4-80 bar (Buttler and Spliethoff 2018). This study will limit the analysis of the delivery pressure up to 30 bar.

4.1.3 Hydrogen Storage Capital Costs

In certain situations, a storage facility may be necessary to store the produced hydrogen for a later use. The storage device can be a pressure vessel, pipeline storage, or geological storage site. In this study, only pressure vessel tanks are considered. For simplicity, the CAPEX of storage vessels is expressed as:

$$CAPEX_{storage} = \text{Storage Cost Factor} \times \text{Hydrogen Weight at Capacity}$$

Eq. 4.17

where the Storage Cost Factor is the capital cost per kg of hydrogen stored and the Hydrogen Weight at Capacity is the maximum weight of hydrogen stored. In this study, a Storage Cost Factor of \$500/kg H_2 is used (Mallapragada et al. 2020) (Papadias and Ahluwalia 2021).

In steady operations, there is no need for a storage (unless storage is needed for the end-use itself) since the electrolyzer is supplying a steady stream of hydrogen to satisfy the presumed baseload demand. In dynamic operations, however, the ability to store excess hydrogen and dispense it at a later time is an important feature to reduce the overall cost.

4.1.4 Replacement Cost

Replacement costs for the electrolyzer system have two components: Planned replacement and unplanned replacement. Planned replacement occurs at each replacement interval and covers the net expense of stack replacement and other major components. Unplanned replacement cost is a yearly expense that is allocated for replacements of minor components and other repairs. Both planned and unplanned replacement costs are given as percentages of the direct capital cost:

$$C_{PR}(y) = \text{Planned Replacement Cost} = \text{Planned Replacement Rate} \times \text{Direct Capital} \; \forall \; \text{y} = 1 + \text{Ri}, \text{i} = 1,2,3, \ldots$$

Eq. 4.18

$$C_{UPR}(y) = \text{Unplanned Replacement Cost} = \text{Unplanned Replacement Rate} \times \text{Direct Capital}$$

Eq. 4.19

In the current central H2A model, the planned replacement rate is 15%, the replacement interval, R, is 10 years, and the unplanned replacement rate is 0.5% (James et al. 2013).

4.1.5 Fixed Operating Cost

Fixed operating cost accounts for the annual expenses that are required to operate the plant. These costs scale with the size of the plant and do not vary with different operating conditions. There are four components to the fixed operating cost. First, there is the labor cost:

$$\text{Labor Cost} = \text{Num of Staff} \times \text{Hourly Cost} \times 260 \times 8 \qquad \text{Eq. 4.20}$$

Based on the current central H2A model, the number of staffs required to operate the plant is assumed to be 10 and the average hourly cost $70 per hour. 260 is the number of working days in a year and 8 is the number of working hours per day (James et al. 2013).

The second component is the overhead cost. The overhead cost is proportional to the labor cost and is given by:

$$\text{Overhead Cost} = \text{Labor Cost} \times \text{OverheadRate} \qquad \text{Eq. 4.21}$$

In the current central H2A model, the overhead rate is 20% (James et al. 2013).

The third component is the tax and insurance costs. These costs scale with the total value of the plant, which can be approximated by the total CAPEX:

$$\text{Tax and Insurance Cost} = CAPEX_{total} \times \text{Tax and Insurance Rate} \qquad \text{Eq. 4.22}$$

In the current central H2A model, the tax and insurance rate is assumed to be 2%.

Finally, the fourth component is the material costs, which cover the expenses required to purchase different parts and materials to sustain operations:

$$\text{Material Cost} = \text{Direct Capital} \times \text{Material Cost Rate} \qquad \text{Eq. 4.23}$$

The Material Cost Rate in the current central H2A model is 3% of the direct capital (James et al. 2013).

The total annual fixed operating cost is the sum of the four components:

$$C_{fOPEX}(y) = \text{Fixed Operating Cost} = \text{Labor Cost} + \text{Overhead Cost} + \text{Tax and Insurance Cost} + \text{Material Cost} \qquad \text{Eq. 4.24}$$

4.1.6 Variable Operating Cost

Variable operating cost scales with the activity of plant operations. The higher the plant utilization rate, the higher the variable operating cost. The two components of the variable operating cost are electricity cost and water cost:

$$\text{Variable Operating Cost} = \text{Electricity Cost} + \text{Water Cost} \qquad \text{Eq. 4.25}$$

The electricity and water costs are calculated on an hourly basis and aggregated to daily and annual costs. Given hourly prices of electricity and the power curve of the electrolyzer, the hourly electricity cost can be calculated as follows:

$$C_{elec}^{hourly}(\text{t}) = P_{elec}(t) \times Power_{op}(t) + P_{elec}(t) \times U_{elec}^{hourly} \times \dot{m}_{H_2}^{hourly} \qquad \text{Eq. 4.26}$$

where $C_{elec}^{hourly}(\text{t})$ is the hourly electricity cost, $P_{elec}(t)$ the hourly electricity price, $Power_{op}(t)$ the hourly operating power, U_{elec}^{hourly} the BoP Electricity Usage, and $\dot{m}_{H_2}^{hourly}$ the hourly hydrogen production for each hour t. In the current central H2A model, U_{elec}^{hourly} is

assumed to be 5.1 kWh/kg H_2 (James et al. 2013).

As described in Chapter 3, the polarization curve expresses the relationship between operating voltage and operating current density. Then, the corresponding power at any given current density can be calculated by:

$$\text{Power(j)} = \text{V(j)} \times \text{j} \times \text{Active Area} \qquad \text{Eq. 4.27}$$

Furthermore, the hourly hydrogen production mass rate is given by:

$$\frac{i}{2F} \times \frac{3600\ s}{hr} \times \frac{1\ kg}{1000\ g} \times \frac{2.02\ g}{mole} \qquad \text{Eq. 4.28}$$

Figure 4.4 shows the polarization curve in the top panel, the power curve in the middle panel, and the hourly hydrogen production curve in the bottom panel. For an operating current density of 2 A/cm^2, the electrolyzer voltage is 1.88 V, the power consumption is 104 MW, and the hydrogen production is 2,083 kg for each hour. It can also be observed that while the hydrogen production increases linearly with increasing current density, the operating power increases quadratically with increasing current density. This means that incrementally more power is required to increase the hydrogen production by applying a higher current density. Therefore, while operating at a higher current density reduces CAPEX by utilizing more of the given electrolyzer, it increases OPEX due to higher power consumptions, thereby setting up a trade-off between CAPEX and OPEX (Ginsberg et al. 2022).

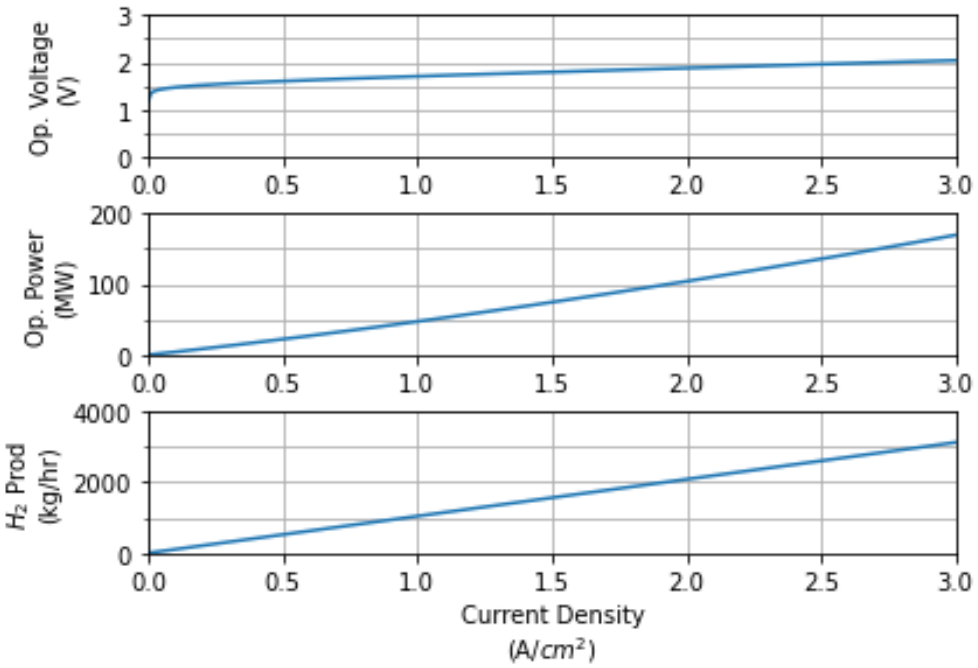

Figure 4.4: (Top) Operating Voltage as a function of Current Density, (Middle) Operating Power Density as a function of Current Density, (Bottom) Hydrogen Production as a function of Current Density.

The hourly cost can be aggregated to the daily and annual costs.

$$C_{elec}^{daily}(\mathrm{d}) = \sum_{t=24d}^{24(d+1)-1} C_{elec}^{hourly}(\mathrm{t}) \;\; \forall\, d = 0,1,2,\ldots,364$$

Eq. 4.29

$$C_{elec}^{annual}(\mathrm{y}) = \sum_{d=0}^{364} C_{elec}^{daily}(\mathrm{d})$$

Eq. 4.30

Similarly, the water cost is calculated on an hourly basis based on the hourly electricity price and the amount of hydrogen production:

$$C_{water}^{hourly}(\mathrm{t}) = P_{water} \times U_{water}^{hourly} \times \dot{m}_{H_2}^{hourly}(t) \qquad \text{Eq. 4.31}$$

where $C_{water}^{hourly}(\mathrm{t})$ is the hourly water cost, P_{water} is the water price per gallon, U_{elec}^{hourly} is the system water usage, and $\dot{m}_{H_2}^{hourly}(t)$ is the hourly hydrogen production for each hour t.

Based on the current central H2A model, P_{water} is assumed to be \$0.00265/gallon, and U_{water}^{hourly} is assumed to be 3.78 gallons per kg of hydrogen produced (James et al. 2013).

The hourly water cost can be aggregated at daily and annual costs:

$$C_{water}^{daily}(\mathrm{d}) = \sum_{t=24d}^{24(d+1)-1} C_{water}^{hourly}(\mathrm{t}) \;\; \forall\, d = 0,1,2,\dots,364$$

Eq. 4.32

$$C_{water}^{annual}(\mathrm{y}) = \sum_{d=0}^{364} C_{water}^{daily}(\mathrm{d})$$

Eq. 4.33

Therefore, the total variable operating cost is:

$$C_{vOPEX}(\mathrm{y}) = C_{elec}^{annual}(\mathrm{y}) + C_{water}^{annual}(\mathrm{y})$$

Eq. 4.34

4.1.7 Summary of Electrolyzer Cost Model Parameters

Table 4.1 summarizes the parameters used for the electrolyzer techno-economic model.

Table 4.1: Summary of Electrolyzer Cost Model Parameters

Cost Category	Value	Units
Stack Capital Cost (Uninstalled)	2	\$/cm
mBoP Capital Cost (Uninstalled)	117	\$/kg H2
eBoP Capital Cost(Uninstalled)	126	\$/kW
Site Preparation Cost	2%	of Direct Capital
Engineering Cost	10%	of Direct Capital
Contingency Cost	15%	of Direct Capital
Permitting Cost	15%	of Direct Capital
Storage Cost	\$500	kg/H2
Planned Replacement Cost	15%	of Direct Capital
Unplanned Replacement Cost	0.50%	of Direct Capital
Overhead Cost	20%	of Labor Cost
Tax and Insurance Cost	2%	of Total Capital Cost
Material Cost	3%	of Direct Capital
BoP Electricity Usage	5%	kWh/kg H2
Water Usage	3.78	gallons/kg H2

4.1.8 Discounted Cash Flow Analysis and Levelized Cost of Hydrogen (LCOH)

The discounted cash flow calculates the total revenue (or cost) of a project in present value. To an investor, there are many different investment options that compete for the same capital. Only those projects whose return is higher than the majority of the options will be funded and allowed to proceed. As a result of these different investment opportunities, $100 today is more valuable than $100 in the future; if a particular project was not funded, another project would have been chosen and generated a profit that the investor can reap in the future.

In order to incorporate such time-dependent value of money, the discounted cash flow analysis is used to calculate the present value of the all the costs, both today and in the future, associated with the electrolysis plant. For the discounted cash flow analysis, the following assumptions are made:

- The project is built and all CAPEX incur in year 0.
- The plant starts to operate in year 1.
- The project lifetime is 40 years.
- The discount rate, d, stays the same throughout the project. The annual discount rate is assumed to be 8%.
- All costs increase at a constant inflation rate of π throughout the project. The annual inflation rate is assumed to be 1.9%.

Then, the present value of the total cost is calculated by:

$$PV(C_{Total}) = C_{CAPEX} + C_{storage} + \sum_{y=1}^{40}\left[\left(C_{PR}(y) + C_{UPR}(y) + C_{fOPEX}(y) + C_{vOPEX}(y)\right)\frac{(1+\pi)^y}{(1+d)^y}\right]$$

Eq. 4.35

where C_{CAPEX} is the total capital expenditure (Eq. 4.1), $C_{storage}$ is the cost of storage (Eq. 4.17), $C_{PR}(y)$ is the planned replacement cost (Eq. 4.18), $C_{UPR}(y)$ is the unplanned replacement cost (Eq. 4.19), $C_{fOPEX}(y)$ is the fixed operating cost (Eq. 4.24), and $C_{vOPEX}(y)$ is the variable operating cost (Eq. 4.34). Note that $C_{PR}(y)$ only incurs at a fixed replacement interval (every 10 years, for example) and is zero in other periods.

Similarly, the discounting principle can be applied to the production of hydrogen:

$$PV(M_{Total}) = \sum_{y=1}^{40} \frac{m_{H_2}(y)}{(1+d)^y}$$

Eq. 4.36

The discounted total cost and the discounted hydrogen production are used to calculate the LCOH, which is a measure of the overall cost of hydrogen over the lifetime of the production plant:

$$Levelized\ Cost\ of\ Hydrogen\ (LCOH) = \frac{Discounted\ Total\ Cost}{Discounted\ Hydrogen\ Production}$$

$$= \frac{PV(C_{Total})}{PV(M_{Total})}$$

Eq. 4.37

4.2 Techno-Economic Model of the Compression System

Depending on the end-use applications, hydrogen needs to be compressed to different pressures ranging from 20 bar to 700 bar, as shown in Figure 4.5. Pipeline transmission requires a pressure of 70-100 bar while a hydrogen charging station of fuel cell electric vehicles (FCEV) is dispensed at 500-700 bar (Khan et al. 2021; Chen 2010; IRENA 2020; Brandon and Kurban 2017). In this study, the target delivery pressure is set to 30 bar by assuming a collocated (i.e., no transmission considered) end-use case for the industrial feed/heat and power generation.

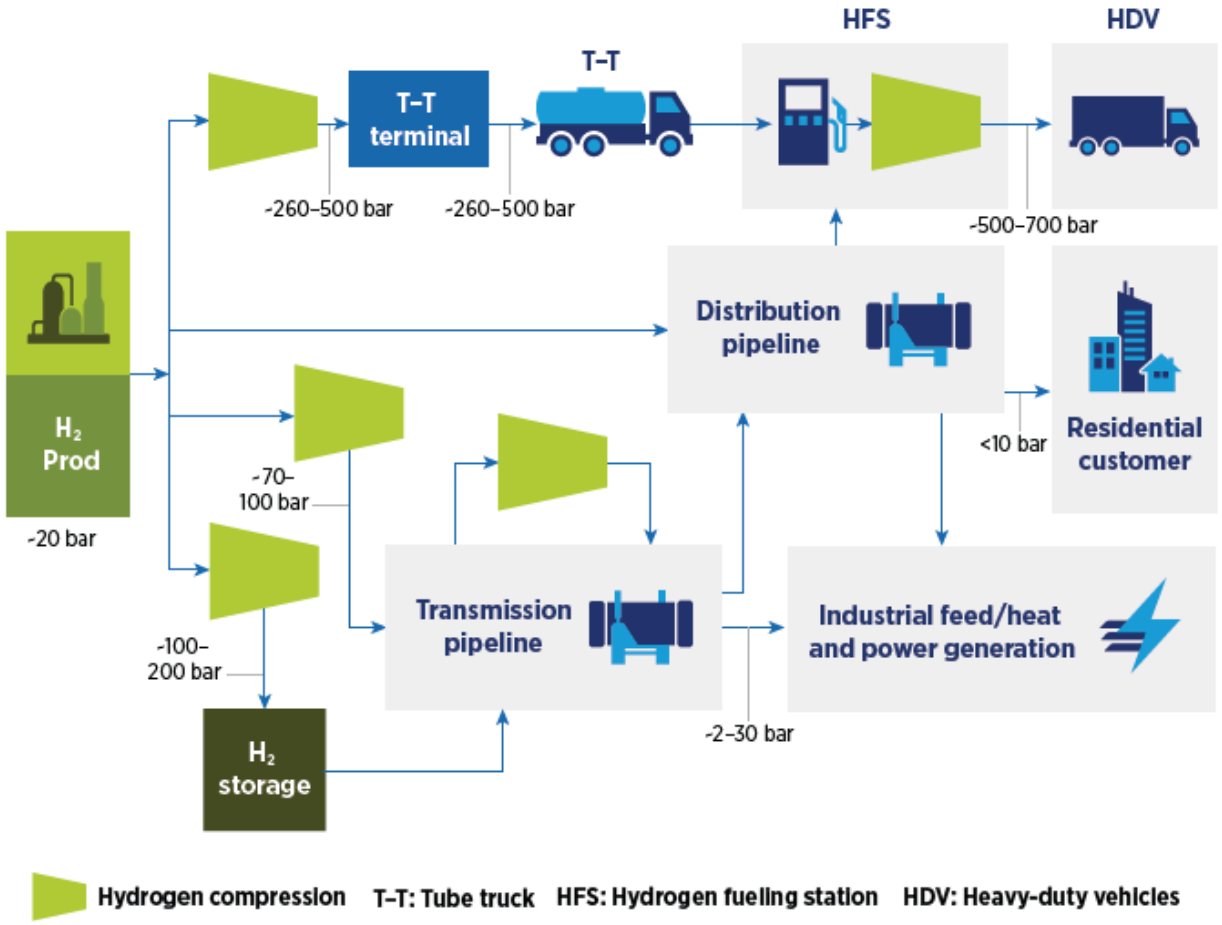

Figure 4.5: Hydrogen Delivery Pressure by Application. Adapted from (Khan et al. 2021).

There are three ways to meet the target delivery pressure. The first option is the direct electrochemical compression. In this mode, the electrolyzer is operated with a differential pressure by setting the cathode pressure to the delivery pressure. The second option is the mechanical compression. The electrolyzer can produce hydrogen at the ambient pressure and the produced hydrogen can be mechanically compressed to the target pressure. The third option is the hybrid of the two. The electrolyzer can deliver the hydrogen at a pressure less than the target pressure and the mechanical compressor can do the rest of the work to meet the target pressure.

Since the cost implications of differential pressure operations are already included in the electrolyzer model as well as the cost model, a techno-economic model for mechanical compression needs to be incorporated in order to evaluate the three compression alternatives.

4.2.1 Number of Compression Stages

In the case that the inlet pressure (or suction pressure) differs significantly from the outlet pressure (or discharge pressure), multiple compression stages are required to reach the target discharge pressure. The number of compression stages, N, required for high compression ratios (>2) is given by (Khan et al. 2021):

$$N = \frac{log\left(\frac{P_{disc}}{P_{suc}}\right)}{log(x)}$$

Eq. 4.38

where P_{disc} is the discharge pressure at the outlet of the compressor, P_{suc} is the suction pressure at the inlet of the compressor, and x is the compression ratio for each stage which is between 2.1 and 4.0. In this study, x is assumed to be 2.1.

4.2.2 Required Compression Power

Compression is typically modeled as a simple isentropic process and later corrected by an isentropic efficiency factor. For such an ideal multi-stage compression process, the power requirement is given by (Khan et al. 2021):

$$Power = N\left(\frac{k}{k-1}\right)\left(\frac{Z}{\eta_{isen}}\right)T_{suc}(q_M)R\left[\left(\frac{P_{disc}}{P_{suc}}\right)^{\left(\frac{k-1}{Nk}\right)} - 1\right]$$

Eq. 4.39

where k (1.41 for hydrogen) is the ratio of specific heat under constant pressure (C_p) to specific heat under constant volume (C_v), Z is the average compressibility factor, η_{isen} is the isentropic efficiency, T_{suc} is the suction temperature (usually ambient) at the inlet of the compressor, q_M is the molar flow rate, and R is the universal gas constant.

The rated power is calculated by dividing the actual compression power by the motor efficiency, which is assumed as 90% in this study (Khan et al. 2021).

$$\text{Rated Power} = \frac{Power}{Motor\ Efficiency}$$

Eq. 4.40

In order to calculate the compressibility factor Z, the average temperature and pressure inside the compression need to be computed. Typically, we know the inlet pressure (suction pressure), the outlet pressure (discharge pressure), and the inlet temperature (suction temperature). Based on the assumptions of an isentropic system, the outlet temperature (discharge temperature) can be calculated by (Khan et al. 2021):

$$T_{disc} = T_{suc}\left[1 + \frac{\left(\frac{P_{disc}}{P_{suc}}\right)^{\left(\frac{k-1}{Nk}\right)} - 1}{\eta_{isen}}\right]$$

Eq. 4.41

The average temperature is (Khan et al. 2021):

$$T_{average} = \frac{T_{suc} + T_{dis}}{2}$$

Eq. 4.42

The average pressure is given by the following equation (Khan et al. 2021):

$$P_{avg} = \frac{2}{3}\left(\frac{P_{disc}^3 - P_{suc}^3}{P_{disc}^2 - P_{suc}^2}\right)$$

Eq. 4.43

Finally, Z is evaluated as a function of the average temperature and pressure using the Redlick-Kwong equation of state.

η_{isen} accounts for the non-ideality that the compression process is not adiabatic and reversible and some of the work can go into increasing the internal energy or temperature of the system. η_{isen} for large reciprocating compressors range from 65 to 70% while η_{isen} for small reciprocating compressors range from 40 to 50% (Khan et al. 2021; Chen 2010). In this study, an η_{isen} of 65% is assumed (Parks et al. 2014).

4.2.3 Compression Cost Calculations

The uninstalled cost (UC) of a compressor scales with the rated power of the compressor. For a high-flow, moderate-compression system, the following scaling factor is applicable (Khan et al. 2021):

$$\text{UC} = 2695.03 \times Rated\ Power^{0.8335}$$

Eq. 4.44

The total installed cost (TIC) of a compressor is calculated by applying an installation factor (IF) to UC:

$$\text{TIC} = \text{UC} \times \text{IF}$$

Eq. 4.45

In this model, the installation factor is assumed to be 2 (Khan et al. 2021).

There are other indirect costs associated with the total capital investment (TCI) of a compressor. Site preparation, which is 5% of the TIC, covers the purchase of land and other auxiliary equipment. Engineering and design amounts to 10% of the TIC. Project contingency, which is allocated to deal with any unforeseen issues, takes another 10% of the TIC. Permitting to get the appropriate approvals and control equipment is 3% of the TIC (Chen 2010). Finally, the owner's cost, which account for the owners' engineering, debt origination, closure costs, and due diligence studies, takes 12% of the TIC (Chen 2010). Therefore, the TCI is calculated by adding all these indirect costs to the TIC:

$$\text{TCI} = \text{TIC} + \text{Indirect Costs} \quad \text{Eq. 4.46}$$

Next, the operating expenses of a hydrogen compressor are calculated. The electricity cost is based on the hourly hydrogen production rate and the corresponding rate power of the compressor:

$$\text{Electricity Cost(h)} = \text{Compressor Rate(h)} \times 1\text{hr} \times \text{ElectricityPrice(h)} \quad \text{Eq. 4.47}$$

The labor cost is the product of the labor hours and the hourly labor rate.

$$Labor\ Cost(\$/year) = Labor\ Hour\ (\#hours/year) \times Hourly\ Labor\ Rate\ (\$/hour)$$

Eq. 4.48

The required labor hour is given by (Khan et al. 2021):

$$Labor\ Hour = 288 \times \left(\frac{Daily\ Compressor\ Flow\ Rate}{100{,}000}\right)^{0.25} \quad \text{Eq. 4.49}$$

where $Daily\ Compressor\ Flow\ Rate$ is in kg/day. The average hourly labor rate for 2021 is $42.48/hour (Bureau of Labor Statistics- NAICS code# 2212).

The overhead cost are 50% of the labor cost (Khan et al. 2021):

$$Overhead = 50\% \times Labor\ Cost \quad \text{Eq. 4.50}$$

Insurance, Property Taxes, Licensing and Permits, and Operating/Maintenance/Repairs costs are given as (Khan et al. 2021; Chen 2010):

$$Insurance\ Cost = 1\% \times TCI \quad \text{Eq. 4.51}$$

$$Property\ Taxes\ Cost = 1\% \times TCI \quad \text{Eq. 4.52}$$

$$Licensing\ and\ Permits\ Cost = 0.1\% \times TCI \quad \text{Eq. 4.53}$$

$$Operating/Maintenance/Repairs\ Costs = 4\% \times TIC \quad \text{Eq. 4.54}$$

In addition, the lifetime of a compressor is 15 years. Therefore, the compressor needs to be replaced every 15 years. The replacement cost for the compressor is TIC adjusted for inflation.

4.2.4 Summary of Compressor Cost Model Parameters

Table 4.2 summarizes the parameters used for the compressor techno-economic model.

Table 4.2: Summary of Compressor Cost Model Parameters

Cost Category	Value	Units
Uninstalled Cost Factor	2695.03	-
Uninstalled Cost Exponent	0.8335	-
Installation Factor	2	
Site Preparation Cost	5%	of Total Installed Cost (TIC)
Engineering Cost	10%	of Total Installed Cost (TIC)
Contingency Cost	10%	of Total Installed Cost (TIC)
Permitting Cost	3%	of Total Installed Cost (TIC)
Owner's Cost	12%	of Total Installed Cost (TIC)
Overhead Cost	50%	of Labor Cost
Insurance Cost	1%	of Total Capital Investment (TCI)
Property Tax	1%	of Total Capital Investment (TCI)
Licensing and Permitting Cost	0.1%	of Total Capital Investment (TCI)
Operating/Maintenance/Repairs Cost	4%	of Total Capital Investment (TCI)

4.3 Techno-Economic Analysis of Steady Operations

4.3.1 Electricity Data

The hourly electricity price data used in this section come from locational marginal pricing (LMP) at LAFRESA_6_N007, which is located just north of Torrance, CA, as shown in Figure 4.6. LMP is a location-specific cost of producing incremental power from the generation system (Helman, Singh, and Sotkiewicz 2010) and serves as the wholesale price that is traded in the electricity market. Large-scale customers may be able to secure this wholesale price in their contract, but typically the end-users must pay additional transmission tariffs for transmission and distribution on top of the wholesale price.

The average electricity from this node in 2021 was $52/MWh. Figure 4.7 shows the historical electricity price on a typical summer day and typical winter day as well as for the whole year. The price fluctuates based on the season and time of the day. The typical summer day plot shows a peak in the afternoon while the typical winter day plot shows a steady profile. The fluctuations in the electricity price become an important consideration in the dynamic operations of the electrolyzer, as will be discussed in Chapter 5.

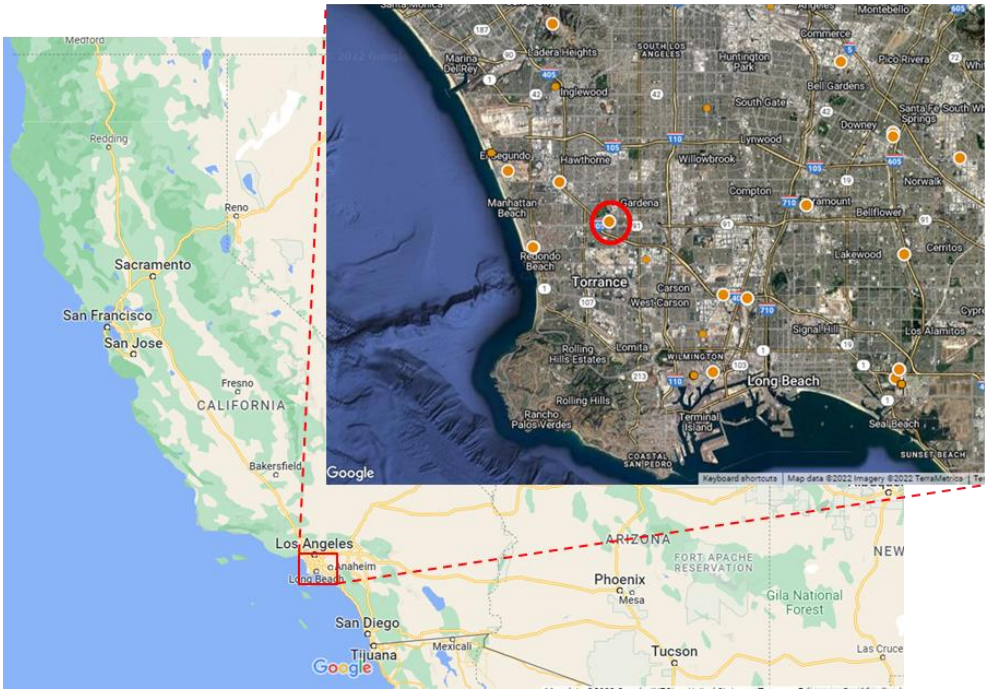

Figure 4.6: Location of LMP LAFRESA_6_N007. Maps from Google and CAISO.

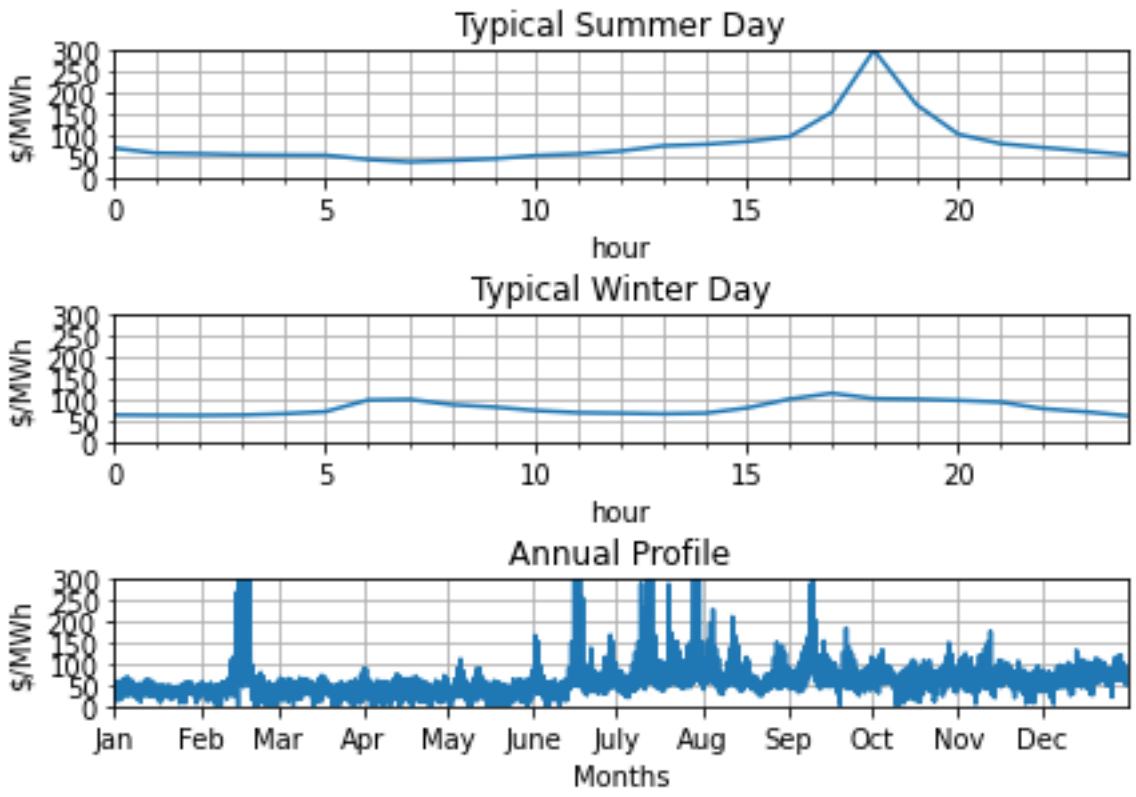

Figure 4.7: Hourly electricity price on a typical summer day (top), on a typical winter day (middle) and for the year (bottom) in 2021 at the node LAFRESA_6_N007 located in Torrance, CA.

4.3.2 Model Input

In order to build a representative electrolyzer system, the electrolyzer model was constructed with the parameters in Table 4.3. Instead of the thicker 254 μm membrane used in the experiment, the commercially popular Nafion 117 with a thickness of 178 μm is chosen in the simulation (IRENA 2020). The temperature is set to 80°C in order to increase the thermodynamic efficiency. However, the energy requirement to maintain the elevated temperature of the feedwater is not considered in this study. Finally, the cathode pressure is set to ambient pressure (1 bar).

The parameters for the electrolyzer techno-economic model are shown in Table 4.4. The nominal operating current density is set to 2 A/cm^2. The 104 MW electrolyzer plant produces 50 tons of hydrogen per day. Electrolyzers are commonly sized based on the energy input rather than the output. A brief note on why this approach is not a useful basis for comparison—unless the corresponding operating current density and efficiency are defined—is available in Appendix B: Calculations of Electrolyzer Size and Cost.

Table 4.3: Electrolyzer Model Parameters

Parameters	Values	Units
Membrane Thickness, t	178	μm
Cathode Exchange Current Density, $j_{0,cathode}$	2.3×10^{-3} (Calculated)	A/cm^2
Anode Exchange Current Density, $j_{0,anode}$	3.0×10^{-6} (Calculated)	A/cm^2
Temperature, T	80	°C
Cathode Pressure, P_{cat}	1	bar
Anode Pressure, P_{an}	1	bar

Table 4.4: Techno-Economic Model Parameters

Parameters	Values	Units
Production	50	Tonne/day
System Size	104	MW
Nominal Current Density	2	A/cm^2
Electrolyzer Lifetime	10	Years
Project Lifetime	40	Years
Stack Cost	2.0	\$/cm^2
mBoP Cost Factor	117	\$/kg H_2 per day
eBoP Cost Factor	126	\$/kW$_{electric}$
Uninstalled Capital Cost	715	\$/kW$_{input}$
Specific CAPEX	1,005	\$/kW$_{input}$
Electricity Cost in Torrance, CA	Variable (Average 52)	\$/MWh
Electrolyzer Electrical Usage	50	kW/kg H_2
BoP Electrical Usage	5.1	kW/kg H_2
Labor Cost	70	\$/hour
Target Delivery Pressure	30	Bar
Cathode Pressure	1	Bar
Temperature	80	°C

The parameters for the compression techno-economic model are shown in Table 4.5. The target delivery pressure is assumed to be 30 bar, requiring a compression ratio of 30. The parameters for the associated compression model are shown in Table 4.5.

Table 4.5: Compression Techno-Economic Model Parameters

Parameters	Values	Units	Source
Target Delivery Pressure	30	Bar	Assumed
Compression Ratio per Stage	2.1	-	(Khan et al. 2021; Chen 2010)
Motor Efficiency	90	%	(Khan et al. 2021; Chen 2010)
Isentropic Efficiency	65	%	(Parks et al. 2014)
Lifetime	15	Years	(Chen 2010)
Scale Factor	2695	-	(Khan et al. 2021)
Scale Exponent	0.8335	-	(Khan et al. 2021)
Number of Stages	5	-	Calculated
Number of Units	2	-	(Chen 2010)
Number of Backup Unit	1	-	(Chen 2010)
Specific CAPEX	1,974	$/kW	Calculated for 1 Compressor

4.3.3 Results from Steady Operations

Figure 4.8 and Figure 4.9 show the hourly electricity price, operating current density, and hydrogen production on a typical summer day and a typical winter day, respectively. Because the size of the electrolyzer is determined by the target production rate and the nominal operating current density, the electrolyzer operates at a constant 2 A/cm^2, producing 2.1 tonne of hydrogen per hour.

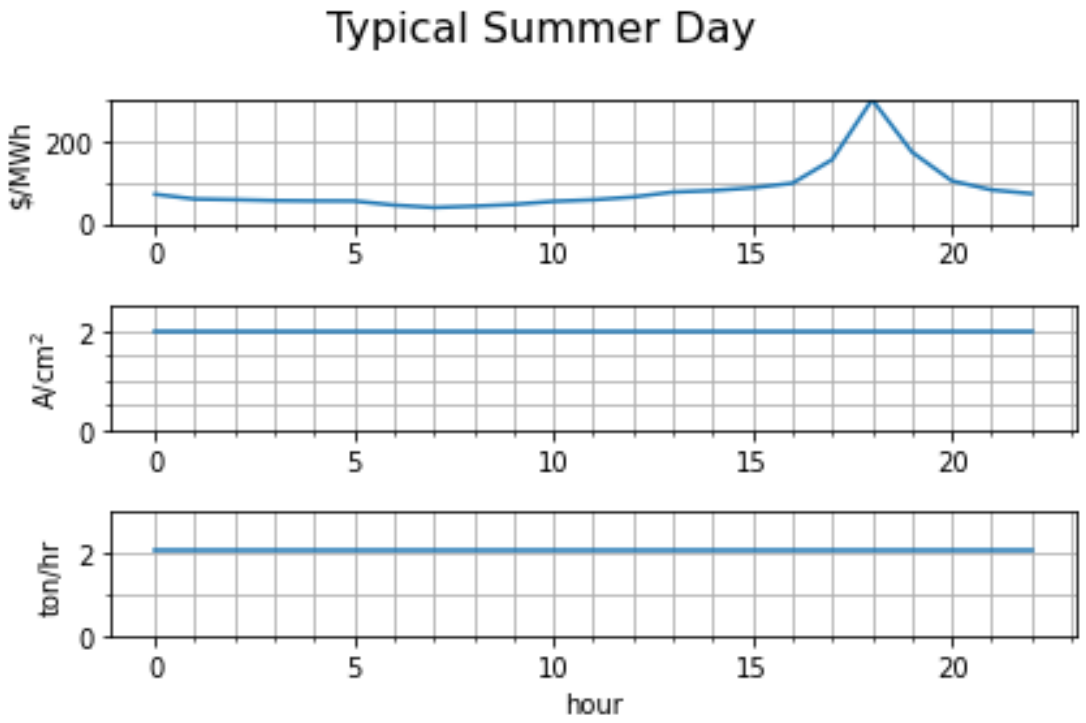

Figure 4.8: Hourly electricity price (top), operating current density (middle), and hydrogen production (bottom) on a typical summer day from steady-operations simulation.

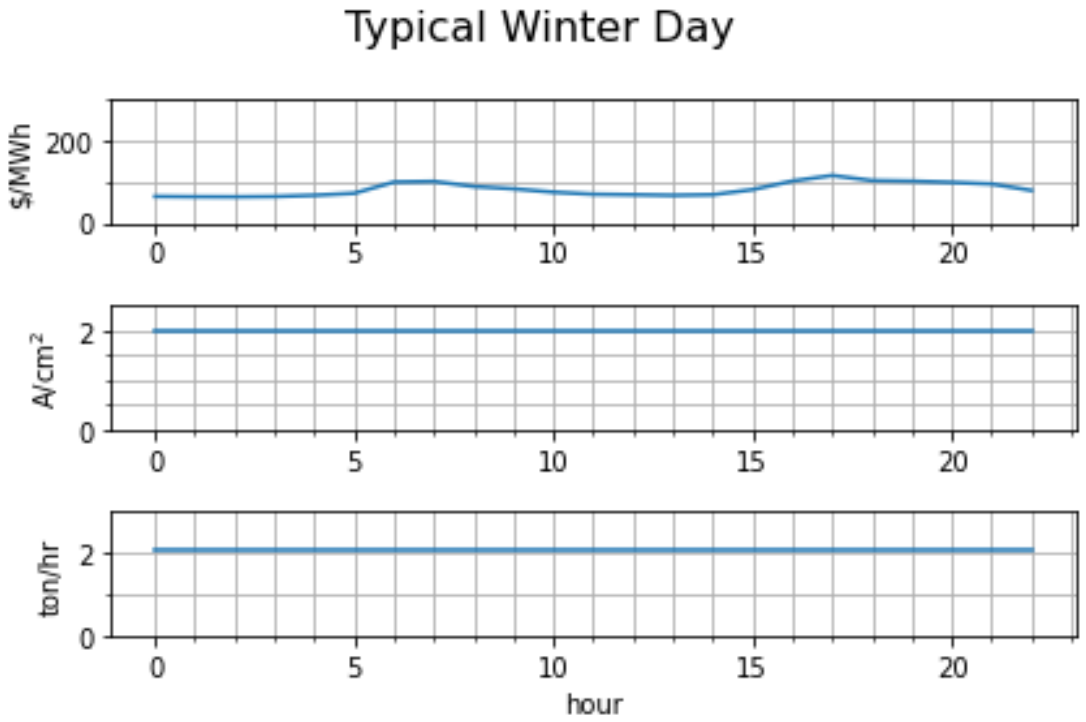

Figure 4.9: Hourly electricity price (top), operating current density (middle), and hydrogen production (bottom) on a typical winter day from steady-operations simulation.

Based on the discounted cash flow analysis, the LCOH for electrolysis and compression can be calculated. The total discounted costs for the electrolyzer over 40 years come out to be $1,003,978,753. Dividing this number by the discounted hydrogen production (217,627,087 kg H_2) gives an LCOH of $4.61/kg H_2, attributed to electrolysis alone (electrolysis LCOH).

After the electrolyzer produces hydrogen at 1 bar, the mechanical compression system further compresses it to 30 bar. The LCOH for compression can be calculated by dividing the total discounted costs of compression ($69,043,820) by the discounted hydrogen production from the electrolysis model (217,627,087 kg H_2). The calculated LCOH is $0.32/kg H_2 (compression LCOH). Therefore, the total cost of producing hydrogen (total LCOH) and delivering it at 30 bar is $4.93/kg H_2.

Comparison of LCOHs from electrolysis and compression shows that the electrolysis cost is 94% of the total costs, as shown in Figure 4.10. 74% of the total cost is attributed to the variable OPEX, the majority of which is the cost of electricity. Previous studies have also found the cost of electricity to contribute 65% to 71% of the total cost (Dutta, Block, and Port 1990; Orella et al. 2020). The oversized impact of variable OPEX means that any effort to decrease the electricity cost has potentially significant impact on the overall cost. This reduction can come from lower electricity price, more efficient electrolyzer that uses less power, or dynamic operations, which is the subject of Chapter 5.

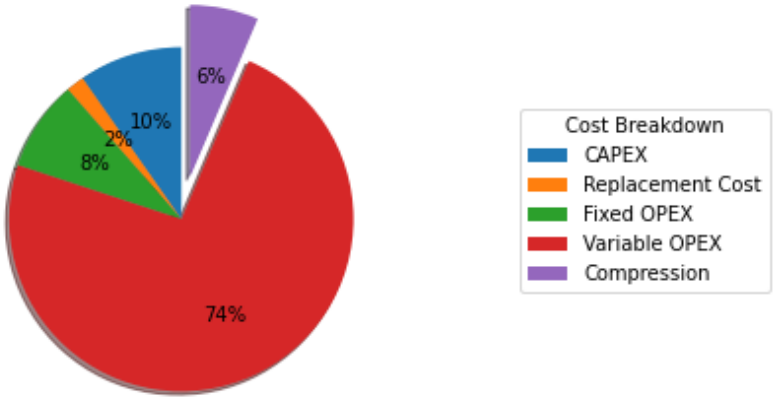

Figure 4.10: Contributions of different cost components to the total production and compression costs during steady operations.

4.3.4 Benchmarking with Previous Studies

Many studies have performed techno-economic analysis to come up with estimates of LCOH. Notably, (IRENA 2020) reports 2020 LCOH of \$4.86/kg H_2 based on the plant cost of \$770/kW, electricity price of \$53/MWh, and a discount rate of 10%. The LCOH of the DOE Current Central H2A model is \$4.83/kg H_2 based on the uninstalled plant cost of \$460/kW, electricity price of \$73.5/MWh, all in 2016 dollar. Table 4.6 summarizes the PEM electrolysis hydrogen costs from various studies.

Table 4.6: Summary of PEM electrolysis hydrogen production costs as reported in the literature. Table and data adapted from (El-Eman 2019).

Energy Source	Plant Capacity (tonne/day)	Electricity Cost ($/MWh)	H_2 Cost ($/kg)	Reference
Wind		60	9.37	Olateju 2016
Wind		60	8.27	Olateju 2016
Wind	1200	88	6.22	Choi 2005
Wind		71	5.27	Bertuccioli 2014
Onshore Wind		-	5.97	Saur and Ramdsen 2011
25% Solar + 75% Grid		98	6.35	Shaner 2016
Solar Thermal—Natural Gas		20	6.35	Boudries 2018
Solar PV		58	11.96	Choi 2005
Solar PV		-	12.6	Shaner 2016
Solar (SPT)		-	6.21	Kolb 2007
Nuclear (APWR)		-	5.46	El-Emam 2017b
Nuclear (APWR)		60	4.14	El-Emam 2017b
Nuclear (APWR)		89	3.56	El-Emam 2017b
Biomass		97	3.7	Choi 2005
Biogas		60	3.57	Agusoglu 2016
Grid		70	8.54	Choi 2005
Grid		20	6.29	Steward 2008

Table 4.6 shows that LCOH estimates can vary widely depending on the energy source, plant size, electricity cost, and other factors. The average of the presented database is \$6.70/kg H_2. The model LCOH of \$4.93/kg H_2 is closer to the H2A/IRENA estimates than the average value from the literature, which include some studies that may not reflect the latest cost information.

4.4 Sensitivities

4.4.1 Impact of Operating Current Density

In the first sensitivity case, the operating current density is varied from 0.5 to 4 A/cm^2 while the rest of the parameters are held constant as shown in Table 4.3 to Table 4.5. The resulting total LCOHs from these cases are illustrated in Figure 4.11. Because a constant stream of hydrogen is being produced and compressed at the same compression ratio, the compression LCOH stays constant. The electrolysis LCOH decreases as the nominal current density goes from 0.5 to 4 A/cm^2.

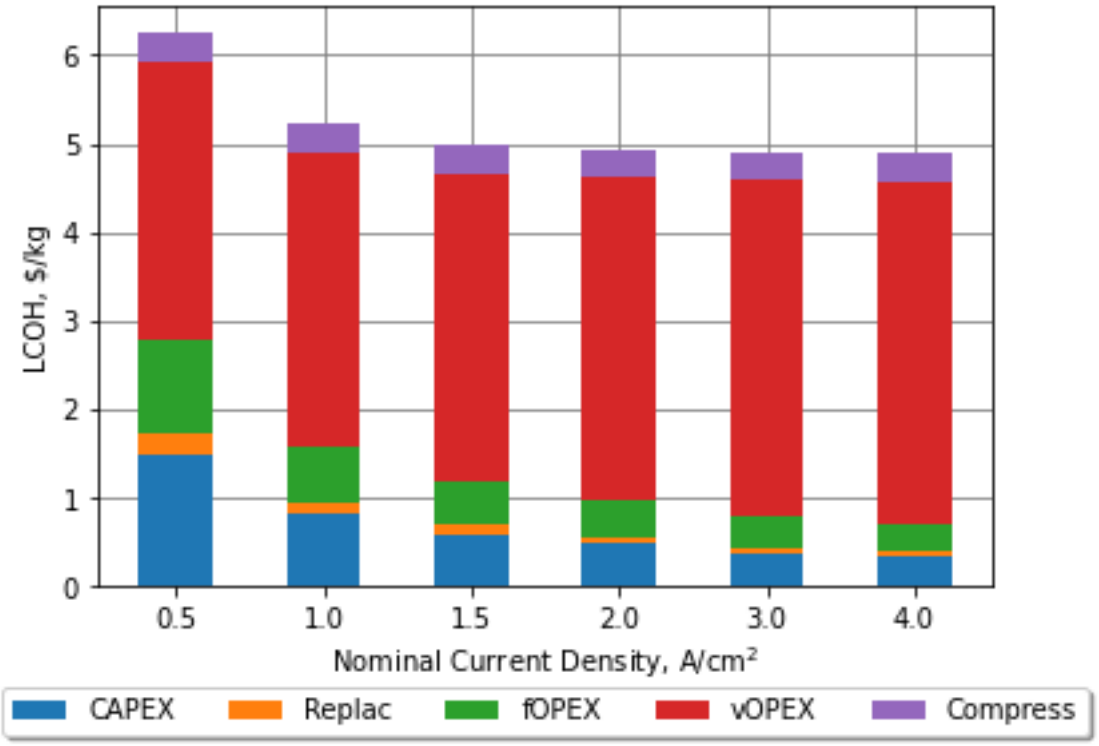

Figure 4.11: Bar charts of LCOH attributed to CAPEX, replacement cost, fixed OPEX, variable OPEX, and compression as a function nominal current density during steady operations.

As the nominal current density increases, CAPEX decreases because the same amount of hydrogen can be produced with a smaller electrolyzer. Replacement cost and fixed operating cost, which scale with CAPEX, exhibit the same declining trend. On the other

hand, variable OPEX increases with increasing nominal current density. Because the power consumption increases quadratically with current density, as previously shown in Figure 4.4, the increase in variable OPEX accelerates at higher current densities. Hence, the LCOH does not fall significantly beyond the current density of 1.5 A/cm^2. In light of this trend, it may be tempting to choose a high operating current density. However, it is important to consider that higher operating current densities cause accelerated degradation of the electrolyzer system, which have not been modeled in this study (Gago et al. 2018; Feng et al. 2017; Li, Araya, and Kær 2021; Weiß et al. 2019). As the limits of the electrolyzer are pushed towards operating at higher current densities, the incorporation of such degradation effects will be critical.

4.4.2 Impact of Cathode Operating Pressure

The next sensitivity study explores the benefits of differential pressure operations where the cathode side is pressurized while the anode side remains at the ambient pressure. Figure 4.12 shows the effect on LCOH. As the cathode pressure increases, the electrolysis LCOH increases in tandem, driven by the higher capital costs of the electrolyzer stack and the increased power consumptions at higher pressures. The initial decline in compression LCOH is very steep because it takes the most amount of energy to achieve compression at a lower pressure range. In this range, the reduction in the compression cost outweighs the increase in the electrolysis cost, resulting in a slight reduction in the total LCOH with the minimum at 5 bar. As the operating pressure continues to increase, the rate of decline in compression LCOH slows down and the incremental benefits of decreasing compression load are not enough to overcome the increase in the electrolysis cost.

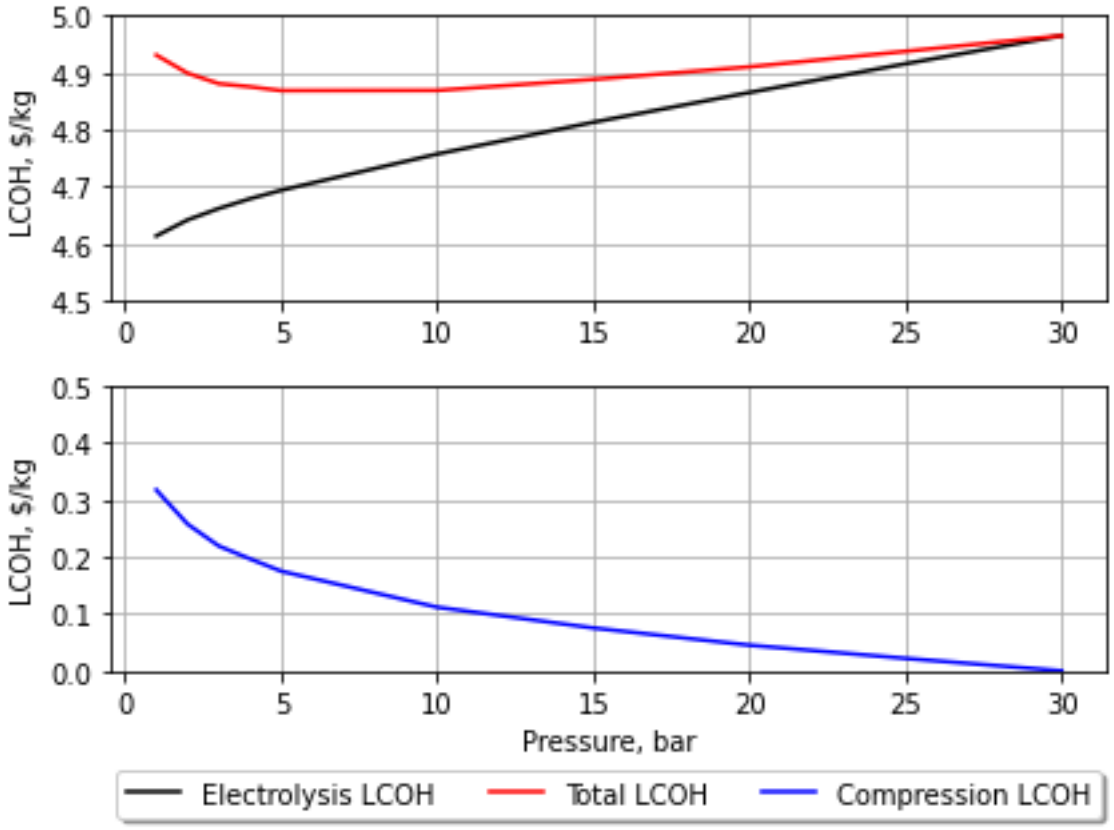

Figure 4.12: Electrolysis LCOH (black), Compression LCOH (blue), and Total LCOH (red) as a function of operating pressure.

These sensitivity results show that a hybrid approach of operating the electrolyzer at 5 bar and mechanically compressing the produced hydrogen to 30 bar gives the optimal economic result. As the costs of electrolyzer come down and the efficiencies improve, the economics of direct electrochemical compression may be more favorable, a hypothesis that will be tested in Chapter 6.

4.5 References

Brandon, N. P., and Z. Kurban. 2017. "Clean Energy and the Hydrogen Economy." *Philosophical Transactions of the Royal Society A: Mathematical, Physical and Engineering Sciences* 375 (2098): 20160400. https://doi.org/10.1098/rsta.2016.0400.

Briguglio, N., L. Andaloro, M. Ferraro, A. Di Blasi, G. Dispenza, F. Matteucci, L. Breedveld, and V. Antonucci. 2010. "Renewable Energy for Hydrogen Production and Sustainable Urban Mobility." *International Journal of Hydrogen Energy* 35 (18): 9996–10003. https://doi.org/10.1016/j.ijhydene.2009.09.065.

Buttler, Alexander, and Hartmut Spliethoff. 2018. "Current Status of Water Electrolysis for Energy Storage, Grid Balancing and Sector Coupling via Power-to-Gas and Power-to-Liquids: A Review." *Renewable and Sustainable Energy Reviews* 82 (February): 2440–54. https://doi.org/10.1016/j.rser.2017.09.003.

Chen, Tan-Ping. 2010. "Hydrogen Delivey Infrastructure Option Analysis". United States. https://doi.org/10.2172/982359. https://www.osti.gov/servlets/purl/982359.

Dutta, S, D Block, and R Port. 1990. "Economic Assessment of Advanced Electrolytic Hydrogen Production." *International Journal of Hydrogen Energy* 15 (6): 387–95. https://doi.org/10.1016/0360-3199(90)90195-5.

Feng, Qi, Xiao−Zi Yuan, Gaoyang Liu, Bing Wei, Zhen Zhang, Hui Li, and Haijiang Wang. 2017. "A Review of Proton Exchange Membrane Water Electrolysis on Degradation Mechanisms and Mitigation Strategies." *Journal of Power Sources* 366 (October): 33–55. https://doi.org/10.1016/j.jpowsour.2017.09.006.

Gago, Aldo Saul, Jörg Bürkle, Philipp Lettenmeier, Tobias Morawietz, Michael Handl, Renate Hiesgen, Fabian Burggraf, Pilar Angel Valles Beltran, and Kaspar Andreas Friedrich. 2018. "Degradation of Proton Exchange Membrane (PEM) Electrolysis: The Influence of Current Density." *ECS Transactions* 86 (13): 695–700. https://doi.org/10.1149/08613.0695ecst.

Ginsberg, Michael J., Maya Venkatraman, Daniel V. Esposito, and Vasilis M. Fthenakis. 2022. "Minimizing the Cost of Hydrogen Production through Dynamic Polymer Electrolyte Membrane Electrolyzer Operation." *Cell Reports Physical Science* 3 (6): 100935. https://doi.org/10.1016/j.xcrp.2022.100935.

Grigoriev, S.A., V.I. Porembskiy, S.V. Korobtsev, V.N. Fateev, F. Auprêtre, and P. Millet. 2011. "High-Pressure PEM Water Electrolysis and Corresponding Safety Issues." *International Journal of Hydrogen Energy* 36 (3): 2721–28. https://doi.org/10.1016/j.ijhydene.2010.03.058.

Hancke, Ragnhild, Thomas Holm, and Øystein Ulleberg. 2022. "The Case for High-Pressure PEM Water Electrolysis." *Energy Conversion and Management* 261 (June): 115642. https://doi.org/10.1016/j.enconman.2022.115642.

Helman, Udi, Harry Singh, Paul Sotkiewicz. 2010. "Chapter 19 – RTOs, Regional Electricity Markets, and Climate Policy." In *Generation Electricity in a Carbon-Constrained World*, edited by Fereidoon P. Sioshansi, 527-563. Academic Press. https://doi.org/10.1016/B978-1-85617-655-2.00019-5.

IRENA. 2020. "Green Hydrogen Cost Reduction: Scaling up Electrolyzers to Meet the 1.5C Climate Goal." International Renewable Energy Agency, Abu Dhabi.

James, Brian, and Strategic Analysis. n.d. "Hydrogen Pathways Analysis for Polymer Electrolyte Membrane (PEM) Electrolysis," 28.

James, Brian, Whitney Colella, Jennie Moton, G. Saur, and T. Ramsden. 2013. "PEM Electrolysis H2A Production Case Study Documentation." NREL/TP--5400-61387, 1214980. https://doi.org/10.2172/1214980.

Khan, Mohd Adnan, Cameron Young, Catherine MacKinnon, and David B Layzell. 2021. "The Techno-Economics of Hydrogen Compression" 1 (1): 49.

Li, Na, Samuel Simon Araya, and Søren Knudsen Kær. 2021. "Investigating Low and High Load Cycling Tests as Accelerated Stress Tests for Proton Exchange Membrane Water Electrolysis." *Electrochimica Acta* 370 (February): 137748. https://doi.org/10.1016/j.electacta.2021.137748.

Mallapragada, Dharik Sanchan, Emre Gençer, Patrick Insinger, David William Keith, and Francis Martin O'Sullivan. 2020. "Can Industrial-Scale Solar Hydrogen Supplied from Commodity Technologies Be Cost Competitive by 2030?" *Cell Reports Physical Science* 1 (9): 100174. https://doi.org/10.1016/j.xcrp.2020.100174.

Mayyas, Ahmad T, Mark F Ruth, Bryan S Pivovar, Guido Bender, and Keith B Wipke. 2019. "Manufacturing Cost Analysis for Proton Exchange Membrane Water Electrolyzers." NREL/TP-6A20-72740, 1557965. https://doi.org/10.2172/1557965.

Millet, Pierre, Diana Dragoe, Serguey Grigoriev, Vladimir Fateev, and Claude Etievant. 2009. "GenHyPEM: A Research Program on PEM Water Electrolysis Supported by the European Commission." *International Journal of Hydrogen Energy* 34 (11): 4974–82. https://doi.org/10.1016/j.ijhydene.2008.11.114.

Orella, Michael J., Steven M. Brown, McLain E. Leonard, Yuriy Román-Leshkov, and Fikile R. Brushett. 2020. "A General Technoeconomic Model for Evaluating Emerging Electrolytic Processes." *Energy Technology* 8 (11): 1900994. https://doi.org/10.1002/ente.201900994.

Papadias, D.D. and R.K. Ahluwalia. 2021. "Bulk storage of hydrogen." *International Journal of Hydrogen Energy* 46 (70): 34527-34541. https://doi.org/10.1016/j.ijhydene.2021.08.028.

Parks, G., R. Boyd, J. Cornish, and R. Remick. 2014. "Hydrogen Station Compression, Storage, and Dispensing Technical Status and Costs: Systems Integration." NREL/BK-6A10-58564, 1130621. https://doi.org/10.2172/1130621.

Peters, Max Stone, Klaus D. Timmerhaus, and Ronald E. West. 2003. *Plant Design and Economics for Chemical Engineers*. 5th ed. McGraw-Hill Chemical Engineering Series. New York: McGraw-Hill.

Peterson, D., Vickers, J., & Desantis, D. (2019). DOE Hydrogen and Fuel Cells Program Record: Hydrogen Production Cost from PEM Electrolysis.

Rashidi, Saman, Nader Karimi, Bengt Sunden, Kyung Chun Kim, Abdul Ghani Olabi, and Omid Mahian. 2022. "Progress and Challenges on the Thermal Management of Electrochemical Energy Conversion and Storage Technologies: Fuel Cells, Electrolysers, and Supercapacitors." *Progress in Energy and Combustion Science* 88 (January): 100966. https://doi.org/10.1016/j.pecs.2021.100966.

Saba, Sayed M., Martin Müller, Martin Robinius, and Detlef Stolten. 2018. "The Investment Costs of Electrolysis – A Comparison of Cost Studies from the Past 30 Years." *International Journal of Hydrogen Energy* 43 (3): 1209–23. https://doi.org/10.1016/j.ijhydene.2017.11.115.

Sadighi, Sepehr, Mahdi Asgari, Hossein Mohammadi, and Farshid Noorbakhsh. 2016. "INCREASING THE EFFICIENCY OF A TEMPERATURE SWING ADSORPTION (TSA) NATURAL GAS DEHYDRATION PLANT." *Petroleum and Coal*, 11.

Tiktak, W J. 2019. "Heat Management of PEM Electrolysis," M.S. Thesis, Delft University of Technology.

U.S. Bureau of Economic Analysis, Gross Domestic Product: Implicit Price Deflator [GDPDEF], retrieved from FRED, Federal Reserve Bank of St. Louis; https://fred.stlouisfed.org/series/GDPDEF, August 4, 2022.

U.S. Bureau of Labor Statistics, Average Hourly Earnings of Production and Nonsupervisory Employees, Chemicals, Not Seasonally Adjusted; https://data.bls.gov/timeseries/CEU3232500008?data_tool=Xgtable

Weiß, A., A. Siebel, M. Bernt, T.-H. Shen, V. Tileli, and H. A. Gasteiger. 2019. "Impact of Intermittent Operation on Lifetime and Performance of a PEM Water Electrolyzer." *Journal of The Electrochemical Society* 166 (8): F487–97. https://doi.org/10.1149/2.0421908jes.

Chapter 5
Dynamic Operations

One of the advantages of PEM electrolyzer systems is its ability to operate dynamically by responding quickly to load variations (El-Emam and Özcan 2019). PEM electrolyzers are capable of changing its operating voltage in less than one second and reaching cold startup within a few seconds (IRENA 2020). With such capabilities, PEM electrolyzers can potentially participate in the grid-balancing market by absorbing surplus electricity that cannot be readily consumed by the grid (Siracusano et al. 2020). In addition, utilizing cheap excess energy means that the production cost of hydrogen can be reduced. By changing the load dynamically in response to price fluctuations in the electricity market, the electrolyzer can reduce the electricity cost, which covers 74% of the total costs, as seen in Chapter 4. In such concept, the electrolyzers must be strategically oversized in order to produce excess amount of hydrogen when the energy prices are affordable. This also means that a storage facility would be required to store the excess hydrogen, especially if a steady rate of supply needs to be delivered to the customers, such as by contractual requirement. This chapter develops an optimization framework to model dynamic operations of PEM electrolyzers and evaluates its effect on LCOH.

5.1 Optimization Framework for Dynamic Operations

In order to explore the economic benefits of dynamic operations, an optimization framework is formulated with two objectives: 1) Find the plant capacity that is big enough to allow dynamic operations but not too big to overblow the capital costs; 2) Find the operating current densities that minimize the power usage and the total cost.

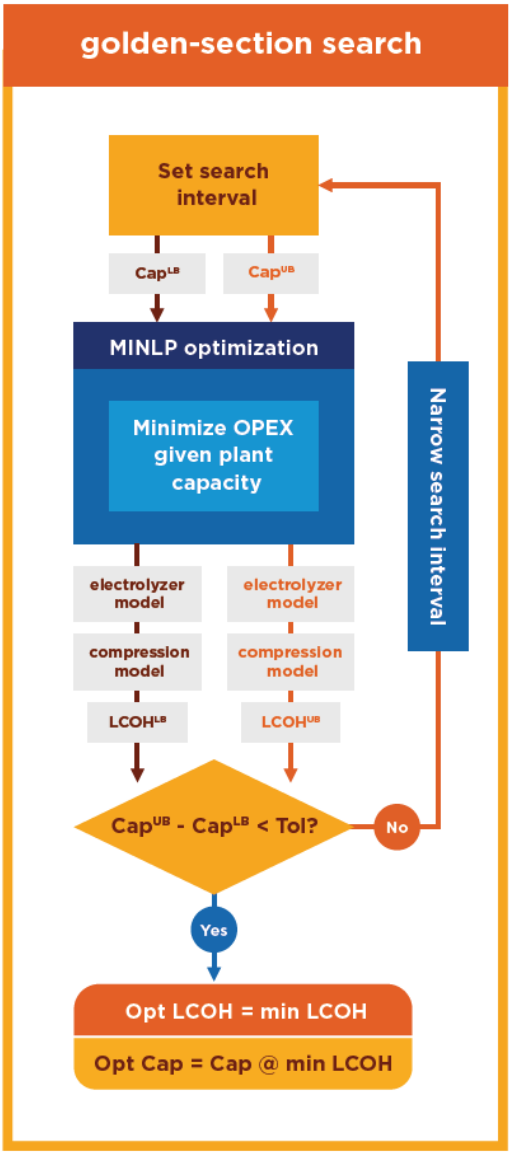

Figure 5.1: Diagram of the Optimization Framework. The outer-loop Golden-Section Search algorithm (the yellow frame) finds the plant production capacity (tonne/day) that results in the minimum LCOH between an upper bound (UB) and a lower bound (LB) defined by the user. The inner-loop Mixed Integer Non-Linear Programming (MINLP) (the blue box) finds the operating conditions that result in the minimum LCOH for a given plant capacity.

In order to achieve these objectives, the optimization framework utilizes two optimization algorithms, as shown in Figure 5.1. In the yellow outer-loop, a Golden-Section Search (GSS) algorithm chooses two plant capacities to test, based on the initial search interval. The plant capacities are sent to the blue inner-loop for evaluation. The blue inner-loop uses a Mixed-Integer Non-Linear Programming (MINLP) implemented with Gurobi optimizer to find the operating parameters that result in the minimum LCOH for a given plant capacity. Based on the LCOH values from the two plant capacities, a new search interval is set for the GSS algorithm. If the search interval is less than the desired tolerance level, then the algorithm terminates and the optimal capacity is set to be the minimum of all the search attempts. Otherwise, the GSS algorithm recursively carries on with the new search interval.

In the section below, detailed descriptions of each optimization model are provided. Since the MINLP algorithm is recursively used within the GSS algorithm, the MINLP algorithm will be described first followed by the GSS algorithm.

5.1.1 MINLP Algorithm to Optimize Operating Expense

The PEM techno-economic model described in Section 4 is formulated into an optimization problem. The problem is designed to find the operating current density and hydrogen storage size for a given electrolyzer plant size and a target production rate. Hence, the decision variables are as follows:

$$j_{op}(t) = [0, j_{max}] \quad \text{Eq. 5.1}$$

$$S_{max} \geq 0 \quad \text{Eq. 5.2}$$

The operating current density at time t, $j_{op}(t)$, has to be greater than 0 and less than or equal to the maximum current density allowed by design. The size of the hydrogen storage tank has to be greater than or equal to 0. The optimization algorithm chooses operating current density at each hour and storage size that minimize the present value of the total cost. Therefore, the objective function can be written as:

$$\text{minimize } PV(C_{Total}) =$$

$$minimize\ C_{CAPEX} + C_{storage} + \sum_{y=1}^{40}\left[\left(C_{PR} + C_{UPR} + C_{fOPEX} + C_{vOPEX}\right)\frac{(1+\pi)^y}{(1+d)^y}\right]$$

Eq. 5.3

In Eq. 5.3, C_{CAPEX} stays constant for a given electrolyzer size, which is already determined by the GSS algorithm, regardless of the operating current density or the storage size. $C_{storage}$ increases with the size of storage. The total replacement cost, which is the sum of $C_{PR}(y)$ and $C_{UPR}(y)$, is proportional to the direct capital cost, which stays constant for a given electrolyzer size. Finally, $C_{fOPEX}(y)$ comprises of labor cost, overhead cost, tax and insurance cost, and material cost. Labor and overhead costs are fixed for each calendar year. Tax and insurance cost is proportional to C_{CAPEX}. Material cost is proportional to the direct capital cost. As a result, $C_{fOPEX}(y)$ does not change as a function of the decision variables. Therefore, Eq. 5.3 can be simplified as:

$$minimize\ C_{storage} + \sum_{y=1}^{40}\left[C_{vOPEX}\frac{(1+\pi)^y}{(1+d)^y}\right]$$

Eq. 5.4

where

$$C_{storage} = Unit\ Cost\ Factor \times Hydrogen\ Weight\ at\ Capacity$$

Eq. 5.5

$$C_{vOPEX} = \sum_{d=0}^{364}\sum_{t=24d}^{24(d+1)-1} P_{elec}(t) \times Power_{op}\left(j_{op}(t)\right) + P_{elec}(t) \times U_{elec}^{hourly} \times \dot{m}_{H_2,prod}^{hourly}(t) + P_{water} \times U_{water}^{hourly} \times \dot{m}_{H_2,prod}^{hourly}(t)$$

Eq. 5.6

The operating power, $Power_{op}(t)$, is a non-linear function of the operating current density,

$j_{op}(t)$. For implementation in the Gurobi solver, the non-linear power function is linearized with five piecewise linear functions as shown in Figure 5.2.

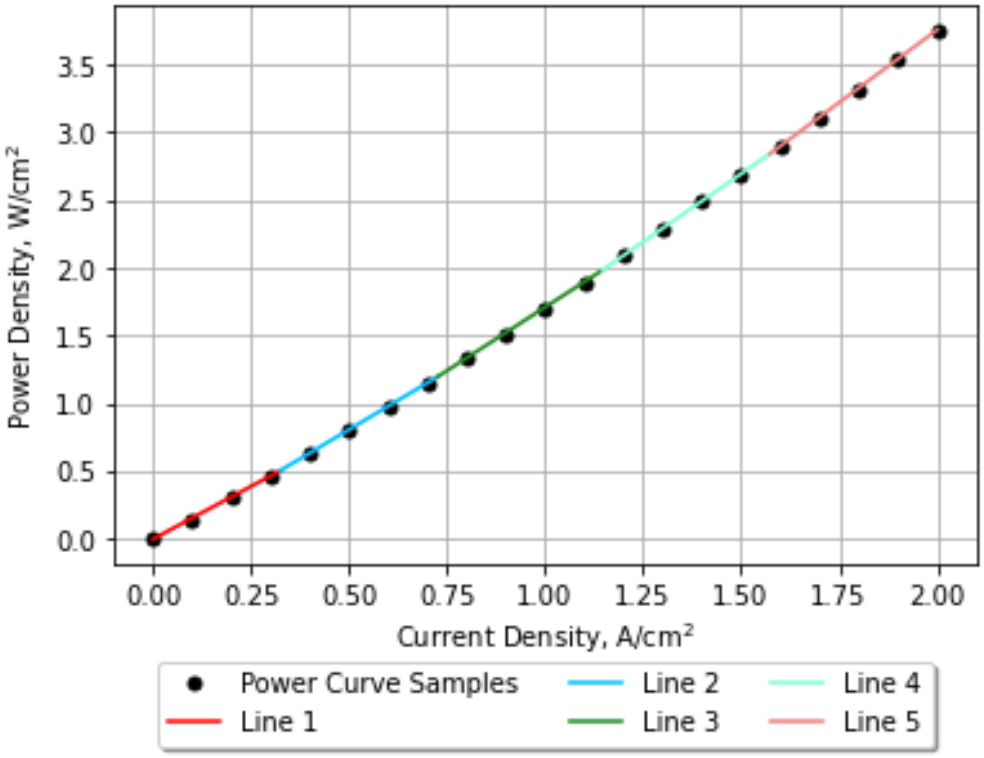

Figure 5.2: The power curve showing the operating power as a function of current density for a given electrolyzer area. The black dots are sampled data from the electrolyzer model. The colored lines are piece-wise linear functions that are fitted to the model.

Each piecewise linear power function, l, is implemented in the optimization formulation by introducing a binary variable w_l:

$$j_{op}(t) \geq x_{1,l} - M \times \left(1 - w_l(t)\right) \forall\, l = 1,2,3,4,5 \qquad \text{Eq. 5.7}$$

$$j_{op}(t) \leq x_{2,l} + M \times (1 - w_l(t)) \forall\, l = 1,2,3,4,5 \qquad \text{Eq. 5.8}$$

$$Power_{op}(t) \geq Slope_l \times j_{op}(t) + Intercept_l - \mathrm{M} \times (1 - w_l(t)) \forall\, l = 1,2,3,4,5 \qquad \text{Eq. 5.9}$$

$$Power_{op}(t) \leq Slope_l \times j_{op}(t) + Intercept_l + \mathrm{M} \times (1 - w_l(t)) \forall\, l = 1,2,3,4,5 \qquad \text{Eq. 5.10}$$

$$\sum_{l=1}^{5} w_l(t) = 1 \qquad \text{Eq. 5.11}$$

Eq. 5.7 and Eq. 5.8 activate the linear function that corresponds to the operating current density at each hour. For example, if the current density is 0.25 A/cm^2, then $w_1(t) = 1$ and Line 1 is activated. Eq. 5.9 and Eq. 5.10 calculate the power density corresponding to the operating current density. Finally, Eq. 5.11 ensures that the model is able to pick only one of the five lines for power calculations.

The hourly hydrogen production, $\dot{m}_{H_2}^{hourly}(t)$ in Eq. 5.6, is directly proportional the operating current density:

$$\dot{m}_{H_2,prod}^{hourly}(t) = \frac{j_{op}(t) \times A}{2F} mole \times \frac{3600\ s}{1\ hr} \times \frac{1\ kg}{1000\ g} \times \frac{2.02\ g}{1\ mole}$$

Eq. 5.12

The produced hydrogen can either be stored or exit the system for sales, as shown in Figure 5.3.

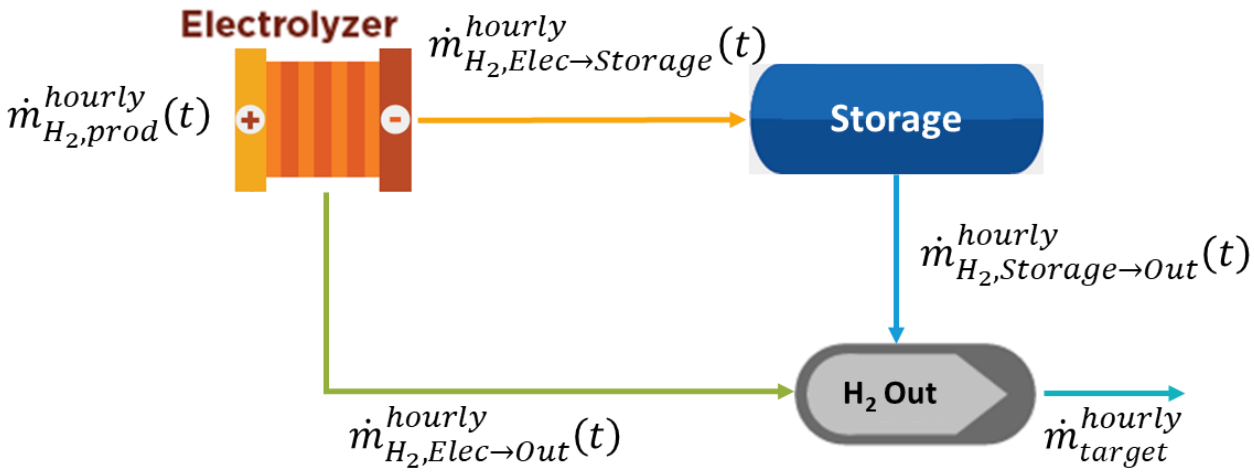

Figure 5.3: Illustration of hydrogen flow paths from electrolyzer to storage to system outlet.

There is a target amount of hydrogen that needs to be delivered. The demand can be met by production from the electrolyzer and/or discharge from the storage. If it is deemed economical to produce and store excess hydrogen at certain hours (such as when the electricity is cheap) and discharge it later, the system is allowed to do so. For simplicity,

the storage can only be charged or discharged, not both at the same time. These mass balance principles and the charging-discharging dual mode of storage are implemented as follows:

$$\dot{m}_{H_2,prod}^{hourly}(t) \geq \dot{m}_{target}^{hourly} - M \times (1 - ws(t)) \quad \text{Eq. 5.13}$$

$$\dot{m}_{H_2,prod}^{hourly}(t) \leq \dot{m}_{target}^{hourly} - M \times ws(t) \quad \text{Eq. 5.14}$$

$$\dot{m}_{H_2,Storage\rightarrow Out}^{hourly}(t) = \left(\dot{m}_{target}^{hourly} - \dot{m}_{H_2,prod}^{hourly}(t)\right) \times (1 - ws(t)) \quad \text{Eq. 5.15}$$

$$\dot{m}_{H_2,Elec\rightarrow Storage}^{hourly}(t) = \left(\dot{m}_{H_2,prod}^{hourly}(t) - \dot{m}_{target}^{hourly}\right) \times ws(t) \quad \text{Eq. 5.16}$$

$$\dot{m}_{H_2,prod}^{hourly}(t) = \dot{m}_{H_2,Elec\rightarrow Storage}^{hourly}(t) + \dot{m}_{H_2,Elec\rightarrow Out}^{hourly}(t) \quad \text{Eq. 5.17}$$

$$\dot{m}_{H_2,Elec\rightarrow Out}^{hourly}(t) + \dot{m}_{H_2,Storage\rightarrow Out}^{hourly}(t) \geq \dot{m}_{target}^{hourly} \quad \text{Eq. 5.18}$$

Eq. 5.13 and 5.14 are used to determine whether the electrolyzer is producing excess amount of hydrogen compared to the target rate. Eq. 5.15 and 5.16 ensure that the storage is either in a charging mode or a discharging mode with a binary variable $ws(t)$. Eq. 5.17 and Eq. 5.18 ensure the mass balance illustrated in Figure 5.3.

The storage facility itself is subject to three constraints:

$$S(t) = S(t-1) + \dot{m}_{H_2,Elec\rightarrow Storage}^{hourly}(t) - \dot{m}_{H_2,Storage\rightarrow Out}^{hourly}(t) \; \forall \; t \neq 0 \quad \text{Eq. 5.19}$$

$$S(1) = S(8760) + \dot{m}_{H_2,Elec\rightarrow Storage}^{hourly}(1) - \dot{m}_{H_2,Storage\rightarrow Out}^{hourly}(1) \quad \text{Eq. 5.20}$$

$$S(t) \leq S_{max} \quad \text{Eq. 5.21}$$

Eq. 5.19 ensures the mass balance for storage. Eq. 5.20 is a special case of Eq. 5.19 which requires the system to start with the same storage amount as it ends with for each calendar year. Eq. 5.21 defines the maximum storage capacity, which feeds into the storage capital cost in the objective function (Eq. 5.4). Additional operating or compression costs associated with storage have not been considered in this study.

Another constraint that is considered in this study is the minimum operating current density limit. Due to safety and efficiency constraints, there may be a limit to how low the operating current density can drop. In such case, rather than operating at a current density below the minimum threshold, the electrolyzer should shut down. These constraints are implemented in the model as follows:

$$j_{op}(t) \geq j_{min} - M \times (1 - w(t)) \quad \text{Eq. 5.22}$$

$$j_{op}(t) \leq 0 + M \times w(t) \quad \text{Eq. 5.23}$$

Eq. 5.22 determines whether the operating current density is below the minimum. If so, Eq. 5.23 sets the operating current density to 0.

In addition, there are non-negativity constraints introduced in the formulation since none of the variables discussed above can be negative in value.

$$j_{op}(t) \geq 0 \quad \text{Eq. 5.24}$$

$$S(t) \geq 0 \quad \text{Eq. 5.25}$$

$$\dot{m}_{H_2,prod}^{hourly}(t) \geq 0 \quad \text{Eq. 5.26}$$

$$\dot{m}_{H_2,Elec \rightarrow Storage}^{hourly}(t) \geq 0 \quad \text{Eq. 5.27}$$

$$\dot{m}_{H_2,Storage \rightarrow Out}^{hourly}(t) \geq 0 \quad \text{Eq. 5.28}$$

$$\dot{m}_{H_2,Elec \rightarrow Out}^{hourly}(t) \geq 0 \quad \text{Eq. 5.29}$$

Table 5.1 summarizes all the variables are used in the MINLP algorithm.

Table 5.1: Nomenclature for MINLP Optimization Algorithm

A	Total Active Area of the Electrolyzer (cm2)
C_{CAPEX}	Capital Expenditure (CAPEX) ($)
C_{fOPEX}	Fixed Operating Expenses (OPEX) ($)
C_{PR}	Planned Replacement Cost ($)
$C_{storage}$	Storage Cost ($)
C_{Total}	Total Cost ($)
C_{UPR}	Unplanned Replacement Cost ($)
C_{vOPEX}	Variable Operating Expenses (OPEX) ($)
d	Discount Rate (fraction)
F	Faraday's Number (96485.3 C/mol e-)
j_{max}	Maximum Current Density (A/cm2)
j_{min}	Minimum Current Density (A/cm2)
j_{op}	Operating Current Density (A/cm2)
M	"Big M"
$\dot{m}^{hourly}_{H_2,Elec\rightarrow Out}$	Hourly Hydrogen Flow from Electrolyzer to Outlet (kg/hr)
$\dot{m}^{hourly}_{H_2,Elec\rightarrow Storage}$	Hourly Hydrogen Flow from Electrolyzer to Storage (kg/hr)
$\dot{m}^{hourly}_{H_2,Storage\rightarrow Out}$	Hourly Hydrogen Flow from Storage to Outlet (kg/hr)
$\dot{m}^{hourly}_{target}$	Hourly Hydrogen Production Target (kg/hr)
P_{elec}	Electricity Price ($/MWh)
P_{water}	Price of Water ($/gallon)
$Power_{op}$	Operating Power (MW)
S	Hydrogen Storage (tonne)
S_{max}	Maximum Hydrogen Storage Capacity (tonne)
U^{hourly}_{elec}	Hourly Electrolyzer Electrical Usage (kW/hour)
U^{hourly}_{water}	Hourly Water Usage (gallon/kg H2)
w	Binary Variable for Minimum Current Density
w_l	Binary Variable for Power Function l
ws	Binary Variable for Charing-Discharging Mode for Storage
$x_{1,l}$	Lower Limit of Current Density Range for Power Function l
$x_{2,l}$	Upper Limit of Current Density Range for Power Function l
π	Inflation Rate (fraction)

The Gurobi implementation of this MINLP is available in Appendix C: Python Code for Techno-Economic Model.

5.1.2 GSS Algorithm to Optimize Plant Capacity

While the MINLP algorithm looks for the optimal operating current densities and hydrogen storage size to minimize the operating cost and LCOH for a given electrolyzer plant size, the GSS algorithm looks for the optimal plant size that results in the lowest overall LCOH. As shown in Figure 5.4, the GSS algorithm searches for an extremum of a unimodal function within a specified interval, between a lower bound, x_1, and an upper bound, x_2. It evaluates the function at two different points, x_3 and x_4. The two points are determined such that:

$$\frac{x_2 - x_3}{x_3 - x_1} = \varphi = \frac{1+\sqrt{5}}{2} \qquad \text{Eq. 5.30}$$

$$\frac{x_4 - x_1}{x_2 - x_4} = \varphi = \frac{1+\sqrt{5}}{2} \qquad \text{Eq. 5.31}$$

The algorithm looks at the values of $y_3=f(x_3)$ and $y_4=f(x_4)$. If $y_4 > y_3$, then the new search interval is set between x_1 and x_4. If $y_3 > y_4$, then the new search interval is set between x_3 and x_2. The new search interval is shaded in light blue in Figure 5.4 for the two different scenarios. The algorithm continues until the search interval is sufficiently narrowed down within a desired tolerance. The extreme point (minimum in the case shown in Figure 5.4) is taken as the minimum of all the search iterations that the algorithm performed.

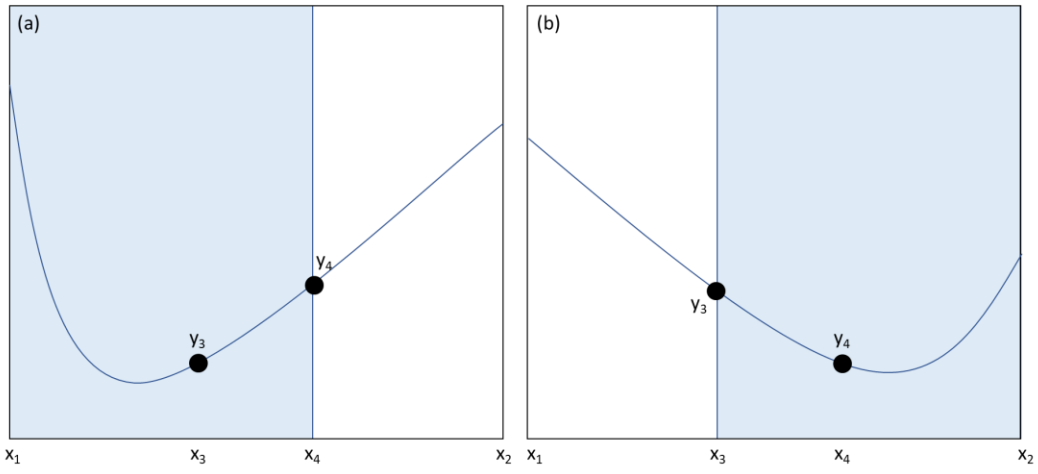

Figure 5.4: Illustration of how the GSS algorithm works with two unimodal functions with different shapes. In (a), the upper bound of the search interval is updated to x_4 from x_2. In (b), the lower bound of the search interval is updated to x_3 from x_1.

5.2 Techno-Economic Analysis of Dynamic Operations

5.2.1 Model Input

For consistency, the electrolyzer model and the techno-economic model used for dynamic operations are fitted with the same set of parameters as those used for steady operations modeling, as shown in Table 5.2 and Table 5.3. The table indicates which of the parameters are varied as the optimization algorithm searches for the optimal set of operating current densities, plant capacity, and storage capacity.

Table 5.2: Electrolyzer Model Parameters for Dynamic Operations

Parameters	Values	Units
Membrane Thickness, t	178	μm
Cathode Exchange Current Density, $j_{0,cathode}$	2.3×10^{-3} (Calculated)	A/cm²
Anode Exchange Current Density, $j_{0,anode}$	3.0×10^{-6} (Calculated)	A/cm²
Temperature, T	80	°C
Cathode Pressure, P_{cat}	20	bar
Anode Pressure, P_{an}	1	bar

Table 5.3: Techno-Economic Model Parameters for Dynamic Operations

Parameters	Values	Units
Target Production	50	Tonne/day
System Size	Varied	MW
Operating Current Density	Varied	A/cm²
Max Current Density	2	A/cm²
Min Current Density	0	A/cm²
Electrolyzer Lifetime	10	Years
Project Lifetime	40	Years
Stack Cost	2.0	$/cm²
mBoP Cost Factor	117	$/kg H_2 per day
eBoP Cost Factor	126	$/$kW_{electric}$
Uninstalled Specific CAPEX	Varied	$/$kW_{input}$
Total Specific CAPEX	Varied	$/$kW_{input}$
Electricity Cost	Variable (Average 52)	$/MWh
Electrolyzer Electrical Usage	50	kW/kg H_2
BoP Electrical Usage	5.1	kW/kg H_2
Labor Cost	70	$/hour

The parameters for the compression techno-economic model are shown in Table 5.4. The target delivery pressure is assumed to be 30 bar, requiring a compression ratio of 1.5.

Table 5.4: Compression Techno-Economic Model Parameters

Parameters	Values	Units
Target Delivery Pressure	30	Bar
Compression Ratio per Stage	2.1	-
Motor Efficiency	90	%
Isentropic Efficiency	65	%
Lifetime	15	Years
Scale Factor	2695	-
Scale Exponent	0.8335	-
Number of Stages	5	-
Number of Units	2	-
Number of Backup Unit	1	-
Compressor Specific CAPEX	1,415	$/kW

5.2.2 Results from Dynamic Operations

Figure 5.5 shows the different search iterations of the GSS algorithm (blue) along with the LCOH value obtained from steady operation (green). Compared to the LCOH of $4.93/kg for steady operation, the LCOH for dynamic operation goes down by 9% to $4.48/kg H_2 by oversizing the plant capacity by 40%.

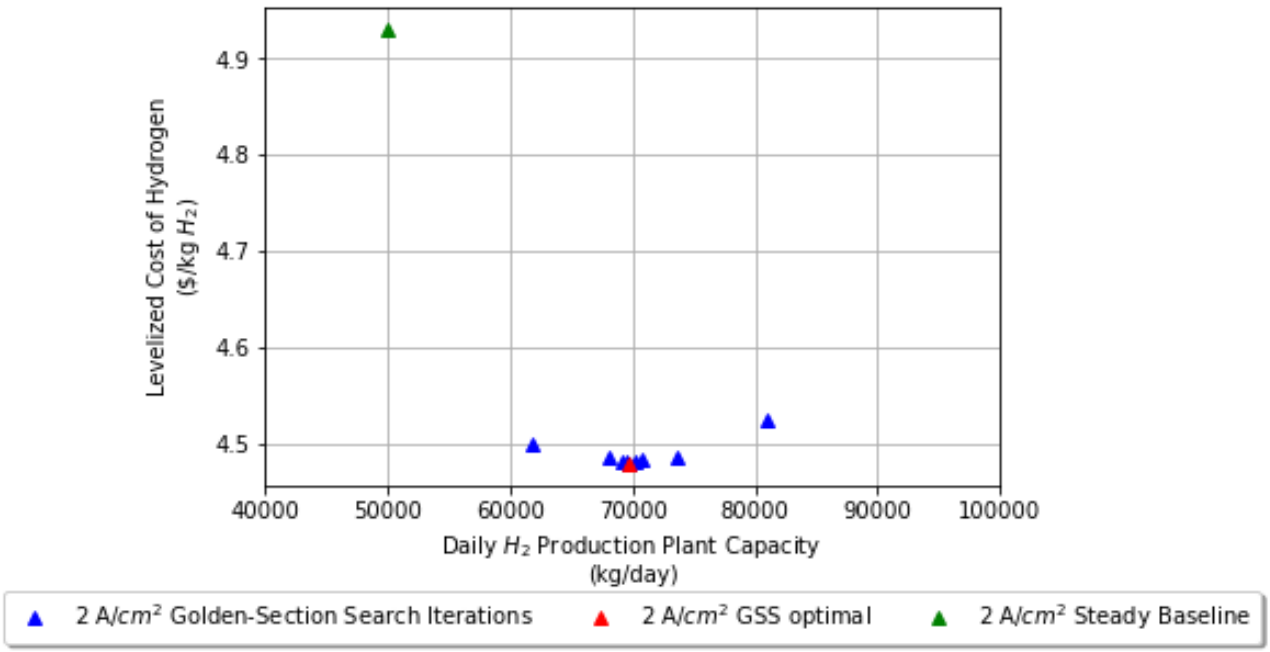

Figure 5.5: Plot of LCOH as a function of daily production plant capacity with a maximum current density of 2A/cm². The blue points are iterations evaluated by the GSS algorithm. The red point is the optimal case with the lowest total LCOH. The green point is the LCOH from steady operation.

By increasing the capacity, the electrolyzer is able to produce and store excess amount of hydrogen when electricity is cheap. When electricity is expensive, the electrolyzer operates at less than its full capacity (or even completely shuts down) and the production target is met by discharging hydrogen from the storage facility. These dynamics are well captured in Figure 5.6 and Figure 5.7, which show the hourly electricity price, operating current density, and hydrogen production on a typical summer day and winter day, respectively, for the optimal case identified by the GSS algorithm (red triangle in Figure 5.5).

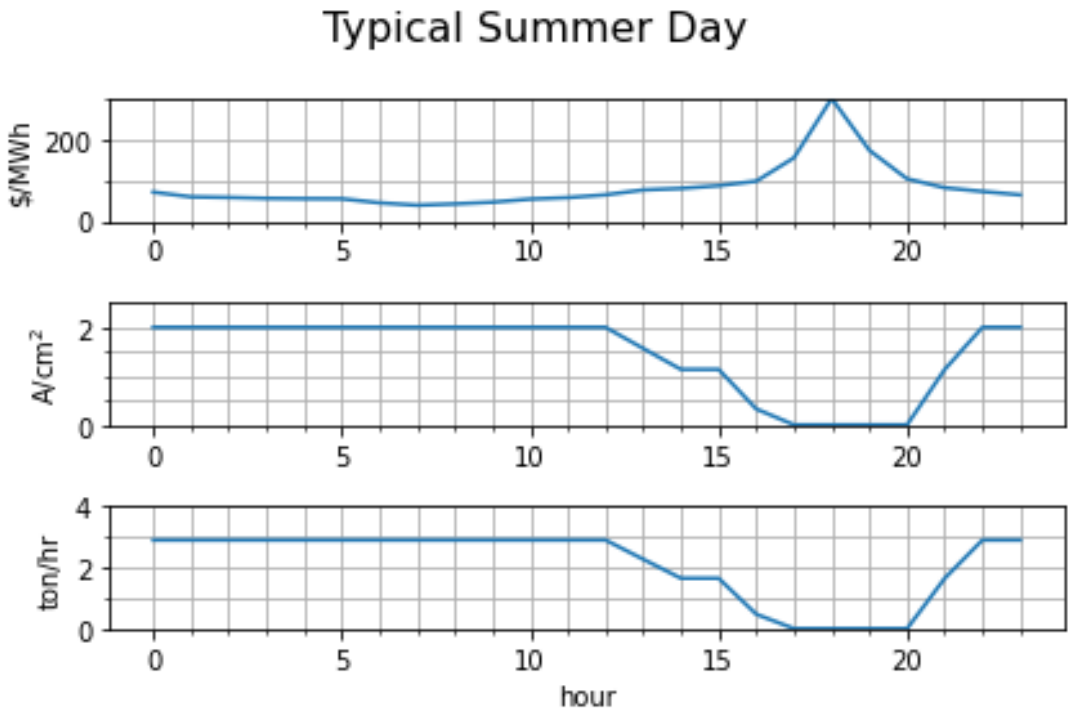

Figure 5.6: Hourly electricity price (top), operating current density (middle), and hydrogen production (bottom) on a typical summer from the dynamic operations simulation.

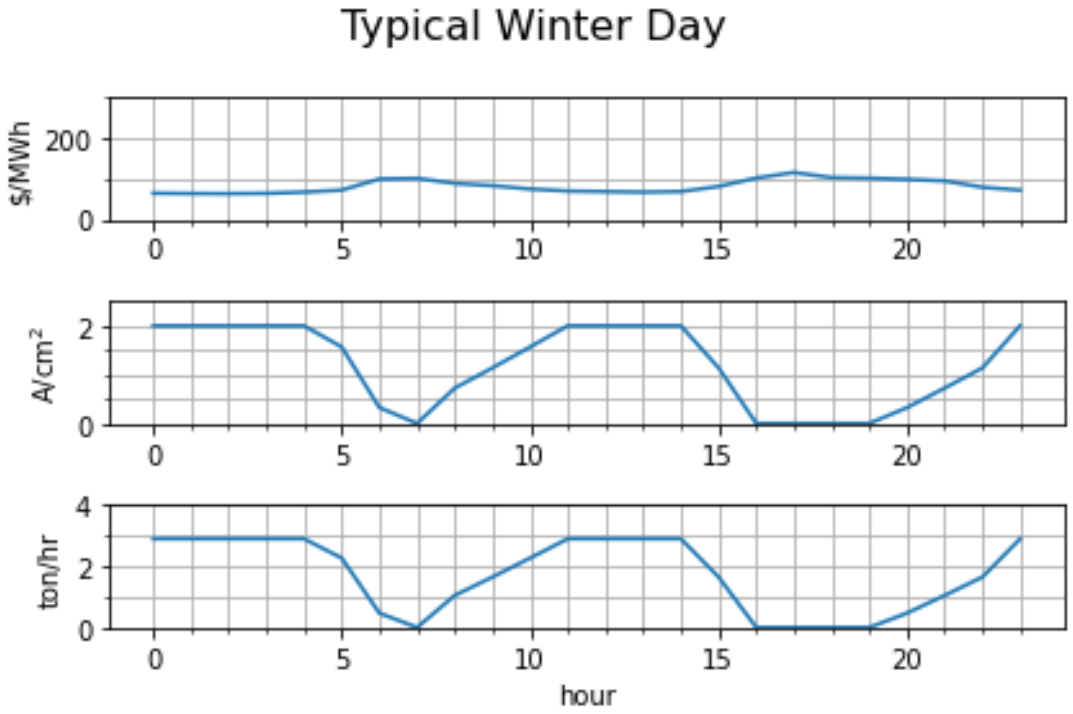

Figure 5.7: Hourly electricity price (top), operating current density (middle), and hydrogen production (bottom) on a typical winter day from the dynamic operations simulation.

The top plot in Figure 5.8 shows the inventory in the hydrogen storage facility for the whole year. Seasonal shifting can be observed with more than 50% of the capacity remaining filled up to 2 weeks at a time, especially during the spring. During the summer, the storage level fluctuates more widely as the electrolyzer responds to the sporadic high spikes in electricity prices.

The bottom plot in Figure 5.8 shows the storage level corresponding to the typical summer day from Figure 5.6. During the first 12 hours of high production, the storage gets filled to its capacity (16.7 tonne H_2). As production slows down with rising electricity prices, the storage level goes down as hydrogen is dispensed to meet the hourly hydrogen demand. Between hours 17 and 19, the electrolyzer completely shuts down and the entire hydrogen demand is met by dispensing from the storage facility.

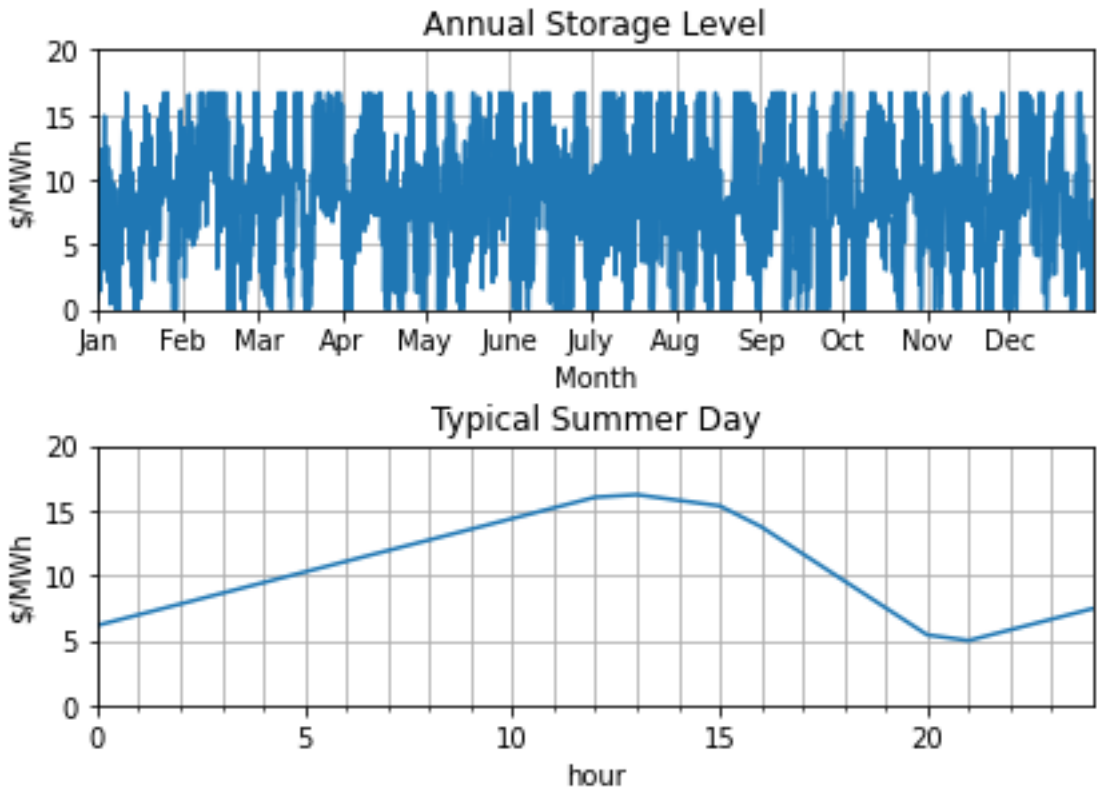

Figure 5.8: Hourly hydrogen storage as a function time for the year (top) and on a typical summer day (bottom) as simulated in the dynamic-operations techno-economic model.

Figure 5.9 shows the cost breakdown of the total LCOH. Compared to the steady operation in which the variable OPEX contributed 74% of the total cost, the variable OPEX contribution in the optimized dynamic case accounts for 63% of the total cost. By oversizing the capacity, CAPEX, replacement cost, and fixed OPEX contribute proportionally more to the overall cost. At the same time, dynamic operations reduce the relative contribution of the variable OPEX by varying the load with the price fluctuations.

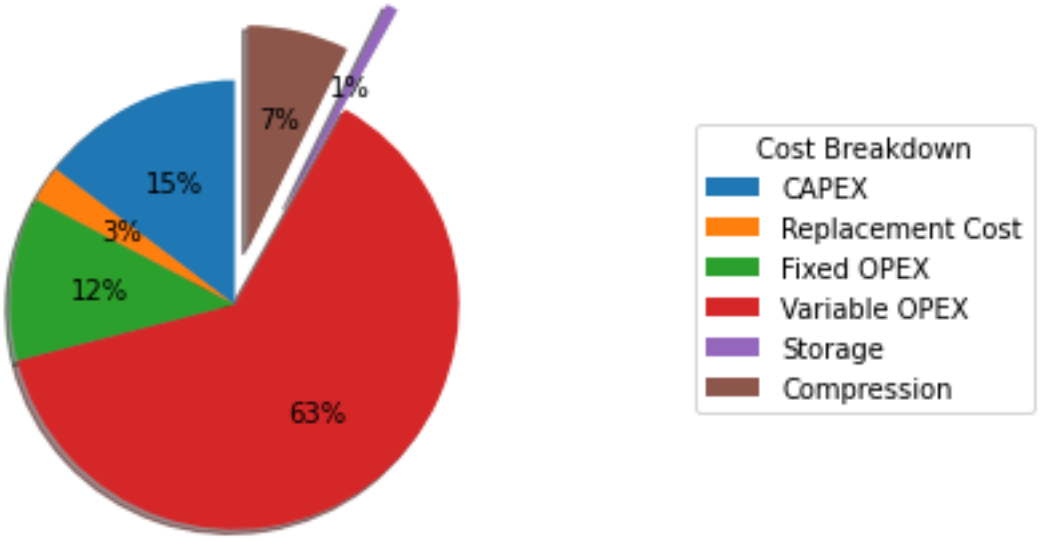

Figure 5.9: Contributions of different cost components to the total production and compression costs during dynamic operations

Table 5.5 summarizes the design and economic parameters for the optimized case. For ease of comparison, these numbers are reported based on a steady operation at 2 A/cm^2. It can be seen that the steady facility and the dynamic facility have the same specific CAPEX. However, the dynamic facility is able to respond to the changing electricity prices and produce hydrogen at a cheaper LCOH than the steady facility. This example further corroborates the argument from Chapter 4 that the economic measures commonly used to compare different electrolyzer systems based on energy input can be misleading unless the operating conditions and design parameters are consistent.

Table 5.5: Techno-Economic Model Parameters of the Dynamic Operation Model

Parameters	Values	Units
Maximum Production Capacity	70	Tonne/day
System Size	145	MW
Operating Current Density	2	A/cm^2
Max Current Density	2	A/cm^2
Min Current Density	0	A/cm^2
Electrolyzer Lifetime	10	Years
Project Lifetime	40	Years
Stack Cost	2.0	\$/cm^2
mBoP Cost Factor	117	\$/kg H_2 per day
eBoP Cost Factor	126	\$/kW$_{electric}$
Uninstalled Capital Specific Cost	715	\$/kW
Total Capital Specific Cost	1,004	\$/kW
Electricity Cost	Variable (Average 52)	\$/MWh
Electrolyzer Electrical Usage	50	kW/kg H_2
BoP Electrical Usage	5.1	kW/kg H_2
Labor Cost	70	\$/hour
Target Delivery Pressure	30	Bar
Cathode Pressure	1	Bar
Temperature	80	°C

5.3 Sensitivities

5.3.1 Impact of Maximum Operating Current Density

The impact of maximum current density on LCOH is summarized in Table 5.6 and illustrated in Figure 5.10. With a maximum current density of 1 A/cm², the electrolyzer system is already oversized to meet the demand target even before considering dynamic operations. Since CAPEX, replacement cost, and fixed operating cost already account for a large portion of the total cost, there is a limited upside to further increasing the plant capacity. As a result, there is a trend where the optimal capacity is bigger for higher maximum current densities; the higher the maximum current density, the lower it costs to add extra production capacity. In addition, there is an economic gain in operating at a high current density during low-price hours even at the expense of lower efficiencies.

Table 5.6: Effect of Maximum Operating Current Density on LCOH during Dynamic Operations

Max Current Density (A/cm²)	Electrolysis LCOH ($/kg H₂)	Compression LCOH ($/kg H₂)	Total LCOH ($/kg H₂)	Normalized Capacity
1	4.61	0.31	4.92	1.14
2	4.15	0.33	4.48	1.40
3	4.04	0.33	4.37	1.38

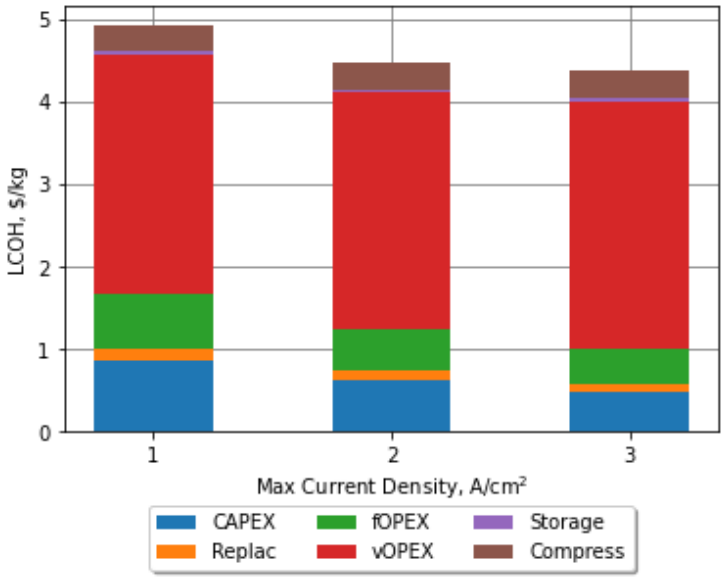

Figure 5.10: Bar charts of LCOH attributed to CAPEX, replacement cost, fixed OPEX, variable OPEX, storage cost, and compression as a function of maximum current density during dynamic operations.

5.3.2 Impact of Cathode Operating Pressure

Figure 5.11 shows the effect of cathode operating pressure on LCOH, which is similar to the trends observed in the steady operation simulation. Economic benefits can be realized in the direct compression pressure range of 5 – 10 bar in which the decrease in the compression cost is more than the increase in the electrolysis cost. Hence, a hybrid compression system makes most sense in this case.

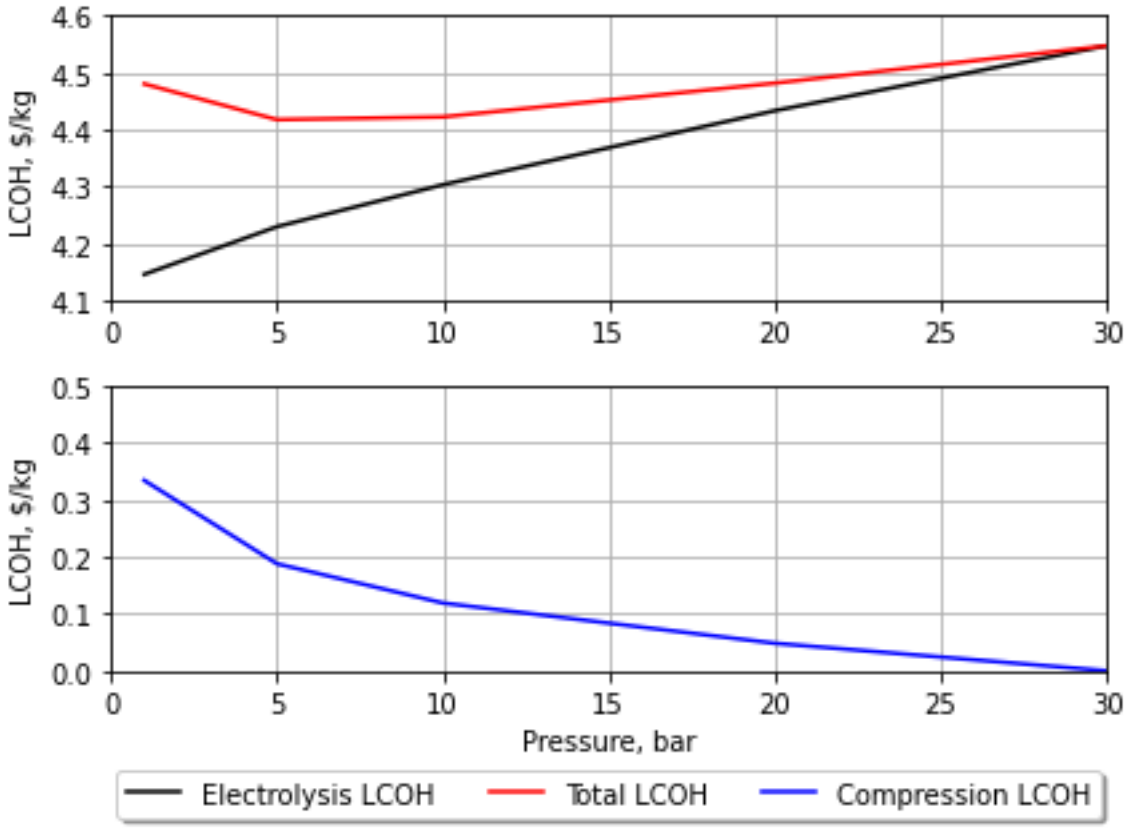

Figure 5.11: Electrolysis LCOH (black), Compression LCOH (blue), and Total LCOH (red) as a function of operating pressure during dynamic operations.

5.3.3 Impact of Minimum Current Density

Hydrogen crossover from the cathode to the anode limits the operations at low loads, especially in a differential-pressure mode (Babic et al. 2017; Schalenbach et al. 2013). Hydrogen crossover presents a serious safety issue as the lower explosion limit (LEL) of hydrogen in oxygen is about 4 mol% under standard conditions (Suermann, Bensmann, and Hanke-Rauschenbach 2019). (Babic et al. 2017) reports that the safe lower limit for a membrane thickness of 200 μm in a 30-bar differential pressure experiment is 0.91 A/cm^2. In addition, hydrogen crossover lowers the Faradic efficiency of the electrolyzer system (Babic et al. 2017; Schalenbach et al. 2013), which have not been incorporated in this study.

A sensitivity study is carried out to study the effect of different minimum current densities on the electrolyzer's operational decisions and economics. Figure 5.12 shows the hourly profile for the same typical summer day as Figure 5.6. It can be seen that the model opts to shut down the electrolyzer rather than operate at a current density below 1 A/cm^2, which is the minimum current density limit set in the model.

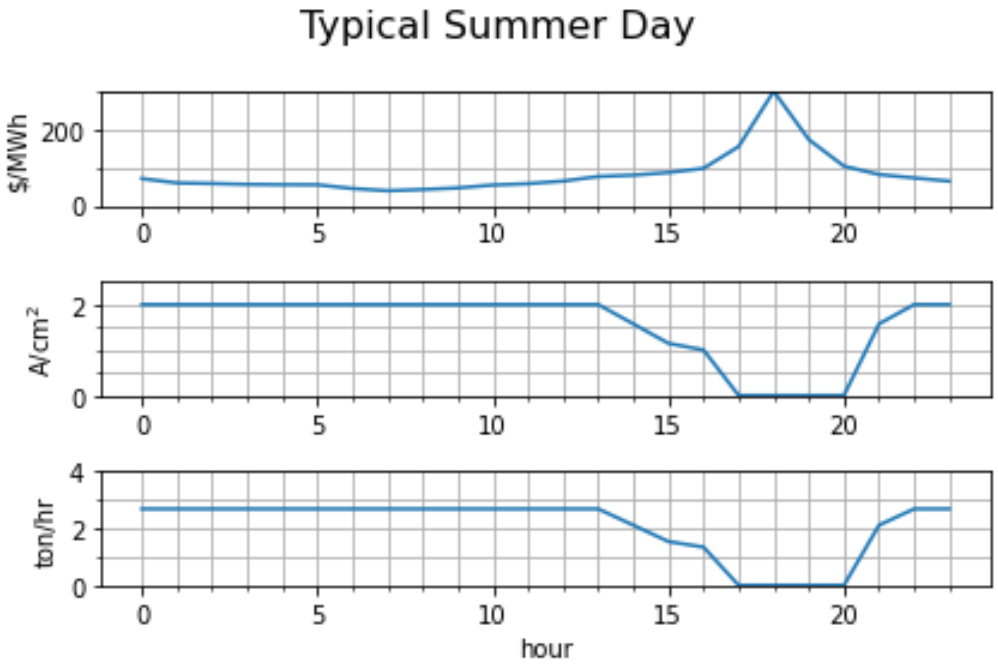

Figure 5.12: Hourly electricity price (top), operating current density (middle), and hydrogen production (bottom) on a typical summer from the dynamic operations simulation with a minimum current density constraint of 1 A/cm^2.

Table 5.7 shows LCOH results for different minimum current densities during dynamic operations. The simulation is subject to the maximum current density of 2 A/cm^2 under ambient pressure at both the cathode and the anode. It is seen that there is no significant impact on the overall economics of hydrogen production. It should be noted that there is no penalty associated with shutting down the plant, so the model is free to shut down and start up the electrolyzer as many times as it is economical to do so. However, in reality, there are operational challenges in restarting an electrolyzer after a complete shutdown. Therefore, it may be necessary to implement an objective that minimizes the number of complete shutdowns in a future study.

Table 5.7: Effect of Minimum Operating Current Density on LCOH during Dynamic Operations

Min Current Density (A/cm^2)	Electrolysis LCOH ($/kg H_2)	Compression LCOH ($/kg H_2)	Total LCOH ($/kg H_2)	Normalized Capacity
0	4.15	0.34	4.48	1.40
0.5	4.15	0.33	4.48	1.36
1	4.14	0.34	4.48	1.42

5.4 Technical Challenges of Dynamic Operations

While the prospect of dynamic operations proffers attractive economic gains, there are technical challenges associated with them, which have not been incorporated in the models in this study.

First, while the PEM electrolyzer may be quick to respond to different loads, the real bottleneck in the system's flexibility may lie with the BoP components. For example, rectifiers have low efficiencies at lower loads. Therefore, a design that is made up of small modular stacks with its own rectifiers may be more flexible than a single-stack, single-rectifier electrolyzer (IRENA 2020).

Second, dynamic operations cause electrolyzers to degrade at a faster rate than steady operations. (Li, Araya, and Kær 2021) reports that high load cycling accelerates membrane thinning, thereby reducing the MEA lifetime. (Weiß et al. 2019) concludes that catalyst degradation occurs when the cell voltage drops to open circuit voltage (OCV). (Feng et al. 2017) writes that dynamic operation can be detrimental to both performance and durability of the electrolyzers.

A further study that involves a much more detailed electrolyzer model capable of simulating transient responses with degradation can be used to understand the operational procedures that minimize such reliability and safety concerns associated with dynamic operations.

5.5 References

Babic, Ugljesa, Michel Suermann, Felix N. Büchi, Lorenz Gubler, and Thomas J. Schmidt. 2017. "Critical Review—Identifying Critical Gaps for Polymer Electrolyte Water Electrolysis Development." *Journal of The Electrochemical Society* 164 (4): F387–99. https://doi.org/10.1149/2.1441704jes.

El-Emam, Rami S., and Hasan Özcan. 2019. "Comprehensive Review on the Techno-Economics of Sustainable Large-Scale Clean Hydrogen Production." *Journal of Cleaner Production* 220 (May): 593–609. https://doi.org/10.1016/j.jclepro.2019.01.309.

Feng, Qi, Xiao−Zi Yuan, Gaoyang Liu, Bing Wei, Zhen Zhang, Hui Li, and Haijiang Wang. 2017. "A Review of Proton Exchange Membrane Water Electrolysis on Degradation Mechanisms and Mitigation Strategies." *Journal of Power Sources* 366 (October): 33–55. https://doi.org/10.1016/j.jpowsour.2017.09.006.

IRENA. 2020. "Green Hydrogen Cost Reduction: Scaling up Electrolyzers to Meet the 1.5C Climate Goal." International Renewable Energy Agency, Abu Dhabi.

Li, Na, Samuel Simon Araya, and Søren Knudsen Kær. 2021. "Investigating Low and High Load Cycling Tests as Accelerated Stress Tests for Proton Exchange Membrane Water Electrolysis." *Electrochimica Acta* 370 (February): 137748. https://doi.org/10.1016/j.electacta.2021.137748.

Schalenbach, Maximilian, Marcelo Carmo, David L. Fritz, Jürgen Mergel, and Detlef Stolten. 2013. "Pressurized PEM Water Electrolysis: Efficiency and Gas Crossover." *International Journal of Hydrogen Energy* 38 (35): 14921–33. https://doi.org/10.1016/j.ijhydene.2013.09.013.

Siracusano, Stefania, Stefano Trocino, Nicola Briguglio, Fabiola Pantò, and Antonino S. Aricò. 2020. "Analysis of Performance Degradation during Steady-State and Load-Thermal Cycles of Proton Exchange Membrane Water Electrolysis Cells." *Journal of Power Sources* 468 (August): 228390. https://doi.org/10.1016/j.jpowsour.2020.228390.

Suermann, Michel, Boris Bensmann, and Richard Hanke-Rauschenbach. 2019. "Degradation of Proton Exchange Membrane (PEM) Water Electrolysis Cells: Looking Beyond the Cell Voltage Increase." *Journal of The Electrochemical Society* 166 (10): F645–52. https://doi.org/10.1149/2.1451910jes.

Weiß, A., A. Siebel, M. Bernt, T.-H. Shen, V. Tileli, and H. A. Gasteiger. 2019. "Impact of Intermittent Operation on Lifetime and Performance of a PEM Water Electrolyzer." *Journal of The Electrochemical Society* 166 (8): F487–97. https://doi.org/10.1149/2.0421908jes.

Chapter 6
Future Cost of Hydrogen

In order to promote the widespread adoption of green hydrogen, the production costs need to be competitive with the traditional means of producing hydrogen from fossil-based fuels. (IEA 2021) reports that in 2021 fossil-based processes can produce hydrogen at $0.5/kg to $1.7/kg, depending on the natural gas prices. As a result, the DOE set a hydrogen production target of $2/kg for transportation end uses and $1/kg for industrial and bulk power applications (McQueen et al. 2020). Therefore, the LCOH of green hydrogen needs to fall below $2/kg to be competitive with the fossil-based production methods. This chapter explores future costs of hydrogen production by examining several cost drivers, including the reductions in CAPEX, different predictions of future electricity prices, and improvement in electrolyzer performance.

6.1 Future Electrolyzer Capital Costs

In the future, dramatic reductions in capital costs are expected for PEM electrolyzers (van der Spek et al. 2022). The move towards a semi or fully automated manufacturing process is expected to significantly reduce the unit cost of electrolyzer (IRENA 2020). Improvements in flow fields, membrane electrode assembly (MEA), labor, economies of scale, improved quality control, and larger cell areas can further drive down the costs (Saba et al. 2018). Several studies indicate that the learning rates for electrolyzers are similar to those for solar PV at a rate between 16% and 21% (IRENA 2020; Lagadec and Grimaud 2020). (IRENA 2020) further projects that a cost reduction of over 40% can be realized by 2030.

(Glenk and Reichelstein 2019) reports that the specific total CAPEX ($/kW) of electrolyzer system declines at an annual rate of 4.8%. Based on the 2021 specific CAPEX of $1,004/kW estimated in the study, the specific CAPEX can reach $504/kW by 2035 and less than $400/kW by 2040.

The DOE H2A model also projects a 40% reduction in the electrolyzer cost, 40% reduction in mBoP costs, and 17% reduction in eBoP costs between their current and future scenarios. These reduction projections in CAPEX were adopted in this study as the Future scenario. As Table 6.1 shows, these reductions translate to a specific CAPEX of $618/kW, which is higher than what is attainable based on the decline rate from (Glenk and Reichelstein 2019). Therefore, a more optimistic scenario, called the Future Optimistic CAPEX, was created, and the electrolyzer stack, mBoP, and eBoP costs were back-calculated – within a reasonable limit – such that the specific CAPEX approaches $400/kW.

Table 6.1: Comparison of Capital Cost Parameters for Current, Future, and Future Optimistic Cases

Capital Cost Parameters	Current	Future	Future Optimistic	Unit
Electrolyzer Stack Cost	2.00	1.13	0.70	$/cm^2
mBoP Cost	117	67	54	$/(kg H2/day)
eBoP Cost	126	99	80	$/kW$_{electric}$
Specific CAPEX	1,006	618	421	$/kW$_{input}$
Storage CAPEX	500	300	300	$/kg
Assumptions/References	(James et al. 2013)	(James et al. 2013)	Estimated based on 4.8% decline rate from (Glenk and Reichelstein 2019)	

The specific CAPEX in Table 6.1 are estimated from the stack and balance of plant costs and assuming an efficiency corresponding to operations at 2 A/cm^2 equal to 68% on an LHV basis (or 49 KWh/kg). The electrolyzer efficiency and performance are also expected to improve in the future. However, this was not considered in the calculation of the specific CAPEX for easy comparison with the current value.

6.2 Future Electricity Prices

Many authors and organizations have provided projections for the future electricity price across the U.S. based on a wide variety of different technology and policy assumptions. In this study, 18 different electricity forecasts have been used to explore the implications of electricity price variations on future LCOHs. The highlighted traits and assumptions for each forecast is provided in Table 6.2.

Table 6.2: Summary of Attributes of 18 Electricity Forecasts used in this Study

Forecast Name	Location(s)	Year	Description	Average Price	Number of Hours of <$5MWh	Number of hours of >100/MWh
NREL-Mid	Southern CA	2040	Mid-level assumptions for demand, resource, cost, price, technology. No new carbon policy	40.61	222	106
NREL-HighRECost	Southern CA	2040	Mid with 2020 ATB RE advanced projections	44.49	33	106
NREL-LowRECost	Southern CA	2040	Mid with 2020 ATB RE conservative projections	31.78	1584	105
NREL-Mid95by2035	Southern CA	2040	Mid with 95% CO_2 reduction by 2035	59.48	3073	112
NREL-Mid95by2050	Southern CA	2040	Mid with 95% CO_2 reduction by 2050	42	431	109
Princeton-BaseCaseTax	Nationwide	2030	$60/tonne carbon tax, AEO2020 REF natural gas prices, mid cost for all resources	47.69	799	262
Princeton-HighWindTax	Nationwide	2030	BaseCaseTax with low cost for wind clusters	45.06	1628	256
Princeton-HighSolarTax	Nationwide	2030	BaseCaseTax with low cost for solar clusters	45.43	1218	241
NREL-MiNg_$100_CAISO	CA	2035	$100/tonne carbon tax, AEO2020 REF natural gas prices	53.08	3413	518
NREL-MiNg_$150_CAISO	CA	2035	$150/tonne carbon tax, AEO2020 REF natural gas prices	45.54	5080	2702
NREL-MiNg_$100_ERCOT	TX	2035	$100/tonne carbon tax, AEO2020 REF natural gas prices	33.76	4049	79
NREL-MiNg_$150_ERCOT	TX	2035	$150/tonne carbon tax, AEO2020 REF natural gas prices	36.34	5199	1401

Table 6.2 Continued

Name	Location(s)	Year	Description	Average Price	Number of Hours of <$5MWh	Number of hours of >100/MWh
NREL-MiNg_$100_MISO-W	AR, IL, IN, IA, KY, LA, MI, MN, MO, MT, ND, SD, TX, WI	2035	$100/tonne carbon tax, AEO2020 REF natural gas prices	35.22	3858	17
NREL-MiNg_$150_MISO-W	AR, IL, IN, IA, KY, LA, MI, MN, MO, MT, ND, SD, TX, WI	2035	$150/tonne carbon tax, AEO2020 REF natural gas prices	28.28	5476	539
NREL-MiNg_$100_NYISO	NY	2035	$100/tonne carbon tax, AEO2020 REF natural gas prices	35.33	4816	185
NREL-MiNg_$150_NYISO	NY	2035	$150/tonne carbon tax, AEO2020 REF natural gas prices	33.84	5834	1421
NREL-MiNg_$100_PJM-W	DE, IL, IN, KY, MD, MI, NJ, NC, OH, PA, TN, VA, WV, DC	2035	$100/tonne carbon tax, AEO2020 REF natural gas prices	48.08	1397	50
NREL-MiNg_$150_PJM-W	DE, IL, IN, KY, MD, MI, NJ, NC, OH, PA, TN, VA, WV, DC	2035	$150/tonne carbon tax, AEO2020 REF natural gas prices	49.94	2666	1903

The profile and short descriptions of each electricity forecast scenario is provided below:

- NREL-Mid: This is NREL's business-as-usual scenario (Gagnon et al. 2021). The 2040 electricity prices from the P10 balancing area (Southern California) were used for this study. The average price is $40.61/MWh. There are spikes of high prices during the summer.

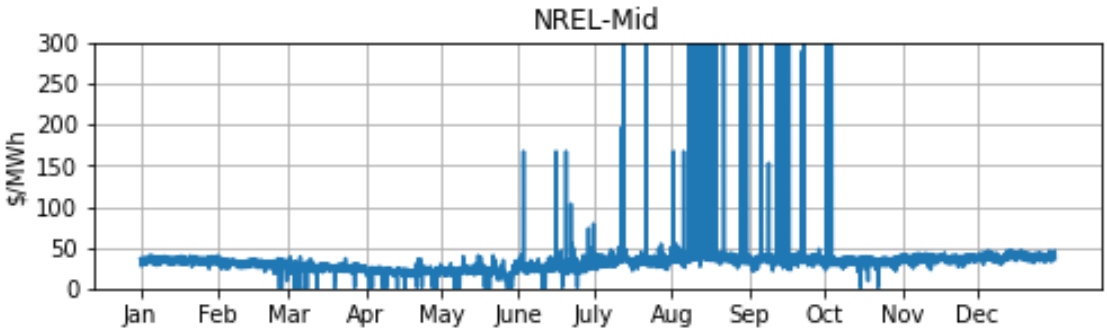

Figure 6.1: Electricity Price Predictions from NREL-Mid Scenario

- NREL-HighRECost: This 2040 scenario has the same assumptions as NREL-Mid scenario, but with higher renewable energy costs (Gagnon et al. 2021). The electricity prices from the P10 balancing area (Southern California) were used for this study. The average price is $44.49/MWh. There are spikes of high prices during the summer.

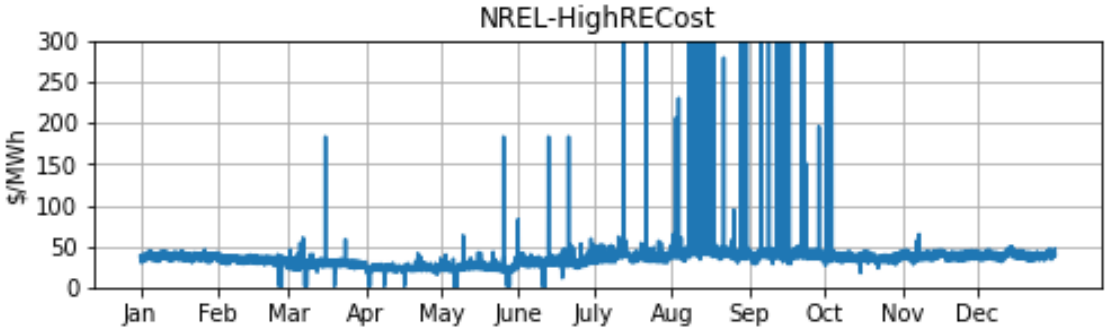

Figure 6.2: Electricity Price Predictions from NREL-HighRECost Scenario

- NREL-LowRECost: This 2040 scenario has the same assumptions as NREL-Mid scenario, but with lower renewable energy costs (Gagnon et al. 2021). The electricity prices from the P10 balancing area (Southern California) were used for this study. The average price is $31.78/MWh. There are spikes of high prices during the summer time. Low electricity prices are available during the spring time.

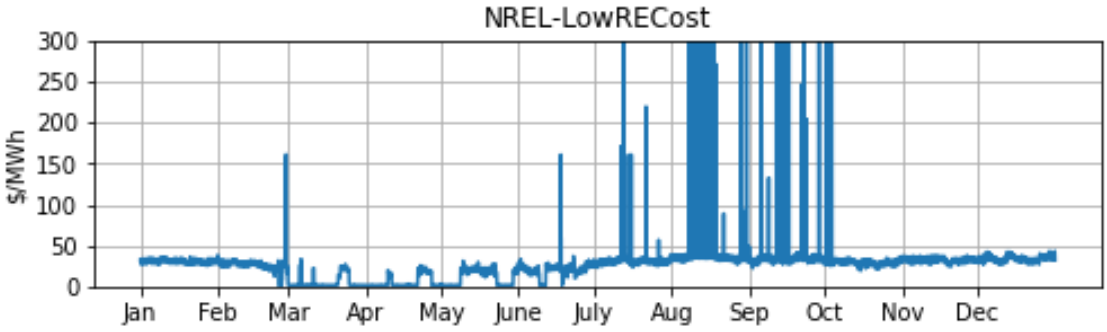

Figure 6.3: Electricity Price Predictions from NREL-LowRECost

- NREL-Mid95by2035: This 2040 scenario has the same assumptions as NREL-Mid scenario, but with 95% decarbonization of the national power sector by 2035 (Gagnon et al. 2021). The electricity prices from the P10 balancing area (Southern California) were used for this study. The average price is $59.48/MWh with higher levels of fluctuations throughout the day. There are spikes of high prices during the summer. Low electricity prices are available during the spring time.

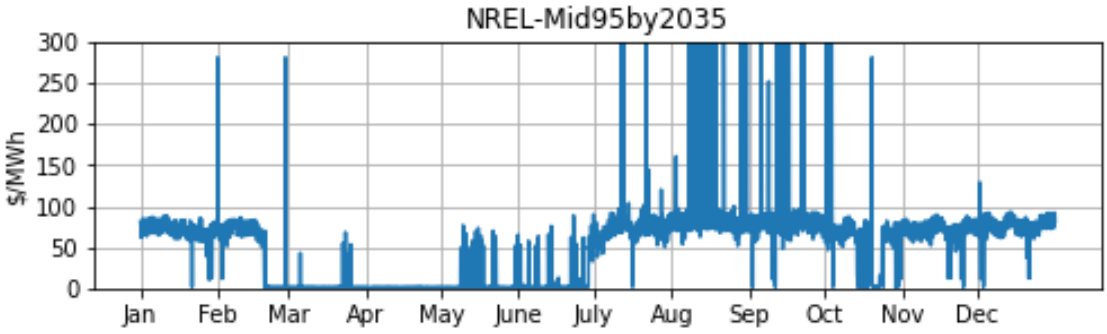

Figure 6.4: Electricity Price Predictions from NREL-Mid95by2035

- NREL-Mid95by2050: This 2040 scenario has the same assumptions as NREL-Mid scenario, but with 95% decarbonization of the national power sector by 2050 (Gagnon et al. 2021). The electricity prices from the P10 balancing area (Southern California) were used for this study. The average price is $42.00/MWh. There are spikes of high prices during the summer. Highly-fluctuating low electricity prices are available during the spring time.

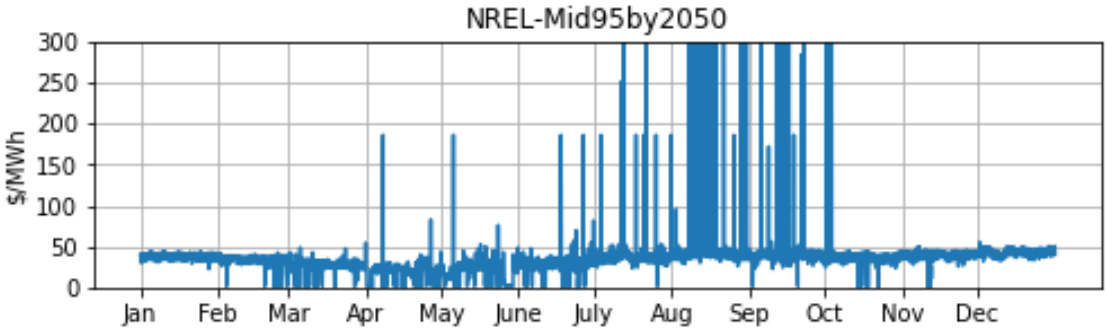

Figure 6.5: Electricity Price Predictions from NREL-Mid95by2050

- Princeton-BaseCaseTax: This 2030 prediction is based on the US-wide aggregate load and existing capacity with Carbon Tax of $60/tonne (Jesse D Jenkins 2021). It assumes AEO2020 REF natural gas prices and ATB2020 mid costs for all resources. The average price is $47.69/MWh. There are high fluctuations throughout the year. The prices are generally higher during the summer.

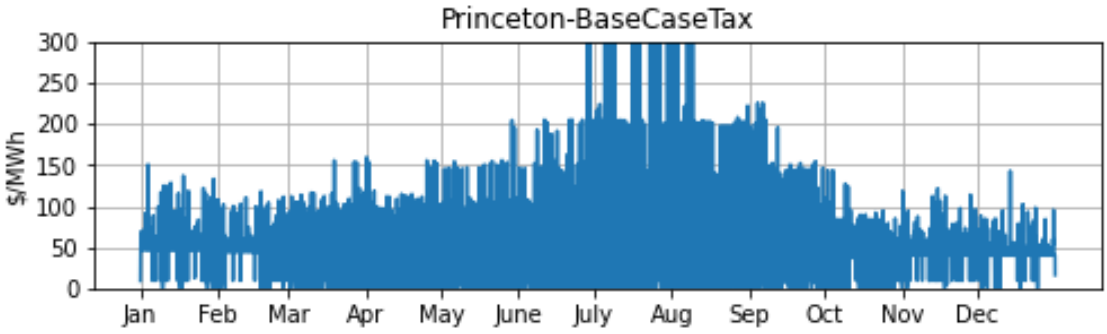

Figure 6.6: Electricity Price Predictions from Princeton-BaseCaseTax

- Princeton-HighWindTax: This 2030 prediction is based on the US-wide aggregate load and existing capacity with Carbon Tax of $60/tonne (Jesse D Jenkins 2021). It assumes AEO2020 REF natural gas prices and ATB2020 low costs for new wind clusters. The average price is $45.06/MWh. There are high fluctuations throughout the year. The prices are generally higher during the summer.

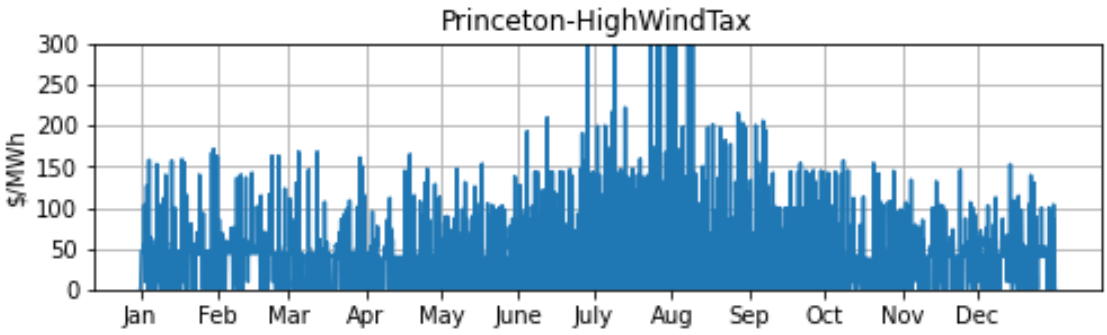

Figure 6.7: Electricity Price Predictions from Princeton-HighWindTax

- Princeton-HighSolarTax: This 2030 prediction is based on the US-wide aggregate load and existing capacity with Carbon Tax of $60/tonne (Jesse D Jenkins 2021). It assumes AEO2020 REF natural gas prices and ATB2020 low costs for new solar clusters. The average price is $45.43/MWh. There are high fluctuations throughout the year. The prices are generally higher during the summer.

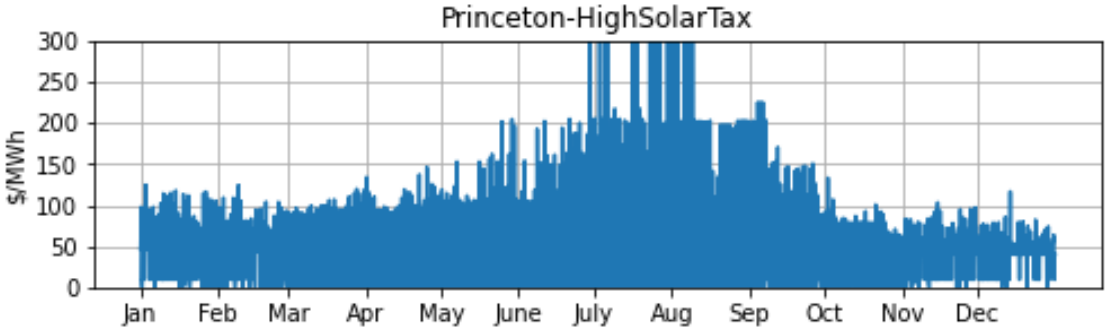

Figure 6.8: Electricity Price Predictions from Princeton-HighSolarTax

- NREL-MiNg_$100_CAISO: This NREL scenario predicts 2035 electricity prices for California Independent System Operator (CAISO) region based on ATB2020 mid technology costs and AEO2020 reference load projections with carbon tax of $100/tonne (Cohen and Durvasulu 2021). The average price is $53.08/MWh. There are high fluctuations throughout the year. The prices are generally higher during the summer.

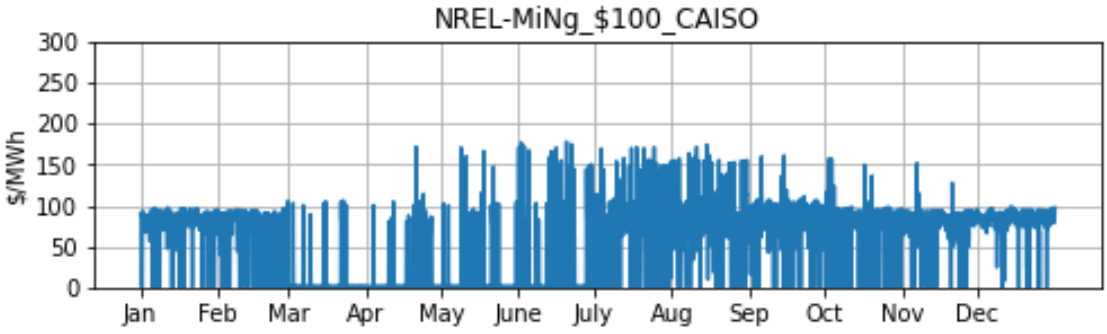

Figure 6.9: Electricity Price Predictions from NREL-MiNg_$100_CAISO

- NREL-MiNg_$150_CAISO: This NREL scenario predicts 2035 electricity prices for California Independent System Operator (CAISO) region based on ATB2020 mid technology costs and AEO2020 reference load projections with carbon tax of $150/tonne (Cohen and Durvasulu 2021). The average price is $45.54/MWh. There are high fluctuations throughout the year. Low electricity prices are available during the spring time. The prices are generally higher during the summer.

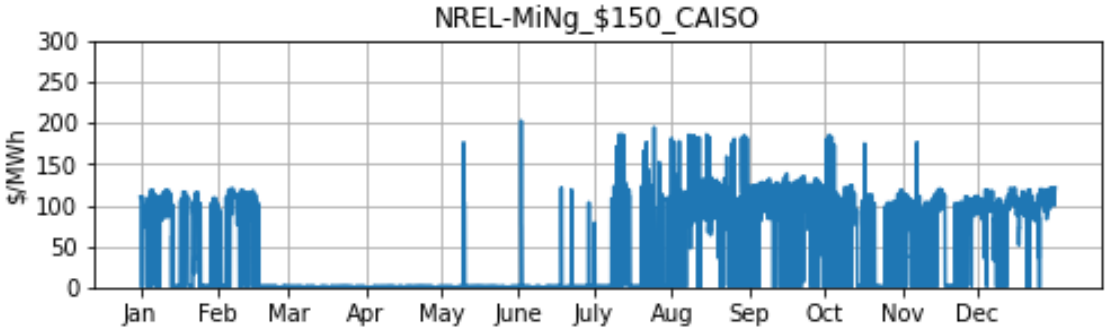

Figure 6.10: Electricity Price Predictions from NREL-MiNg_$150_CAISO

- NREL-MiNg_$100_ERCOT: This NREL scenario predicts 2035 electricity prices for Electric Reliability Council of Texas (ERCOT) region based on ATB2020 mid technology costs and AEO2020 reference load projections with carbon tax of $100/tonne (Cohen and Durvasulu 2021). The average price is $33.76/MWh. There are high fluctuations throughout the year. Low electricity prices are available during the spring time. The prices are generally higher during the summer.

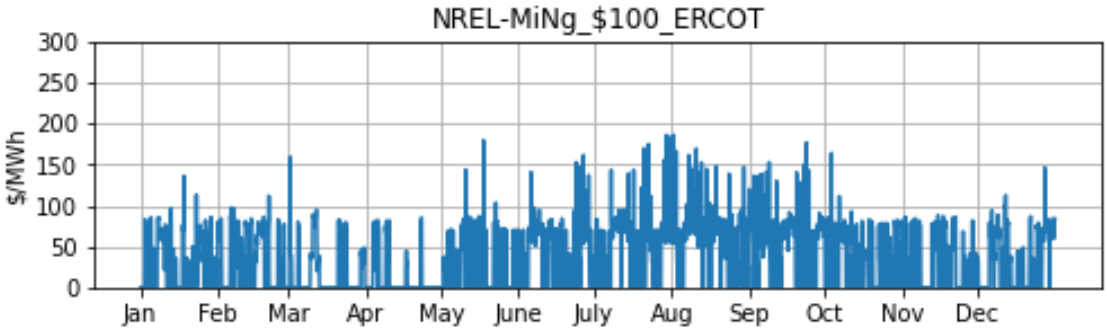

Figure 6.11: Electricity Price Predictions from NREL-MiNg_$100_ERCOT

- NREL-MiNg_$150_ERCOT: This NREL scenario predicts 2035 electricity prices for Electric Reliability Council of Texas (ERCOT) region based on ATB2020 mid technology costs and AEO2020 reference load projections with carbon tax of $150/tonne (Cohen and Durvasulu 2021). The average price is $36.34/MWh. There are high fluctuations throughout the year. Low electricity prices are available during the spring time. The prices are generally higher during the summer.

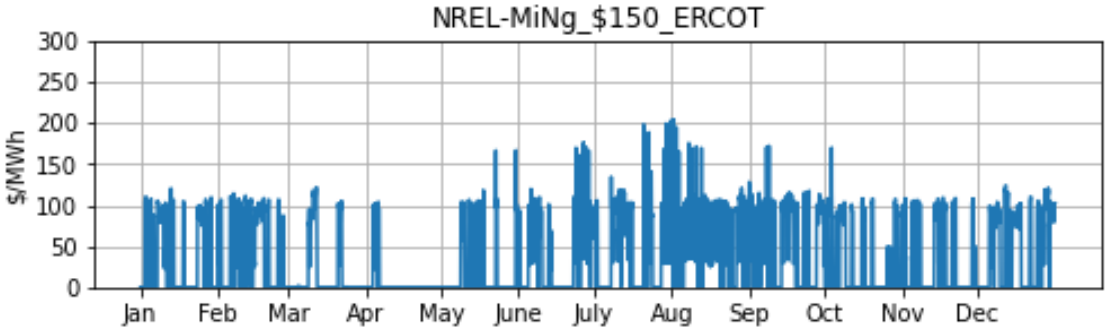

Figure 6.12: Electricity Price Predictions from NREL-MiNg_$150_ERCOT

- NREL-MiNg_$100_MISO-W: This NREL scenario predicts 2035 electricity prices for Midcontinent Independent System Operator (MISO) region based on ATB2020 mid technology costs and AEO2020 reference load projections with carbon tax of $100/tonne (Cohen and Durvasulu 2021). The average price is $35.22/MWh. There are high fluctuations throughout the year. Low electricity prices are available during the spring time. The prices are generally higher during the summer.

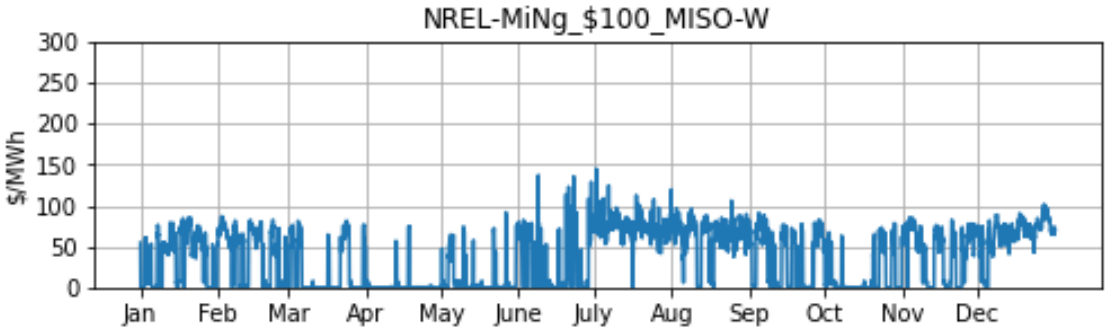

Figure 6.13: Electricity Price Predictions from NREL-MiNg_$100_MISO-W

- NREL-MiNg_$150_MISO-W: This NREL scenario predicts 2035 electricity prices for Midcontinent Independent System Operator (MISO) region based on ATB2020 mid technology costs and AEO2020 reference load projections with carbon tax of $150/tonne (Cohen and Durvasulu 2021). The average price is $28.28/MWh. There are high fluctuations throughout the year. Low electricity prices are available during the spring and fall. The prices are generally higher during the summer.

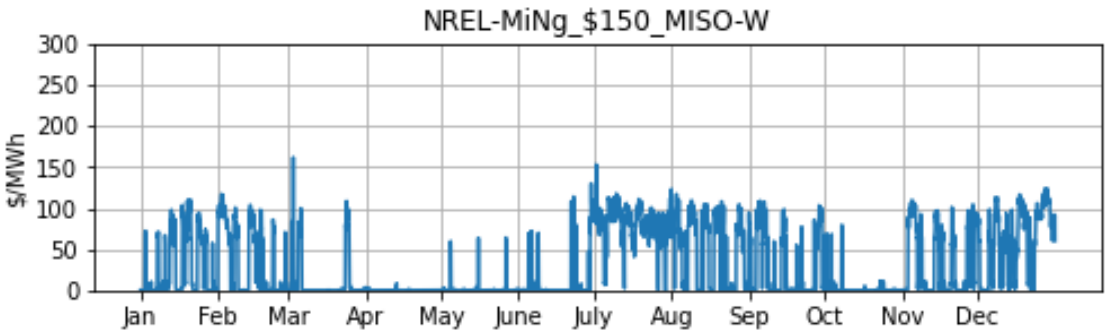

Figure 6.14: Electricity Price Predictions from NREL-MiNg_$150_MISO-W

- NREL-MiNg_$100_NYISO: This NREL scenario predicts 2035 electricity prices for New York Independent System Operator (NYISO) region based on ATB2020 mid technology costs and AEO2020 reference load projections with carbon tax of $100/tonne (Cohen and Durvasulu 2021). The average price is $35.33/MWh. There are high fluctuations throughout the year. Low electricity prices are available during the spring and fall. The prices are generally higher during the summer.

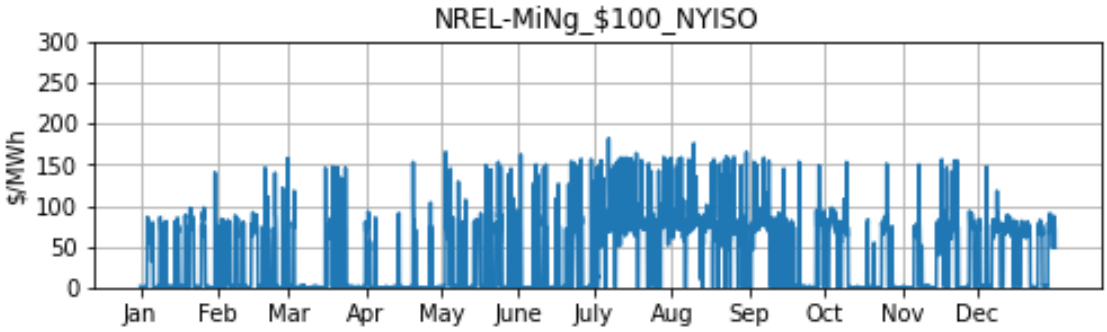

Figure 6.15: Electricity Price Predictions from NREL-MiNg_$100_NYISO

- NREL-MiNg_$150_NYISO: This NREL scenario predicts 2035 electricity prices for New York Independent System Operator (NYISO) region based on ATB2020 mid technology costs and AEO2020 reference load projections with carbon tax of $150/tonne (Cohen and Durvasulu 2021). The average price is $33.84/MWh. There are high fluctuations throughout the year. Low electricity prices are available during the spring and fall. The prices are generally higher during the summer.

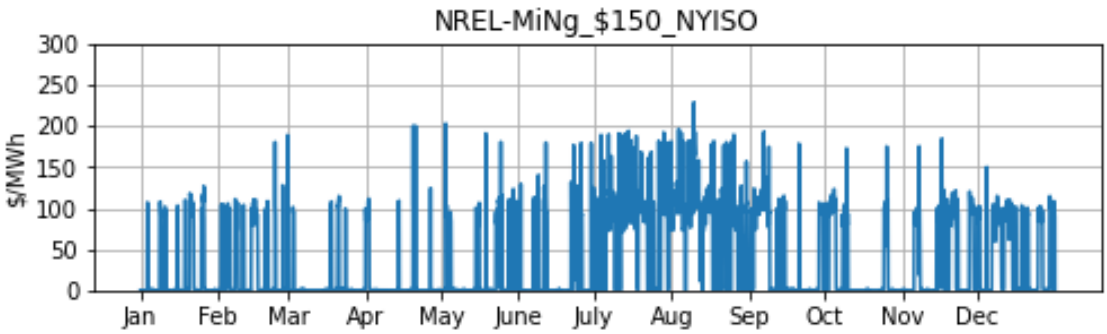

Figure 6.16: Electricity Price Predictions from NREL-MiNg_$150_NYISO

- NREL-MiNg_$100_PJM-W: This NREL scenario predicts 2035 electricity prices for Pennsylvania-New Jersey-Maryland (PJM) region based on ATB2020 mid technology costs and AEO2020 reference load projections with carbon tax of $100/tonne (Cohen and Durvasulu 2021). The average price is $42.00/MWh. Slightly lower electricity prices are available during the spring. There are spikes of high prices during the summer.

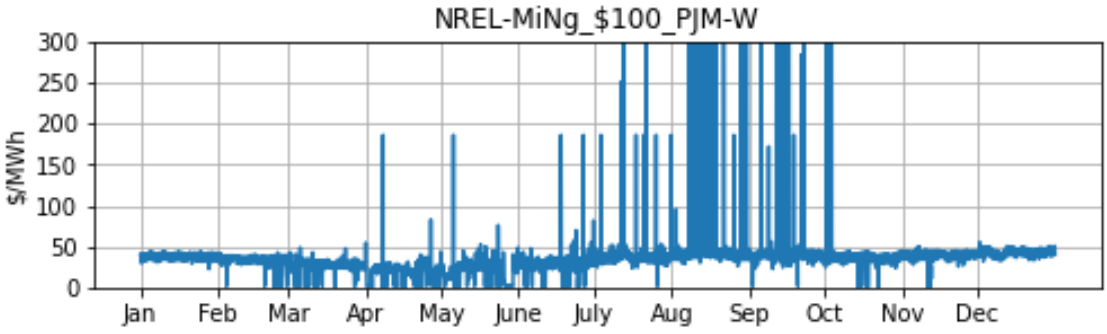

Figure 6.17: Electricity Price Predictions from NREL-MiNg_$100_PJM-W

- NREL-MiNg_$150_PJM-W: This NREL scenario predicts 2035 electricity prices for Pennsylvania-New Jersey-Maryland (PJM) region based on ATB2020 mid technology costs and AEO2020 reference load projections with carbon tax of $150/tonne. The average price is $49.94/MWh. There are high fluctuations throughout the year. Low electricity prices are available during the spring and fall. The prices are generally higher during the summer.

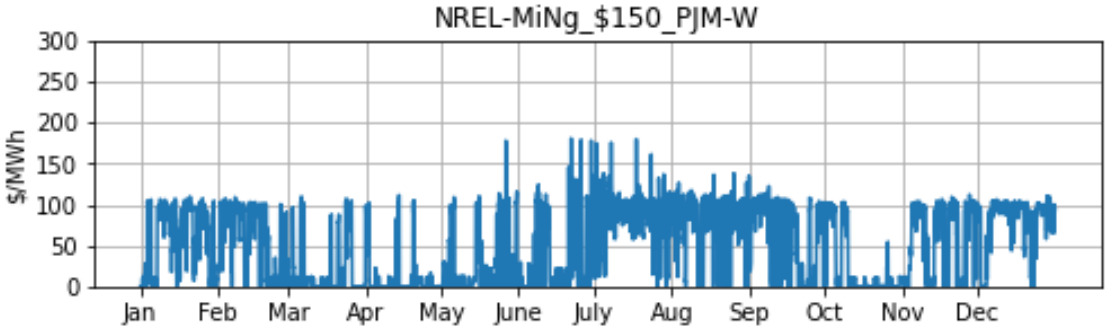

Figure 6.18: Electricity Price Predictions from NREL-MiNg_$150_PJM-W

6.3 Future Electrolyzer Performance

Improvements in the electrolyzer performance and efficiency can come from a number of different factors. First, the membrane thickness can be decreased to reduce the ohmic resistance of the cell while maintaining the mechanical strength to support safe and reliable operations. Second, catalyst layers can be better optimized to improve reaction kinetics while reducing the amount of platinum and iridium loadings (IRENA 2020).

In this study, a moderate improvement in the electrolyzer performance was assumed. In particular, it was assumed that future advancements in membrane design and manufacturing processes would allow the use of a 127-μm membrane (same thickness as Nafion 115) in a wide variety of operating conditions, including dynamic operations and differential-pressure operations. Furthermore, it was assumed that the same level of reaction kinetics could be achieved with lower catalyst loadings in light of the iridium supply issue that can stifle the future deployment of PEM electrolyzers (Minke et al. 2021). In terms of the operating conditions, the electrolyzer was assumed to operate at a differential pressure of 30 bar, removing the need for a separate mechanical compression system. Finally, a minimum current density limit of 0.5 A/cm^2 was assumed in order to minimize gas crossover during differential pressure operations (Schalenbach et al. 2013).

Table 6.3: Electrolyzer Model Parameters for Future Simulations (IRENA 2020)

Parameters	Current Value	Future Value	Units
Membrane Thickness, t	178	127	μm
Temperature, T	80	80	°C
Cathode Pressure, P_{cat}	1	30	bar
Anode Pressure, P_{an}	1	1	bar
Minimum Current Density	0	0.5	A/cm^2

The corresponding polarization curve (blue) is plotted against other benchmark systems from (Buttler and Spliethoff 2018) in Figure 6.19.

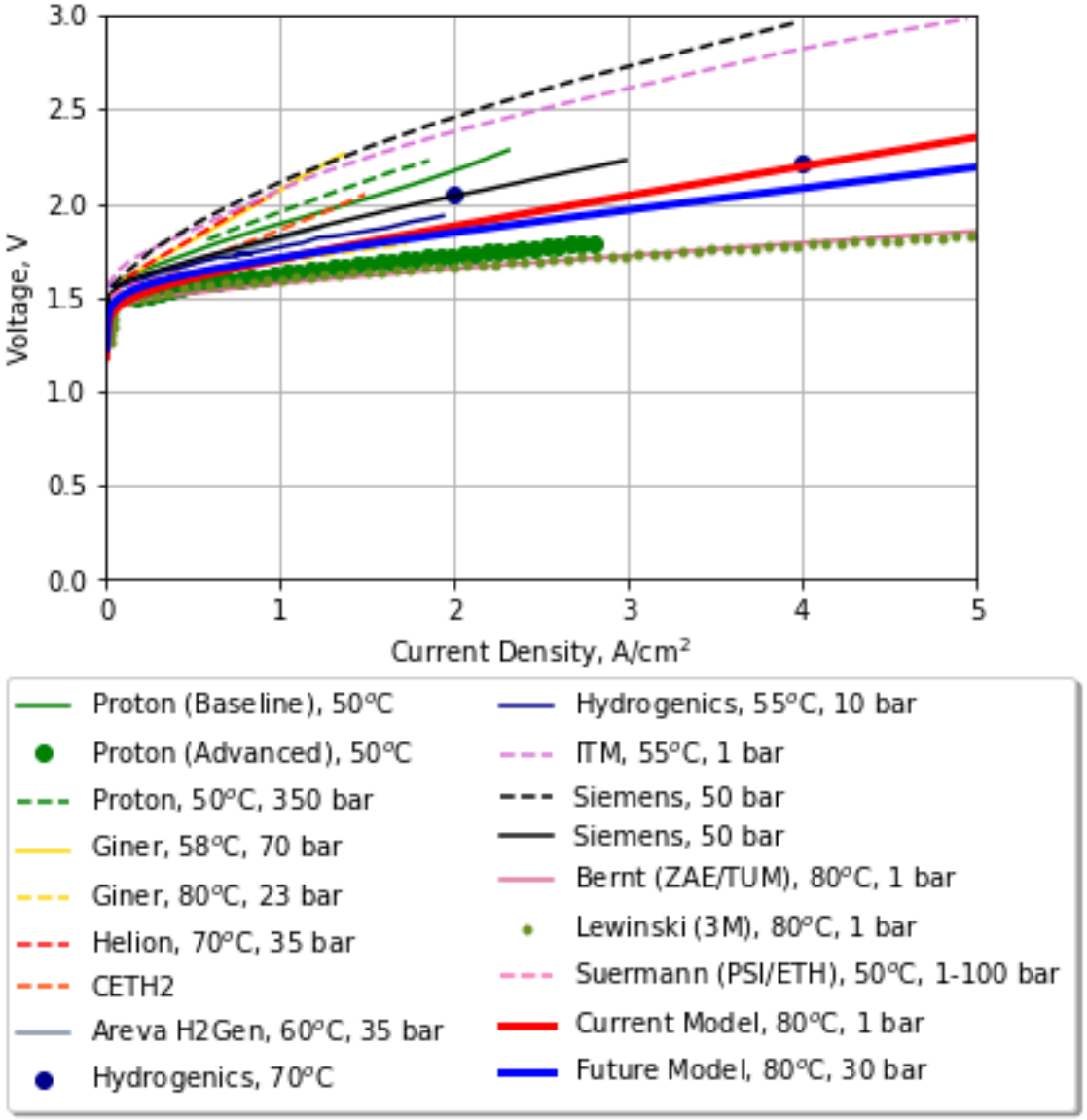

Figure 6.19: Polarization curve showing voltage as a function current density for the future electrolyzer model (blue) and the current electrolyzer model (red) against other PEM electrolyzer IV curves from the literature. Figure adopted from (Buttler and Spliethoff 2018)

6.4 LCOH Projection

Based on 2 future capital cost scenarios, 18 different electricity price projections, projected improvements in electrolyzer performance, and 3 different maximum current density designs, a total of 108 LCOH estimates were developed using the techno-economic model developed in this study. The list below summarizes the experimental design for each parameter.

- CAPEX (2 designs)
    - Future ($618/kW)
    - Future Optimistic ($421/kW)
- Electricity Price Projections (18 designs)
    - 5 2040-Projections for the balancing area 10 (Southern California) from NREL (Gagnon et al. 2021)
    - 3 2030-Projections from Princeton (Jesse D Jenkins 2021)
    - 10 2035-Projections for different grid operators from NREL (Cohen and Durvasulu 2021)
- Electrolyzer Performance (1.97 V at 3 A/cm^2)
- Maximum Current Density (3 designs)
    - 3 A/cm^2
    - 4 A/cm^2
    - 5 A/cm^2
- Minimum Current Density
    - 0.5 A/cm^2

Figure 6.20 shows LCOH projections as a function of average electricity price. Each vertical line (of the same color) represents one electricity forecast scenario. It can be seen that the future optimistic CAPEX scenarios always result in lower LCOHs than the future scenarios, with everything else equal. Furthermore, higher current density designs produce lower LCOHs than lower current density designs: Economic gains from producing more hydrogen during the low-price hours more than make up for the losses in efficiency that ensue from operating at high current density. The general trend of the scatterplot shows that the average electricity price strongly influences the LCOH.

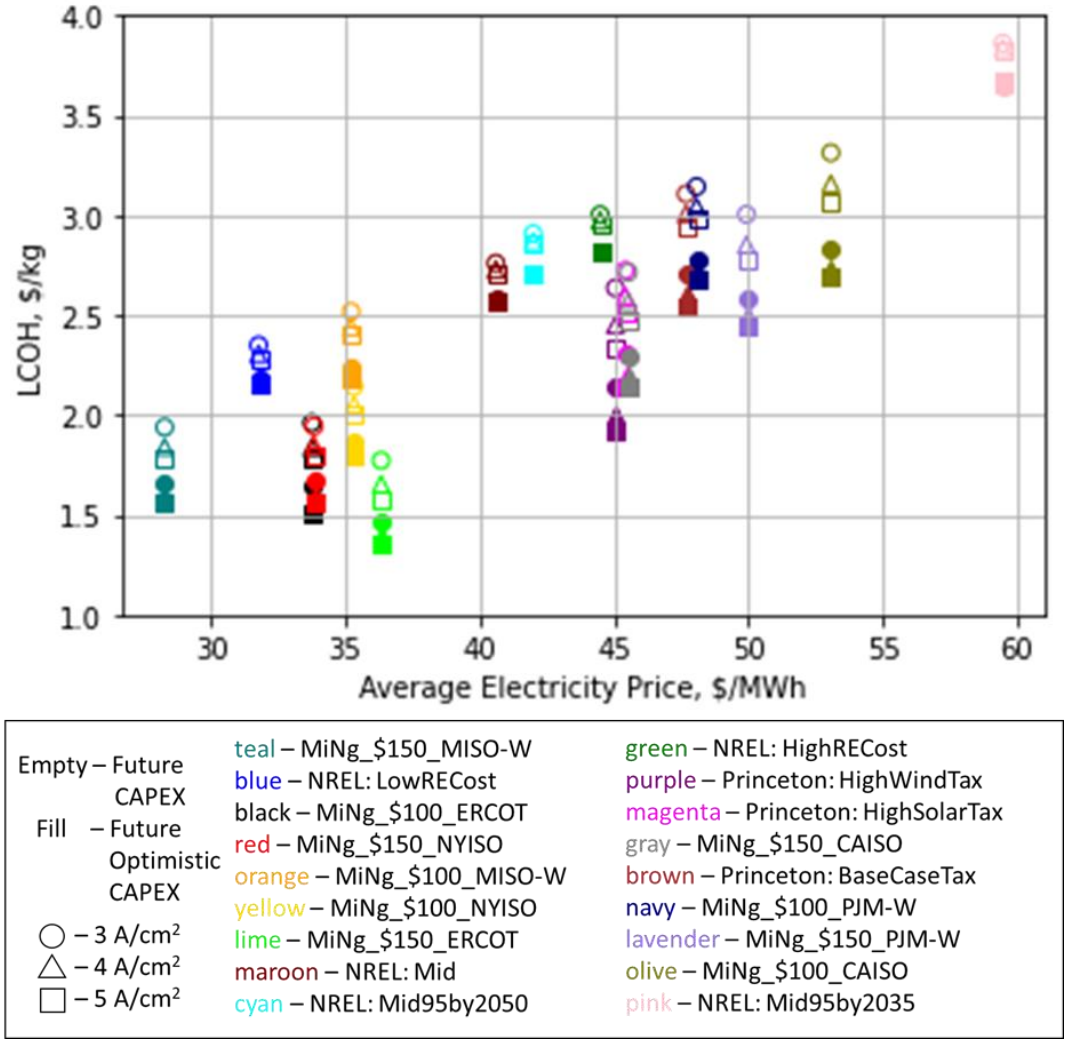

Figure 6.20: LCOH projection as a function of the average electricity price for future electrolyzer systems under various assumptions, including reduced capital costs (empty vs filled), electricity price projection (different colors), electrolyzer performance improvement, and maximum current density design (shapes).

Figure 6.21 shows LCOH projections as a function of the number of hours with electricity price less than $5/MWh in each electricity price forecast. The number of low-price hours is a proxy for the average electricity price. The higher the number of low-price hours, the more opportunities for dynamic operations to produce affordable hydrogen.

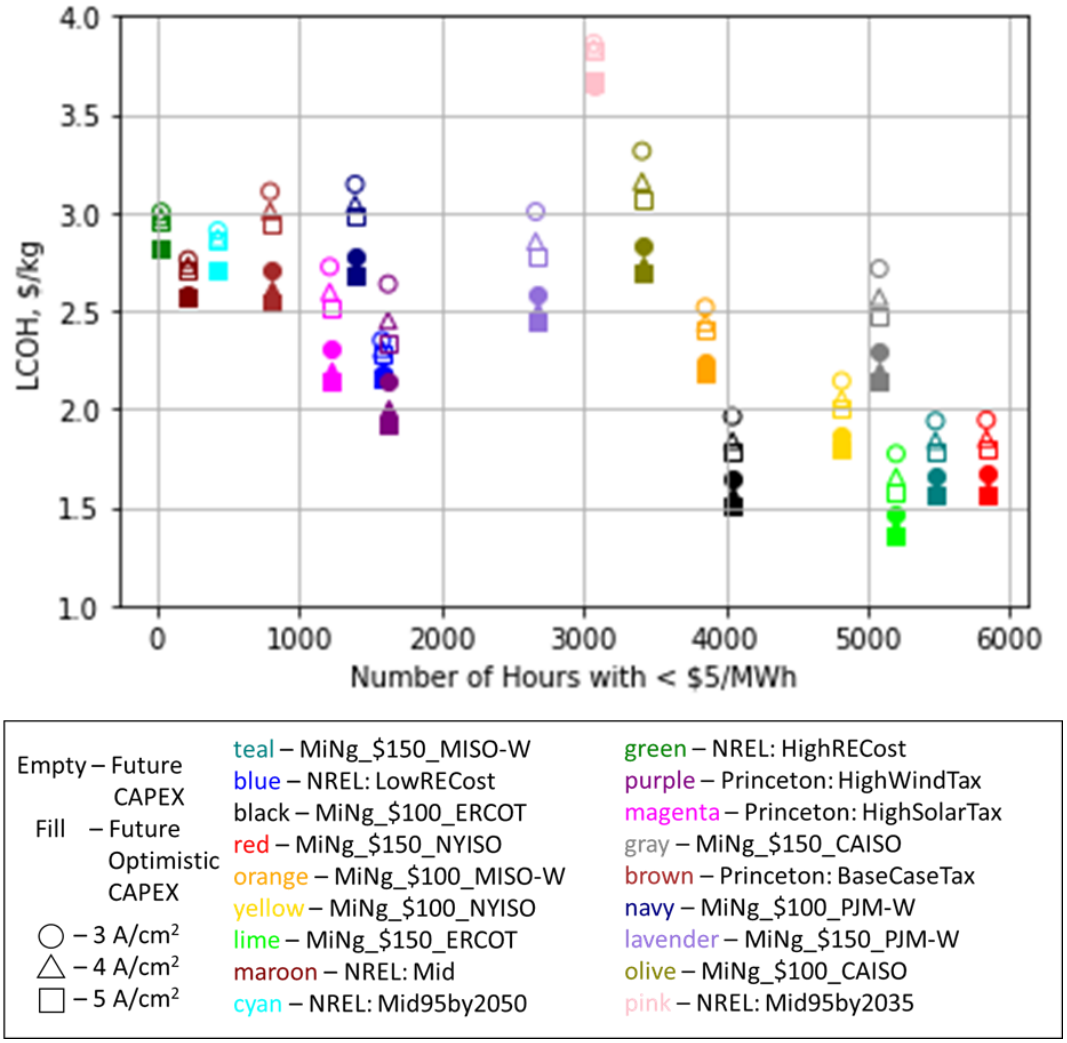

Figure 6.21: LCOH projection as a function of the number of hours with price less than $5/MWh for future electrolyzer systems under various assumptions, including reduced capital costs (empty vs filled), electricity price projection (different colors), electrolyzer performance improvement, and maximum current density design (shapes).

Figure 6.22 shows LCOH projections as a function of the number of hours with electricity price more than $100/MWh in each electricity price forecast. It can be seen that there is no apparent trend in the scatterplot. Dynamic operations insulate the electrolyzer system from high electricity prices by reducing the load or completely shutting off the system. During this time, the hydrogen demand is met by dispensing hydrogen from the storage facility.

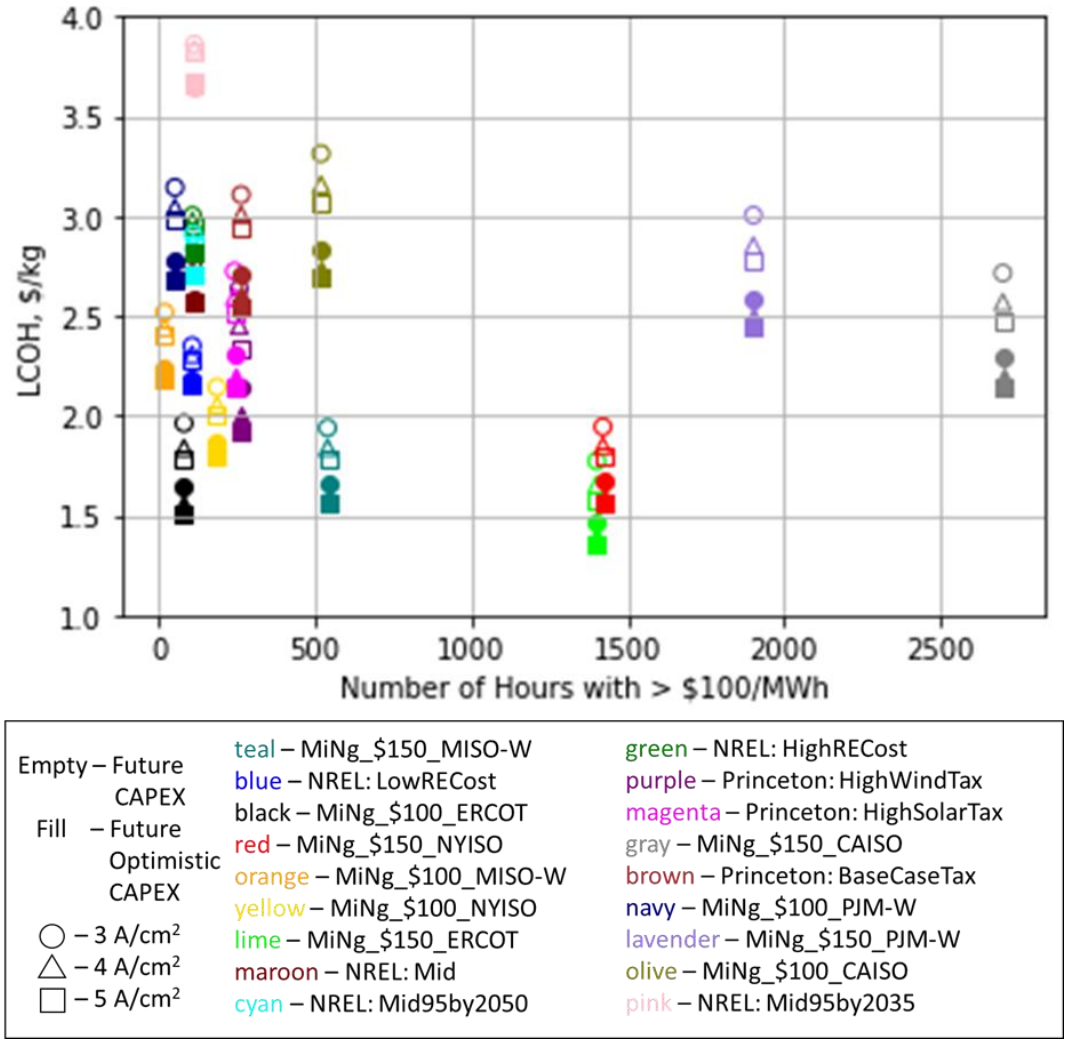

Figure 6.22: LCOH projection as a function of the number of hours with price greater than $100/MWh for future electrolyzer systems under various assumptions, including reduced capital costs (empty vs filled), electricity price projection (different colors), electrolyzer performance improvement, and maximum current density design (shapes).

In order to unlock the full potential of dynamic operations, the electrolyzer system must be equipped with a large enough production capacity to produce and store excess hydrogen when the electricity prices are low. To that effect, Figure 6.23 shows that the LCOHs tend to go down with higher normalized capacity. In most cases, the production capacity is less than 3 times the nominal production target. However, under some circumstances, a production capacity as big as 4 times the nominal production target may be necessary.

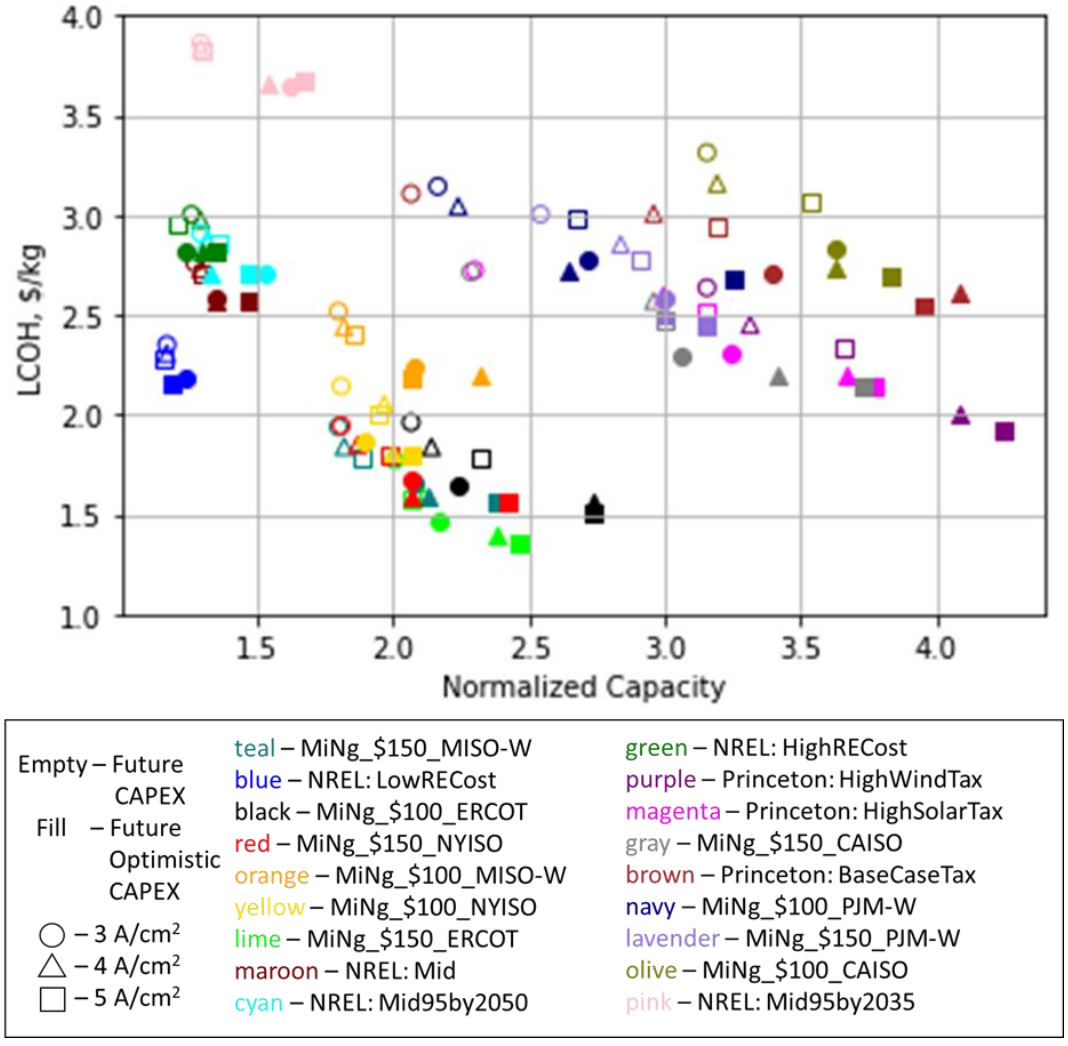

Figure 6.23: LCOH projection as a function of normalized capacity for future electrolyzer systems under various assumptions, including reduced capital costs (empty vs filled), electricity price projection (different colors), electrolyzer performance improvement, and maximum current density design (shapes).

As the production capacity gets oversized, however, the capacity utilization goes down. In steady operations, a high capacity utilization is necessary to achieve favorable economics. However, in dynamic operations, a high capacity is not desirable as it forces the electrolyzer to operate during the high-price hours. A one-week sample of an optimized case running with Future Optimistic CAPEX, MiNg_$150_ERCOT electricity forecast, and a maximum current density of 3 A/cm^2 is shown in Figure 6.24. It can be seen that the electrolyzer only operates when the electricity price is economical to do so. Capacity utilization during this one-week period is 71%. In fact, it is precisely the flexibility afforded by the extra capacity (and low utilization rate) that allows the electrolyzer to produce hydrogen at a low LCOH, in this case $1.49/kg.

It is also important to point out that the model is honoring all the constraints that have been implemented in the optimization model. The operating current density is between 0.5 A/cm^2 and 3 A/cm^2 unless the electrolyzer is completely shut off at 0 A/cm^2. It also honors the maximum storage capacity of 207 tonne that is set by the optimization engine. Finally, the amount of hydrogen that is being delivered is exactly the target rate.

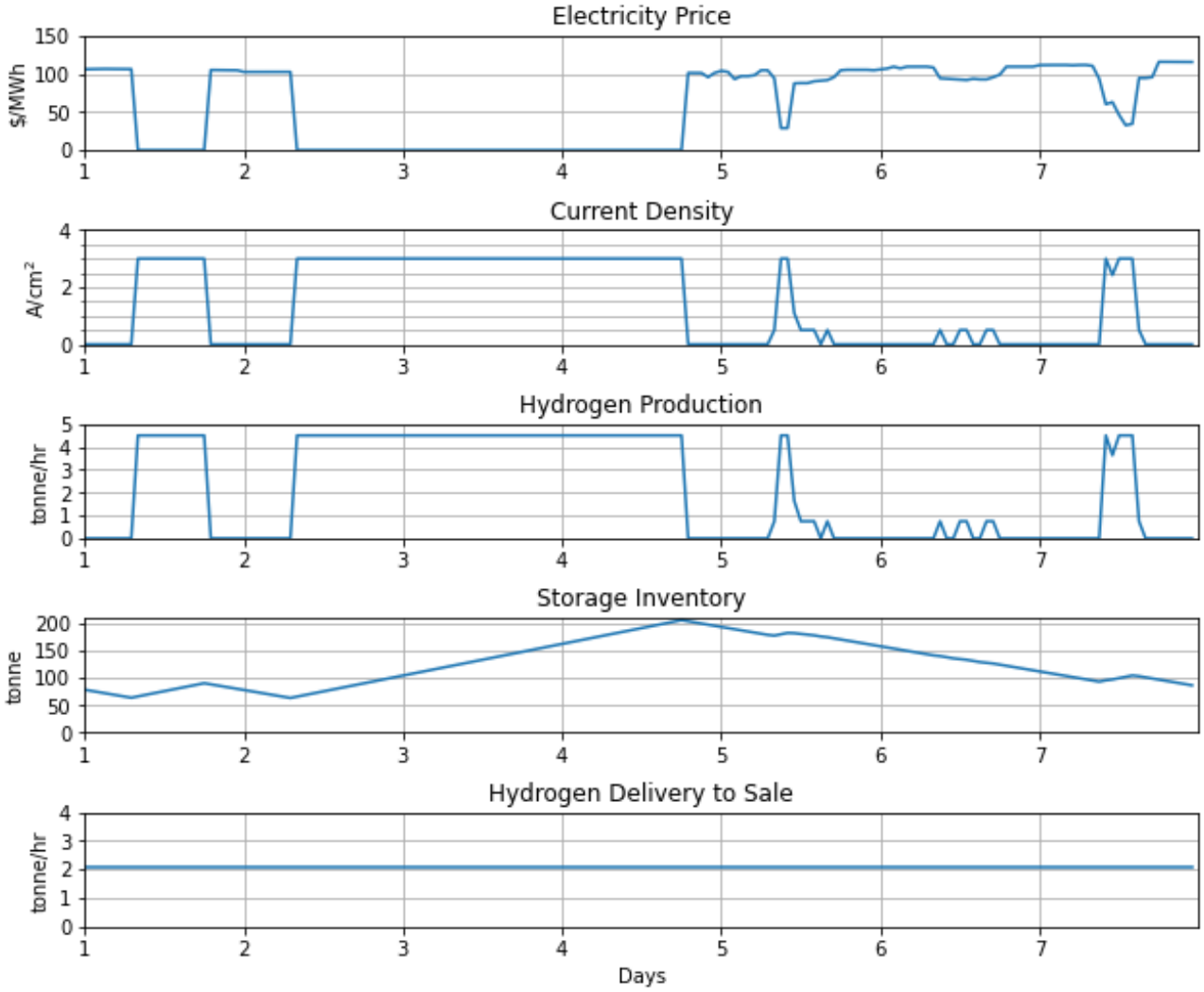

Figure 6.24: One week sample of electricity price, current density, hydrogen production, storage inventory, and hydrogen delivery to sale as a function time for an optimized case running with future optimistic CAPEX, MiNg_$150_ERCOT electricity forecast, and a maximum current density of 3 A/cm².

Finally, dynamical operations responding to volatile electricity prices need to be supported with more storage, as can be seen in Figure 6.25. As the number of low-price hours increases, the model is incentivized to produce and store more hydrogen for a future use. This is precisely what happens in Figure 6.24. During the first four days, there are many hours with low electricity prices, so the electrolyzer produces excess amount of hydrogen and puts it into storage. As a result, the storage inventory goes up during this

time until it hits the capacity. From the fifth day and on, the electricity prices are high. Instead of producing the targeted amount of hydrogen, the electrolyzer system draws hydrogen from the storage facility to meet the demand rate. As a result, the storage inventory goes down from day 5 to day 7.

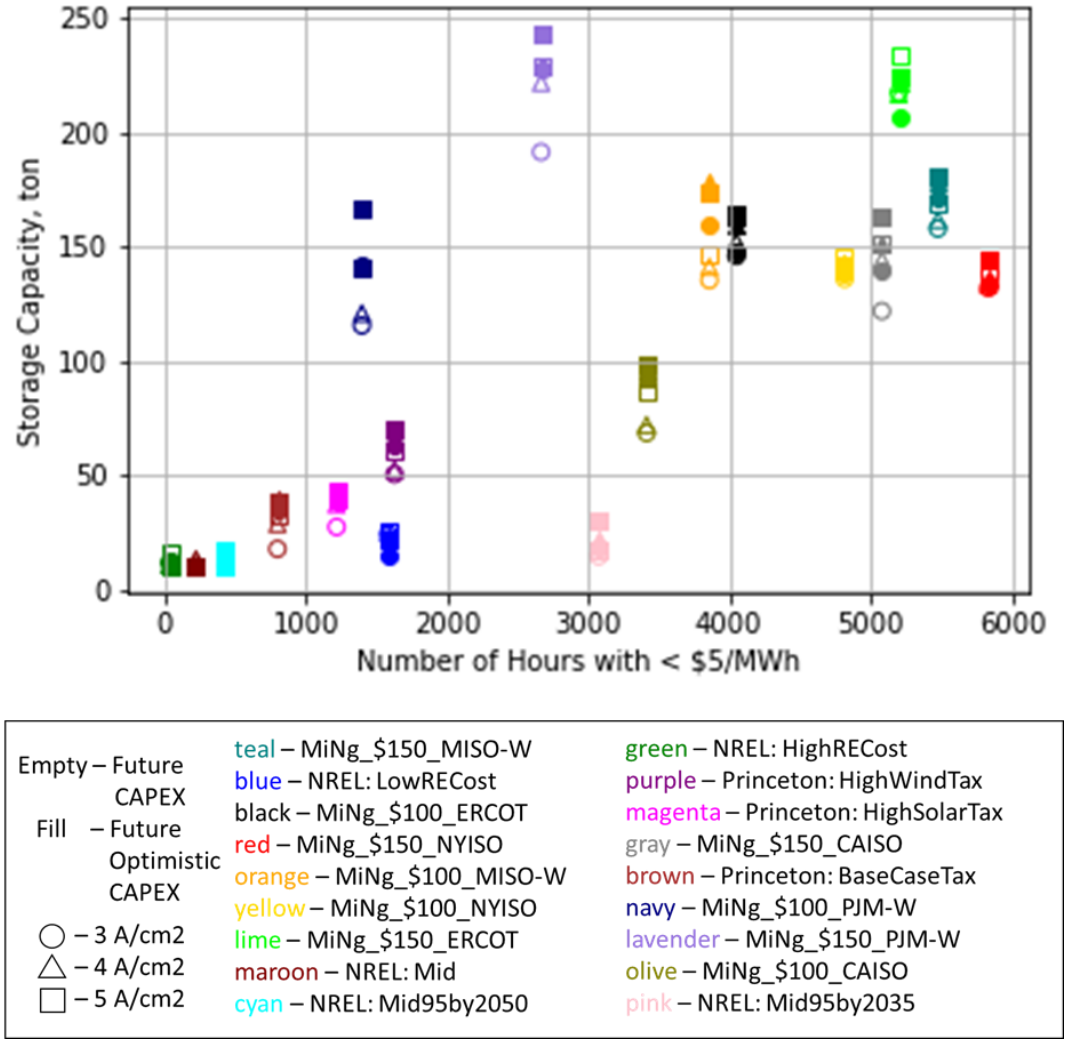

Figure 6.25: Storage capacity as a function of the number of hours with price less than $5/MWh for future electrolyzer systems under various assumptions, including reduced capital costs (empty vs filled), electricity price projection (different colors), electrolyzer performance improvement, and maximum current density design (shapes).

These trends provide several interesting directions to reduce the production cost of hydrogen:

- Low electricity price is an absolute requirement for producing low-cost hydrogen. According to this analysis, an average electricity price of less than $45/MWh is required to even have a chance at reaching a LCOH of $2/kg H_2 while an average price of less than $40/MWh is desirable. More integration of cheap renewable electricity sources would be the right step forward to achieve this feat. For example, in Figure 6.20, NREL's mid case scenario breaks below the $40/MWh mark only with the assumption of low renewable energy cost.

- High capacity utilization is not needed for a low LCOH during dynamic operations. The capacity utilization for the lowest cost scenario was 69%. In fact, strategically decreasing the capacity utilization by oversizing the electrolyzer capacity and storage size allows dynamic operations to more effectively capitalize on the low-electricity-price hours.

- A specific CAPEX of $600/kW or less would be necessary to break below $2.0/kg.

- The electrolyzer must be able to operate at a high current density, preferably more than 3 A/cm^2 without compromising efficiency.

As mentioned previously, these results do not reflect some critical technical and operational challenges with highly dynamic operations. These challenges include degradation, thermal response, and hydrogen crossover which have not been incorporated into the electrolyzer model in this study. Therefore, a future study should look into how to operationalize the findings of this study with a focus on minimizing the safety and reliability issues coming from degradation, thermal response, and hydrogen crossover.

6.5 Benefits of Direct Electrochemical Compression

In Chapter 4 and Chapter 5, the economics of direct electrochemical compression fell short to a hybrid compression model. In order to assess the benefits of differential pressure operations in a more favorable electrolytic hydrogen production scenario (i.e. low electricity prices, low electrolyzer system CAPEX), a scenario based on an electrolyzer model operating at a current density between 0.5 and 3 A/cm^2 with the future-optimistic CAPEX and MiNg_$150_ERCOT electricity scenario was used to evaluate the effect of cathode pressure on LCOH. Table 6.4 and Figure 6.26 show that direct electrochemical compression to 30 bar is the cheapest mode of operation in this scenario.

Table 6.4: Effect of Cathode Pressure on LCOH in a Low-Cost Future Scenario

Cathode Pressure (bar)	Electrolysis LCOH ($/kg H_2)	Compression LCOH ($/kg H_2)	Total LCOH ($/kg H_2)	Normalized Capacity
1	1.37	0.30	1.67	2.08
5	1.39	0.17	1.56	2.05
10	1.41	0.12	1.53	2.12
20	1.45	0.05	1.50	2.15
30	1.49	0.00	1.49	2.09

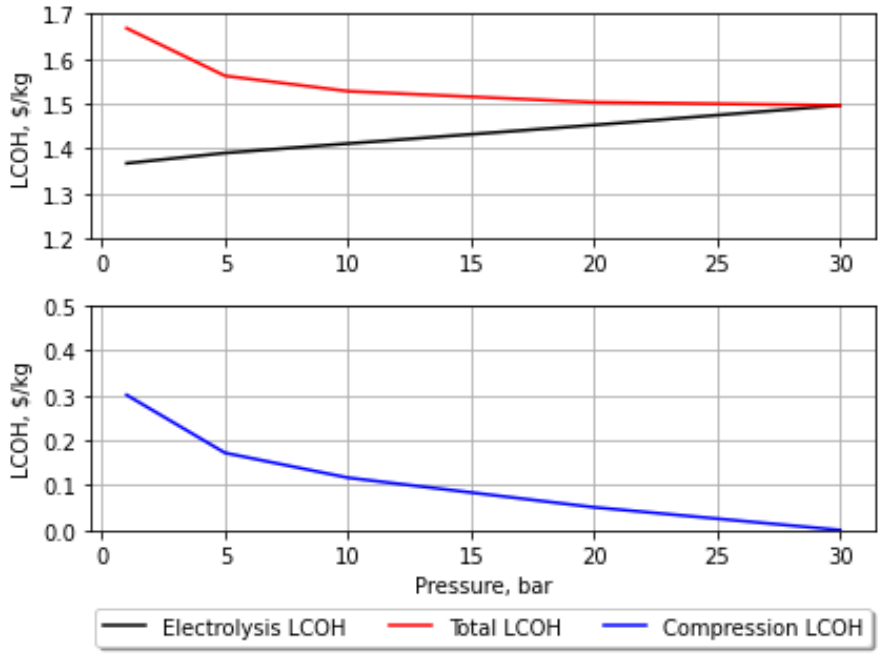

Figure 6.26: Electrolysis LCOH (black), Compression LCOH (blue), and Total LCOH (red) as a function of operating pressure during dynamic operations in a low-cost future scenario.

6.6 References

Buttler, Alexander, and Hartmut Spliethoff. 2018. "Current Status of Water Electrolysis for Energy Storage, Grid Balancing and Sector Coupling via Power-to-Gas and Power-to-Liquids: A Review." *Renewable and Sustainable Energy Reviews* 82 (February): 2440–54. https://doi.org/10.1016/j.rser.2017.09.003.

Cohen, Stuart; Durvasulu, Venkat. 2021. "NREL Price Series Developed for the ARPA-E FLECCS Program." National Renewable Energy Laboratory. 10.7799/1838046

Cole, Wesley, Sean Corcoran, Nathaniel Gates, Trieu Mai, and Paritosh Das. 2020. "2020 Standard Scenarios Report: A U.S. Electricity Sector Outlook." *Renewable Energy*, 51.

Gagnon, Pieter; Frazier, Will; Cole, Wesley; Schwarz, Marty; Hale, Elaine. 2021. "Cambium data for 2021 Standard Scenarios." National Renewable Energy Laboratory. https://cambium.nrel.gov/.

Glenk, Gunther, and Stefan Reichelstein. 2019. "Economics of Converting Renewable Power to Hydrogen." *Nature Energy* 4 (3): 216–22. https://doi.org/10.1038/s41560-019-0326-1.

IEA. 2021. "Global Hydrogen Review 2021." IEA, Paris https://www.iea.org/reports/global-hydrogen-review-2021.

IRENA. 2020. "Green Hydrogen Cost Reduction: Scaling up Electrolyzers to Meet the 1.5C Climate Goal." International Renewable Energy Agency, Abu Dhabi.

Jesse D Jenkins, Sambuddha Chakrabarti. 2021. "Summary Report of the GenX and PowerGenome Runs for Generating Price Series (for ARPA-E FLECCS Project)." Zenodo. https://doi.org/10.5281/ZENODO.5765798.

Lagadec, Marie Francine, and Alexis Grimaud. 2020. "Water Electrolysers with Closed and Open Electrochemical Systems." *Nature Materials* 19 (11): 1140–50. https://doi.org/10.1038/s41563-020-0788-3.

McQueen, Shawna, Stanford, Joseph, Satyapal, Sunita, Miller, Eric, Stetson, Ned, Papageorgopoulos, Dimitrios, Rustagi, Neha, Arjona, Vanessa, Adams, Jesse, Randolph, Katie, Peterson, David, Hill, Laura, Koleva, Mariya, Reinhardt, Tim, Frye, Evan, Schrecengost, Robert, Kokkinos, Angelos, Litynski, John, Conrad, Regis, Soloveichik, Grigorii, Tew, David, Litzelman, Scott, Vetrano, John, Onuschak, Rebecca, Hahn, Alison, Hsieh, Eric, and Costa, Ryan. 2020. "Department of Energy Hydrogen Program Plan". United States. https://doi.org/10.2172/1721803. https://www.osti.gov/servlets/purl/1721803.

Minke, Christine, Michel Suermann, Boris Bensmann, and Richard Hanke-Rauschenbach. 2021. "Is Iridium Demand a Potential Bottleneck in the Realization of Large-Scale PEM Water Electrolysis?" *International Journal of Hydrogen Energy* 46 (46): 23581–90. https://doi.org/10.1016/j.ijhydene.2021.04.174.

Nikolaidis, Pavlos, and Andreas Poullikkas. 2017. "A Comparative Overview of Hydrogen Production Processes." *Renewable and Sustainable Energy Reviews* 67 (January): 597–611. https://doi.org/10.1016/j.rser.2016.09.044.

Saba, Sayed M., Martin Müller, Martin Robinius, and Detlef Stolten. 2018. "The Investment Costs of Electrolysis – A Comparison of Cost Studies from the Past 30 Years." *International Journal of Hydrogen Energy* 43 (3): 1209–23. https://doi.org/10.1016/j.ijhydene.2017.11.115.

Schalenbach, Maximilian, Marcelo Carmo, David L. Fritz, Jürgen Mergel, and Detlef Stolten. 2013. "Pressurized PEM Water Electrolysis: Efficiency and Gas Crossover." *International Journal of Hydrogen Energy* 38 (35): 14921–33. https://doi.org/10.1016/j.ijhydene.2013.09.013.

Spek, Mijndert van der, Catherine Banet, Christian Bauer, Paolo Gabrielli, Ward Goldthorpe, Marco Mazzotti, Svend T. Munkejord, et al. 2022. "Perspective on the Hydrogen Economy as a Pathway to Reach Net-Zero CO_2 Emissions in Europe." *Energy & Environmental Science* 15 (3): 1034–77. https://doi.org/10.1039/D1EE02118D.

Chapter 7
Conclusions

This thesis examined the economics of operating a PEM electrolyzer under various operating conditions using a techno-economic optimization model. The baseline LCOH for a 104-MW electrolyzer with the 2021 techno-economic parameters (i.e., a capital cost of $1,004/kW and an average electricity price of $52/MWh) in a steady operation mode was $4.93/kg, which was in agreement with estimates from other studies. When the electrolyzer was switched to a dynamic operation mode, the LCOH decreased by 9% to $4.48/kg as a result of increasing the plant capacity by 40% and dynamically varying the load.

The electrolyzer operating with a differential pressure of 1-30 bar was also evaluated based on the 2021 techno-economic parameters. The reduction in the compression cost with increasing pressure was offset by the increase in capital cost and electricity cost. The most economical case proved to be a hybrid system where hydrogen is compressed to 5 bar in direct electrochemical compression, followed by mechanical compression to 30 bar.

The current estimated LCOH of $4.48/kg is still far from being competitive with the cost of conventional production methods. However, the production costs of PEM electrolyzers are fast declining and the performance is improving as the membrane gets thinner and the catalyst layers are optimized. In addition, an increasing mix of cheap renewable energy means that more affordable electricity will be available for electrolysis in the future. These developments suggest that PEM electrolysis LCOH has room to fall in the future.

Based on the changes that are expected in the future, the model was used to explore various drivers that affect the LCOH of PEM electrolysis for 2035-2040. The resulting scatter ranging from $1.35/kg to $3.86/kg reflects the uncertainties that are inherent in projecting the future cost of hydrogen. Several interesting trends came out of this plot. First, the average electricity price should be less than $40/MWh for electrolysis to be cost-competitive. The electricity cost accounts for the majority of the total cost, so a low electricity price is crucial to realizing affordable green hydrogen. Second, dynamic operations are effective in a highly volatile price environment, suggesting that PEM electrolysis is an excellent fit for the future electricity market with a greater share of intermittent renewables. Regarding the electrolyzer design, the operators should expect to oversize the plant capacity by 2-3 times the production target to enable dynamic operations. In addition, future PEM electrolyzers should be capable of operating at higher current densities ranging from 3 to 5 A/cm^2.

This techno-economic assessment is by no means complete and offers directions for future studies. First, the electrolyzer model did not incorporate mass transport of reacting species, which is useful for understanding the crossover phenomenon and calculating the mass transport overpotential. Second, the model did not include any thermal behavior of the PEM electrolyzer components. It was assumed that all system components were in thermal equilibrium at the operating temperature. However, the PEM electrolyzer's thermal response can be an important limiter to how freely the load can be varied in dynamic operations. Third, there is no notion of degradation incorporated in the model. Typically, degradation worsens with operating time, high current densities, and load cycling. Therefore, an understanding of the degradation mechanism would be an

important consideration in deciding when to vary the load or not. Finally, reaching cost-parity with conventional methods requires a continued reduction in electrolyzer cost, improvement in performance, and more integration of cheap renewable energy. Therefore, research and development, industry investment, and government policy are indispensable pieces to the puzzle that unlocks the future of the green hydrogen economy and the decarbonized world.

APPENDIX

Single-Phase Region Enthalpy, kJ/kg

T	1 bar	2 bar	4 bar	6 bar	8 bar	10 bar	20 bar	40 bar	60 bar	80 bar	100 bar	120 bar	140 bar	160 bar	180 bar	200 bar	220 bar	240 bar	260 bar	280 bar	300 bar	400 bar	500 bar	600 bar	700 bar	800 bar	1000 bar
25	104.9	105	105.2	105.4	105.6	105.8	106.7	108.5	110.4	112.2	114.1	115.9	117.7	119.6	121.4	123.2	125	126.9	128.7	130.5	132.3	141.3	150.3	159.1	168	176.7	194.1
30	125.8	125.9	126.1	126.3	126.5	126.7	127.6	129.4	131.2	133	134.8	136.6	138.4	140.3	142.1	143.9	145.7	147.4	149.2	151	152.8	161.7	170.6	179.4	188.1	196.8	214
35	146.7	146.8	147	147.2	147.4	147.5	148.4	150.2	152	153.8	155.6	157.4	159.2	161	162.7	164.5	166.3	168.1	169.8	171.6	173.4	182.2	190.9	199.6	208.3	216.9	233.9
40	167.6	167.7	167.9	168.1	168.2	168.4	169.3	171.1	172.8	174.6	176.4	178.1	179.9	181.7	183.4	185.2	186.9	188.7	190.4	192.2	193.9	202.6	211.3	219.9	228.4	237	253.9
45	188.5	188.6	188.8	189	189.1	189.3	190.2	191.9	193.7	195.4	197.2	198.9	200.6	202.4	204.1	205.8	207.6	209.3	211	212.7	214.5	223.1	231.6	240.2	248.7	257.1	273.9
50	209.4	209.5	209.7	209.8	210	210.2	211.1	212.8	214.5	216.2	217.9	219.7	221.4	223.1	224.8	226.5	228.2	229.9	231.6	233.3	235.1	243.6	252	260.5	268.9	277.3	293.9
55	230.3	230.4	230.6	230.7	230.9	231.1	231.9	233.6	235.3	237	238.7	240.4	242.1	243.8	245.5	247.2	248.9	250.6	252.3	254	255.6	264.1	272.4	280.8	289.1	297.4	314
60	251.2	251.3	251.5	251.6	251.8	252	252.8	254.5	256.2	257.9	259.5	261.2	262.9	264.5	266.2	267.9	269.6	271.2	272.9	274.6	276.2	284.6	292.9	301.1	309.4	317.6	334
65	272.1	272.2	272.4	272.6	272.7	272.9	273.7	275.4	277	278.7	280.3	282	283.6	285.3	287	288.6	290.3	291.9	293.6	295.2	296.9	305.1	313.3	321.5	329.7	337.8	354.1
70	293.1	293.2	293.3	293.5	293.6	293.8	294.6	296.3	297.9	299.5	301.2	302.8	304.4	306.1	307.7	309.3	311	312.6	314.2	315.9	317.5	325.6	333.8	341.9	350	358	374.2
75	314	314.1	314.3	314.4	314.6	314.7	315.6	317.2	318.8	320.4	322	323.6	325.2	326.8	328.5	330.1	331.7	333.3	334.9	336.5	338.1	346.2	354.2	362.3	370.3	378.3	394.3
80	335	335.1	335.2	335.4	335.5	335.7	336.5	338.1	339.7	341.3	342.9	344.5	346.1	347.6	349.2	350.8	352.4	354	355.6	357.2	358.8	366.8	374.7	382.7	390.6	398.5	414.4
85	356	356.1	356.2	356.4	356.5	356.7	357.5	359	360.6	362.2	363.8	365.3	366.9	368.5	370	371.6	373.2	374.8	376.3	377.9	379.5	387.4	395.2	403.1	411	418.8	434.5
90	377	377.1	377.2	377.4	377.5	377.7	378.5	380	381.6	383.1	384.7	386.2	387.8	389.3	390.9	392.4	394	395.5	397.1	398.6	400.2	408	415.8	423.5	431.3	439.1	454.7
95	398	398.1	398.3	398.4	398.6	398.7	399.5	401	402.5	404.1	405.6	407.1	408.7	410.2	411.7	413.2	414.8	416.3	417.8	419.4	420.9	428.6	436.3	444	451.7	459.4	474.9

Single-Phase Region Entropy, kJ/(kg K)

T	1 bar	2 bar	4 bar	6 bar	8 bar	10 bar	20 bar	40 bar	60 bar	80 bar	100 bar	120 bar	140 bar	160 bar	180 bar	200 bar	220 bar	240 bar	260 bar	280 bar	300 bar	400 bar	500 bar	600 bar	700 bar	800 bar	1000 bar
25	0.3672	0.3672	0.3672	0.3671	0.3671	0.367	0.3667	0.3662	0.3657	0.3652	0.3646	0.3641	0.3636	0.363	0.3625	0.3619	0.3614	0.3608	0.3602	0.3597	0.3591	0.3562	0.3532	0.3501	0.347	0.3438	0.3372
30	0.4368	0.4367	0.4367	0.4366	0.4366	0.4365	0.4362	0.4356	0.435	0.4343	0.4337	0.4331	0.4325	0.4318	0.4312	0.4306	0.4299	0.4293	0.4287	0.428	0.4274	0.4241	0.4208	0.4174	0.414	0.4105	0.4034
35	0.5051	0.5051	0.505	0.505	0.5049	0.5048	0.5045	0.5038	0.5031	0.5024	0.5017	0.501	0.5003	0.4996	0.4989	0.4981	0.4974	0.4967	0.496	0.4953	0.4946	0.491	0.4873	0.4836	0.4799	0.4762	0.4686
40	0.5724	0.5724	0.5723	0.5722	0.5721	0.572	0.5717	0.5709	0.5701	0.5693	0.5686	0.5678	0.567	0.5662	0.5654	0.5646	0.5639	0.5631	0.5623	0.5615	0.5607	0.5568	0.5529	0.5489	0.5449	0.5409	0.5329
45	0.6386	0.6385	0.6385	0.6384	0.6383	0.6382	0.6378	0.6369	0.6361	0.6352	0.6344	0.6335	0.6327	0.6318	0.631	0.6301	0.6293	0.6284	0.6276	0.6267	0.6259	0.6216	0.6174	0.6132	0.6089	0.6047	0.5962
50	0.7038	0.7037	0.7036	0.7035	0.7034	0.7033	0.7029	0.702	0.701	0.7001	0.6992	0.6983	0.6974	0.6964	0.6955	0.6946	0.6937	0.6928	0.6919	0.691	0.69	0.6855	0.681	0.6765	0.672	0.6675	0.6586
55	0.7679	0.7679	0.7678	0.7677	0.7676	0.7675	0.767	0.766	0.765	0.764	0.763	0.7621	0.7611	0.7601	0.7591	0.7581	0.7572	0.7562	0.7552	0.7542	0.7533	0.7484	0.7437	0.7389	0.7342	0.7295	0.7202
60	0.8312	0.8311	0.831	0.8309	0.8308	0.8307	0.8302	0.8291	0.8281	0.827	0.8259	0.8249	0.8239	0.8228	0.8218	0.8207	0.8197	0.8187	0.8176	0.8166	0.8156	0.8105	0.8054	0.8004	0.7955	0.7905	0.7808
65	0.8935	0.8934	0.8933	0.8932	0.8931	0.893	0.8924	0.8913	0.8902	0.8891	0.888	0.8868	0.8857	0.8846	0.8835	0.8824	0.8813	0.8802	0.8792	0.8781	0.877	0.8716	0.8663	0.8611	0.8559	0.8507	0.8406
70	0.955	0.9549	0.9548	0.9547	0.9545	0.9544	0.9538	0.9526	0.9515	0.9503	0.9491	0.9479	0.9468	0.9456	0.9444	0.9433	0.9421	0.941	0.9398	0.9387	0.9376	0.9319	0.9264	0.9209	0.9155	0.9101	0.8996
75	1.0156	1.0155	1.0154	1.0152	1.0151	1.015	1.0144	1.0131	1.0119	1.0106	1.0094	1.0082	1.0069	1.0057	1.0045	1.0033	1.0021	1.0009	0.9997	0.9985	0.9973	0.9914	0.9856	0.9799	0.9742	0.9687	0.9577
80	1.0754	1.0753	1.0752	1.075	1.0749	1.0748	1.0741	1.0728	1.0715	1.0702	1.0689	1.0676	1.0663	1.065	1.0638	1.0625	1.0612	1.06	1.0587	1.0575	1.0562	1.0501	1.044	1.0381	1.0322	1.0264	1.0151
85	1.1344	1.1343	1.1342	1.134	1.1339	1.1338	1.1331	1.1317	1.1303	1.129	1.1276	1.1263	1.1249	1.1236	1.1223	1.1209	1.1196	1.1183	1.117	1.1157	1.1144	1.108	1.1017	1.0955	1.0894	1.0834	1.0717
90	1.1926	1.1926	1.1924	1.1923	1.1921	1.192	1.1913	1.1898	1.1884	1.187	1.1856	1.1842	1.1828	1.1814	1.18	1.1786	1.1772	1.1759	1.1745	1.1732	1.1718	1.1651	1.1586	1.1522	1.1459	1.1397	1.1276
95	1.2502	1.2501	1.2499	1.2498	1.2496	1.2495	1.2487	1.2473	1.2458	1.2443	1.2428	1.2414	1.2399	1.2384	1.237	1.2356	1.2341	1.2327	1.2313	1.2299	1.2285	1.2216	1.2148	1.2082	1.2017	1.1953	1.1828

Source: Kretzschmar, Hans-Joachim, and Wolfgang Wagner. 2019. International Steam Tables: Properties of Water and Steam Based on the Industrial Formulation IAPWS-IF97. Berlin, Heidelberg: Springer Berlin Heidelberg. https://doi.org/10.1007/978-3-662-53219-5.

Appendix B: Calculations of Electrolyzer Size and Cost

Unlike other industrial plants, most of which are sized based on the amount of power generated, electrolyzers are commonly sized based on the amount of power consumed. Unfortunately, power consumption depends on many parameters such as the efficiency of the electrolyzer stacks and the nominal current density design. As a result, power consumption is not a straightforward indicator that corresponds to the plant's capacity to produce hydrogen. Consider the example scenarios in Table A.1.

Table A.1: Illustration of Three Electrolyzers with the Same System Size but Different Attributes

Parameters	Case 1	Case 2	Case 3
Membrane Thickness (μm)	254	178	178
Temperature(°C)	60	80	80
Cathode Pressure (bar)	1	30	30
Nominal Current Density (A/cm^2)	2	2	1
Electrolyzer Active Area (m^2)	930	1,014	2,449
System Size (MW)	50	50	50
Production Rate (tonne/day)	16.8	18.3	22.1
Total CAPEX ($ million)	45.7	48.9	99.9
Specific CAPEX ($/$kW_{input}$)	914	979	1,999

Even though the three electrolyzers have the same size in terms of the power consumption (50 MW), the hydrogen production capacity can differ by 24%, depending on the electrolyzer design. Similarly, the specific CAPEX, which is commonly reported in literature, varies widely by 30% to 160%. These numbers can exhibit even more variations if different operation modes – steady or dynamic – are considered. Therefore, it is important to specify the nominal operating current density and the corresponding voltage (or efficiency) when reporting the system size and specific CAPEX based on the input energy.

Appendix C: Python Code for Techno-Economic Model

The techno-economic optimization model was implemented in Python and the code files are available at https://github.com/cdhdc77/MSTHESIS. The mix-integer non-linear programming (MINLP) model was solved with Gurobi on a high-performance computing cluster available at MIT.

The author acknowledges the MIT SuperCloud and Lincoln Laboratory Supercomputing Center for providing (HPC, database, consultation) resources that have contributed to the research results reported within this thesis.